공학박사 학위논문

Effects of Various Light Extraction Structures and Orientation Polarization Molecules on Organic Light-Emitting Diodes

유기발광소자에 대한 다양한 광추출 구조와 배향 분극 분자의 효과

2020년 8월

서울대학교 대학원

재료공학 전공

한 윤 제

Abstract

Effects of Various Light Extraction Structures and Orientation Polarization Molecules on Organic Light-Emitting Diodes

Yoonjay Han
Department of Materials Science and Engineering
The Graduate School
Seoul National University

Since the first electroluminescence (EL) of organic compound was observed in the anthracene single crystal in 1965, organic light-emitting diodes (OLEDs) have undergone numerous developments, and have recently become the mainstream of small-sized displays. In addition, as OLEDs will have a modest substrate dependency, it has the potential to receive even more attention as the next generation display like flexible or transparent displays. The remaining challenges for OLEDs are high efficiency, and operational stability.

In general, because organic materials have a wide emission spectrum, OLED can be a good lighting with a high color rendering index (CRI). It can

also be used as a display with high color purity by optimizing the cavity length. However, more than half of the photons generated in OLEDs are dissipated due to total internal reflection by high-refractive-index organic layers and the substrate. Therefore, light extraction technology is required to increase the efficiency and reduce the power consumption of OLEDs. In addition, as mentioned before, it is necessary to consider the lifetime of the device. There have been many studies on the short operation lifetime of OLEDs, and several mechanisms have been proposed, but there is no concrete description of the origin of degradation. Nonetheless, it is obvious that the stability of the layers constituting the OLED should be considered for high operational stability.

This thesis concerns two research topics: (1) simple and efficient light extraction method for OLED lighting and display, and (2) improving operation lifetime of OLED using spontaneous orientation polarization molecule.

In **chapter 1**, a brief introduction of OLEDs will be provided.

In **chapter 2**, a facile and effective method for fabricating random organic microstructures for efficient light extraction from blue OLEDs is presented. Simple drop casting of a TCTA and B4PyMPM mixed solution followed by UV curing results in films with irregular-shaped microstructures (DACMs), ideal for light extraction without diffraction patterns. An external quantum efficiency (EQE) of 44.3% is realized by attaching DACMs formed on a polymer film to a blue phosphorescent OLED. The efficiency is improved by 35% compared to a planar device without the light extraction layer, greater

than the 22% improvement obtained by using microlens arrays. The method is useful for OLED lighting and potentially in displays because of the simple fabrication method that is applicable to a large area on rigid or flexible substrates, the low material cost, the insolubility of the microstructure in alkyl halide solvents such as chloroform, and the controllability of the structure through the solution process.

In **chapter 3**, we show the damageless light extraction structure for top-emittng organic light-emitting diodes (TEOLEDs). TEOLEDs are used in small displays, due to the high aperture ratios, unblurred imaging, and high color purity. However, the strong cavity structures responsible for these advantages result in a high optical loss within metal electrodes. Furthermore, as there is no substrate in the light path, it is rather complicated to form a structure on the emission surface without damage. Here, we present a facile and effective method for light extraction of TEOLEDs. When 1,5-diaminoanthraquinone (DAAQ) is deposited on the Ag electrode, crystallization occurs immediately and nanowire arrays are formed in the out-of-plane direction. The shape and distribution of nanowire arrays can be controlled by deposition thickness and evaporation rate. In addition, morphological changes affect the transmittance of DAAQ-deposited Ag thin films. DAAQ nanowire arrays were applied to a red phosphorescent inverted TEOLED, enhancing the external quantum efficiency (EQE) by 8.6% in a narrow full-width-at-half-maximum (FWHM) device, and by 10.6% in a wide FWHM device. The emission spectra of the out-coupled

devices are similar to those of the reference devices, as the DAAQ layer is located outside the OLED stacks sandwiched between two highly reflective metal electrodes. The method is useful for OLED displays because it is simple, vacuum-processable, and does not compromise device lifetime or the emission spectrum.

In **chapter 4**, we suggest the importance of patternability of internal light extraction layer. Integration of internal light extraction layers in OLED displays requires electrical connection between driving circuits in the backplane and an OLED electrode, therefore needs fabrication of a via hole. Generally, internal light extraction layers consist of two materials with different refractive indices; thus, good patternability may be difficult with the matched etch selectivities of these two materials. Both the patternability of the internal light extraction layer and high out-coupling efficiency are important so, it needs a proper etchant which aren't lowering the extraction efficiency by demolishing its structure. Here, the patternability of light extraction layers is discussed and demonstrated experimentally. The random scattering layer (RSL) composed of SiO_x nano scatterers and a TiO_2 planarization layer was used in this study and it was patterned by photolithography and wet etching processes. For matching the etching selectivity of those two different materials, a mixture of buffered oxide etchant (BOE) and phosphoric acid (H_3PO_4), in a volume ratio of 0.5 of H_3PO_4 to BOE, shows the best results for forming electrical channels through the out-coupling layer. The OLEDs fabricated on this patterned substrate showed

similar current density-voltage (*J-V*) characteristics to OLEDs on a glass substrate with low leakage levels. The device showed over 50% enhancement of external quantum efficiency (EQE; from 21.7% to 32.7%), similar to the device without via holes.

Chapter 5 contains a method for improving the stability of electron transporting layer. After the alignment of permanent dipole moment (PDM) was found in Alq_3, it was revealed that spontaneous orientation polarization (SOP) was observed in several electron transporting materials. Although studies on the electrical effects of the polarization have been reported, there are few reports on the effects of polarization on the lifetime of device. Here, we observed the SOP characteristics and the change in the lifetime of device when BAlq was doped in PO-T2T with different volume ratios. As the polarization increased, the operation lifetime also increased and the applied voltage change decreased. In addition, the lifetime enhancement was only observed when there was a polarized layer at the interface with the emtting layer (EML). This shows that hole blocking layer (HBL) can enhance the lifetime when it has a negative surface charge at the interface with EML, and also indicates that the SOP characteristics of the molecule should be considered for improving the lifetime.

Keywords: Organic light-emittng diodes, Light extraction efficiency, Light extraction structure, Operation lifetime, Spontaneous orientation polarization

Student Number: 2015-20870

Contents

List of Tables

List of Figures

Chapter 1. Introduction

1.1 Brief history of Organic Light-Emitting Diodes (OLEDs)

Organic semiconductors can control material properties through molecular structure modification, which is a unique advantage of organic materials. Organic light-emitting diodes are light-emitting diodes that utilize the above advantage of organic materials, and are composed of several layers of organic semiconductors, each of which plays a specific role. The structure of a typical OLED is as follows, and it is depicted in Figure 1.1: substrate/anode/hole injection layer (HIL)/hole transporting layer (HTL)/electron blocking layer (EBL)/emitting layer (EML)/hole blocking layer (HBL)/electron transporting layer (ETL)/electron injection layer (EIL)/cathode. OLEDs are classified into bottom emission type and top emission type (Figure 1.2), and the former emits light in the direction of the device's substrate, and the latter emits light from the opposite direction of the substrate. Since the pixel area loss shadowed by the thin film transistor (TFT) is more important for small-sized pixel displays, in general, the bottm emission type is used for large-sized pixel devices as television, and the top emission type is used for small-sized pixel devices as moblie. OLED has many advantages to being used as lighting and display. Firstly, OLED does not require a backlight because it has self-emitting property, so it is thin, light and flexible. In addition, it also has surface emission, fast repetition rate, high contrast ratio, high color rendering index (CRI) through a wide full-width-at-half-maximum (FWHM) emission spectrum, and high color

purity due to microcavity structures. As such, OLED has many advantages, and is used as a variety of commercial products today. (Figure 1.3)

Organic semiconductor was discovered by akamatsu and inokuchi in 1950 by measuring the electrical conductivity of violanthrone, iso-violanthrone, and pyranthrone.[1] Furthermore, in 1965, and the first electroluminescence (EL) of organic compound was observed by Helfrich and Schneider to measure EL of anthracene single crystal.[2] In addition, ELs of perylene-based materials, polyvinyl carbazole (PVK) and poly (3-vinyl carbazole) have been reported.[3,4] In 1987, C. W. Tang and S. A. Van Slyke reported the first bilayer OELD with 4,4′-Cyclohexylidenebis[*N*,*N*-bis(4-methylphenyl)benzenamine] (TAPC)/tris(8-hydroxyquinolinato)aluminum (Alq3) structure.[5] The external quantum efficiency (EQE) of the device was 1% and the maximum luminance of the device was over 1,000 cd/m^2. Also, in 1989, they developed a host-guest system to increase efficiency and control the emission spectrum by doping Coumarin 540, DCM1, DCM2 to Alq3.[6] The differences between today's state-of-the-art OLEDs are that they consist of more layers and better performance materials. The above two papers are of great significance in showing the origin of the current structure of OLEDs for the first time.

Although the first OLED was reported, its efficiency was very low. The reasons are that exciton binding energy is high, exchange energy is high, and only singlet excitons participate in radiative decay process. In photoexcitation, only singlet excitons are formed, but in the charge recombination process, 25%

single singlet and 75% triple excitons are formed by spin statistics, and the triple excitons are dissipated through the non-radiative decay. Therefore, if the triplet excitons that dissipated through the non-radiative process can emit phosphorescence at room temperature, the efficiency of OLED can be greatly improved. In 1998, M. A. Baldo and S. R. Forrests reported strong phosphorescence at room temperature using Pt-based organometallic compound, 2,3,7,8,12,13,17,18-octaethyl21H,23H-porphine platinum(II) (PtOEP).[7] Due to the strong spin-orbit coupling at excited state, organometallic compounds with heavy metal atom (Ir, Pt, Os, Ru, Pd) allow the triplet exciton to emit phosphorescence at room temperature by electron spin flipping during the decay. With this development, the efficiency of OLED has been greatly improved and 100% internal quantum efficiency (IQE) (= $\frac{\text{number of generated photons}}{\text{number of injected charge carriers}}$ (%)) is possible.

Meanwhile, despite the high efficiency of organiometaalic compounds, the heavy metal atoms are generally rare earth metals, so a triplet harvesting method without the heavy metal atoms was needed. In 2012, H. Uoyama and C. Adachi reported metal-free organic comound that allow spin up-conversion from triplet to singlet by small energy level gap.[8] They named this process as thermally activated delayed fluorescence (TADF) and spatially separtated donor and acceptor moieties allowed the intramolecular charge transfer that leads small energy gap between the singlet and triplet states, promoting spin mixing by intersystem crossing (ISC) ($S_1 \rightarrow T_1$) and reverse intersystem crossing

($T_1 \rightarrow S_1$). This process allows to harvest the triplet excited states as delayed fluorescence. Similarly, the above properties are also exhibited by intermolecular charge transfer between electron-accpeting molecules and electron-donating molecules, which is called excited charge transfer state (exciplex).[9–11] Furthermore, the systems that doped the TADF emitter to the exciplex host to boost the RISC rate (k_{RISC}) have also been reported.[12,13] In recent years, as the operation lifetime of OLED has become more important, TADF emitter + fluorescent emitter or phosphorescent emitter + fluorescent emitter is doped to EML to utilize triplet exciton while using the high stability properties of fluorescent dopants.[14–17] Figure 1.4 is a schematic illustration of the above three electronic processes.

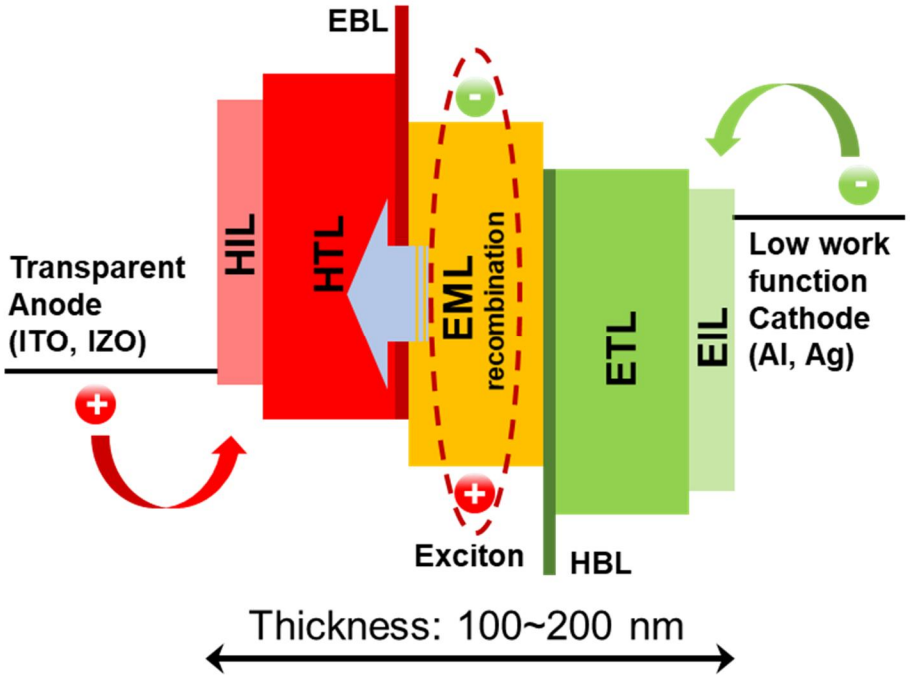

Figure 1.1 Typical structure of organic light-emittig diode (OLED).

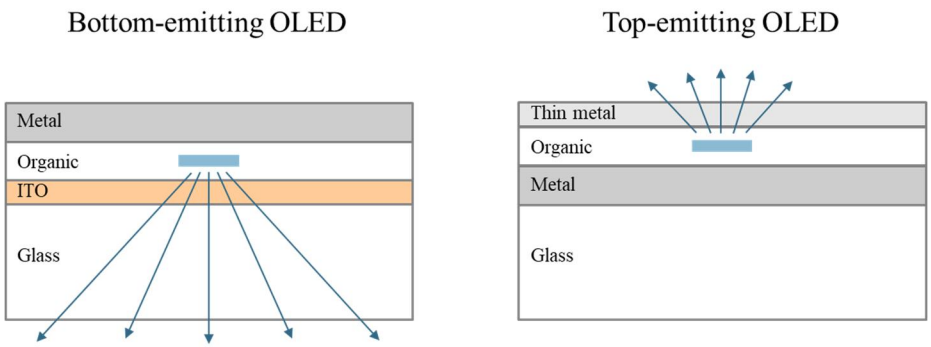

Figure 1.2 Schematic images of the propagating light path depending on the emitting type of OLEDs.

Figure 1.3 Commercial products of OLEDs; (a) Foldable OLED Panel in Samsung Galaxy Z Flip (Samsung Electronics 2020), (b) LG Rollable OLED TV R9 (LG Electronics 2020), (c) OLED lighting in automobile (BMW AG 2017), (d) Virtual exterior mirror (Audi 2018).

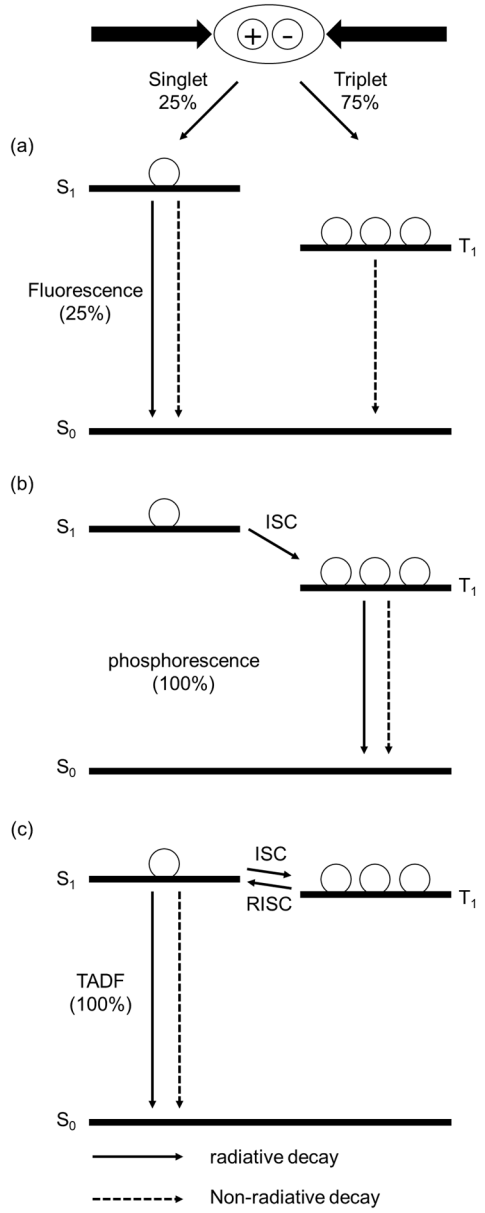

Figure 1.4 Mechanisms of (a) fluorescence, (b) phosphorescence, and (c) thermally-activated delayed fluorescence (TADF) radiation.

1.2 Efficiency of OLEDs

External quantum efficiency (EQE) is one of the parameters indicating the efficiency of OLED, and is defined as the number of photons emitted to the air compared to the number of injected charge carriers. EQE does not take into account eye sensitivity such as candela (cd) or lumen (lm). EQE can be expressed by the following equation.

$$\eta_{\mathrm{EQE}} = \eta_{\mathrm{IQE}} \times \eta_{\mathrm{out}}(\Theta, \Gamma) = \gamma \times \eta_{\mathrm{S/T}} \times q_{\mathrm{eff}}(q_{\mathrm{r}}, \Gamma) \times \eta_{\mathrm{out}}(\Theta, \Gamma)$$

η_{EQE} = external quantum efficiency (EQE)
η_{IQE} = internal quantum efficiency (IQE)
η_{out} = out-coupling efficiency
γ = exciton formation efficiency (charge balance factor)
$\eta_{\mathrm{S/T}}$ = radiative exciton ratio
q_{eff} = effective quantum efficiency

Θ is the emitting dipole orientation (ratio of horizontal transition dipole moment), which greatly affects the efficiency of the device. This can also be expressed as an S (orientation order). The values are different, but they mean the same thing.

(1) $\mathrm{horizontal} : \mathrm{vertical} = \Theta : (1-\Theta) = \langle \sin^2\theta \rangle : \langle \cos^2\theta \rangle$

(2) $S = \dfrac{3\langle \cos^2\theta \rangle - 1}{2}$

θ is the angle between the transition dipole moment vector and the normal

vector of the substrate. $\langle \cdots \rangle$ is an ensemble average. As depicted in Figure 1.5, vertically aligned dipoles are difficult to extract light to the air, and most of the externally emitted light comes from horizontally aligned dipoles. Therefore, the larger Θ, the higher the efficiency. Γ is a geometric factor and is affected by the thickness of the device and the location of the recombination zone in EML. γ means the ratio of exciton formation in EML compared to the injected charge carriers, and $\eta_{S/T}$ refers to the ratio of radiative excitons by spin statistic as mentioned in chapter 1.1. q_{eff} is the ratio of excitons that form photon among radiative excitons in the cavity structure, and is different from q_r . q_r is the radiative quantum efficiency, also called photoluminescence quantum yield (PLQY). PLQY is defined as the ratio of emitted photons by emitting dopant to the excitons. Also, it can be expressed as kinetic parameter as below.

$$q_r = \frac{k_r}{k_r + k_{nr}}$$

$$q_{eff} = \frac{F \cdot k_r}{F \cdot k_r + k_{nr}}$$

k_r = radiative decay rate
k_{nr} = non-radiative decay rate
F = purcell factor

Non-radiative decay means that energy is dissipated into phonon. The difference between q_r and q_{eff} is whether the emitting layer is in the free

space or inside the cavity. Since the excitonic decay rate in the electromagnetic cavities is altered according to the local mode density,[18] the efficiency of the EML located in the cavity called OLED should take F into account. Lastly, η_{out} is the ratio at which photon inside the cavity is extracted to the air. Although lower than light-emitting diodes (LEDs), OLEDs also have a larger refractive index than air, so there is light trapped inside the cavity. Therefore, it should be considered.

In addition to EQE, there are luminous current efficiency (cd/A) and luminous power efficiency (luminous efficacy, lm/W) as parameters indicating the efficiency of OLED. Since 1 candela (cd) is the brightness of 1 candle per 1 sr, cd/A indicates the luminous intensity of 1 sr solid angle according to ampere. Also, the cd value is different for each color even though EQE is the same because the luminous intensity takes into account the human eye's sensitivity. Brightness of OLEDs can be calculated by the following equation

$$I[\text{cd}] = 683.002 \cdot \int_{\lambda} I_e(\lambda) S(\lambda) d\lambda$$

Where $I_e(\lambda)$ is the radiant flux spectrum (watt/nm) and $S(\lambda)$ is the relative human eye's sensitivity. Figure 1.6 depicts the eye sensitivity. 683.002 is the arbitrary term occurs to match the unit between cd and watt. Since Candela is the brightness of one candle, it is a constant created by determining monochromatic radiation of 540×10^{12} Hz frequency to 1 lm/W to precisely define candela. Lumen (lm) is the intensity of light emitted at a solid angle,

which is the same unit as cd·sr. For example, since the light spreads out form a candle in a spherical shape, the intensity of light is $1\,\mathrm{cd} \times 4\pi\ \mathrm{sr} = 4\pi\ \mathrm{lm}$. Therefore, lm/W is the intensity of light from all solid angles, compared to the power applied to the device, so it is a more practical parameter than EQE.

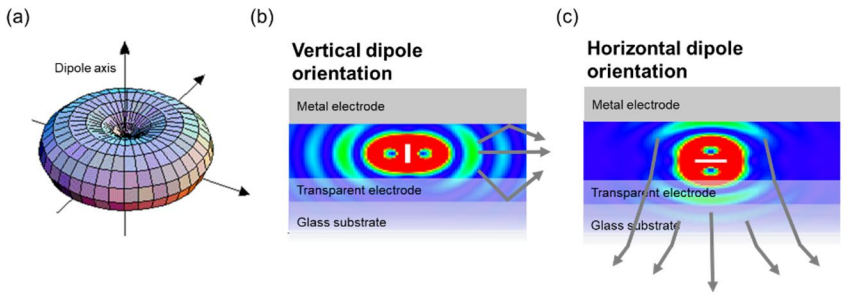

Figure 1.5 (a) Radiation pattern from the dipole. Radiation from (b) horizontal and (c) vertical dipoles in OLED stacks.

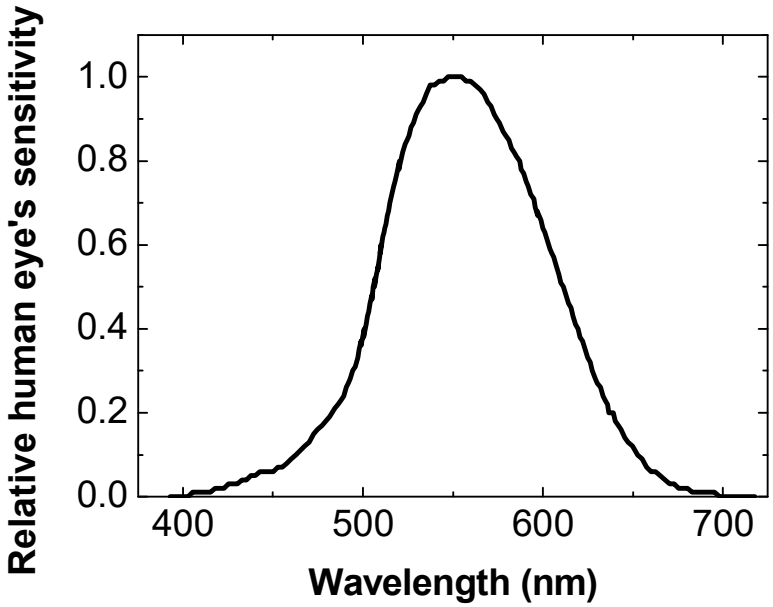

Figure 1.6 Relative human eye's sensitivity as a function of wavelength

1.3 Light extraction methods for OLEDs

As shown in Figure 1.7, organic materials have a higher refractive index than air, so there are confined modes in the OLED. In addition, since the organic material has a larger refractive index than glass, there is light confined inside the oled stack without being extracted to the substrate. Also, because it is located close to the metal electrode, there is a loss due to surface plasmon polariton coupling and intrinsic absorption of the materials. Each of these modes is classified as the air mode, substrate-guided mode, wave-guided mode, surface palsmon polaritons (SPPs), and intrinsic absorption loss. Since the mode distribution is affected by the structure of the device, out-coupling efficiency is affected by device structure. Plus, out-coupling efficiency is also affected by the emitting dipole orientation, because the spp loss is only caused by the transverse magnetic (TM) mode, and the direction of the field is also dependent on the emitting dipole orientation. There are methods to improve the out-coupling efficiency, including (1) emitting dopant with high horizontal dipole orientation, (2) organic materials with low refractive indices, (3) optical structure attachment. Here, we describe how to improve the out-coupling efficiency through the optical structure.

The light extraction structure can be rougly classified into two types; the external light extraction layer which is located outside the substrate and the internal light extractgion layer which is located between the substrate and the OLED stack or inside the OLED stack. Figure 1.8 shows microlens array

(MLA), luminaire, scatter film, and high refractive index substrate, which are representative types of external light extraction methods. The external structure has the advantage that it is easy to fabricate and apply, but there is a limitation that only substrate-guided mode can be extracted. Figure 1.9 is a representative internal light extraction method, photonic crystal embedded high refractive index layer and corrugated device. Because the periodic structure has a distortion of the spectrum due to the wavelength dependency, the structure is usually randomly dispersed. The internal structure has the advantage that it can affect both wave-guided and substrate-guided modes, but there are critical issues. Because the solution process is often used to fabricate the structures, problems with reliablitiy of OLED caused by residual solvent may occur. In the case of the corrugated structure which can extract the spp modes, it is important to ensure electrical uniformity because the curvature of device can cause local thickness differences. Therefore, the light extraction structure should be easy, fast, reliable and should not affect the reliability of the device.

Light extraction is used for lighting, but it is still limited in OLED displays due to image blurring issue. This is because the image blurring issue is not critical in lighting, but the display has an important requirement not to interrupt small-sized pixels. Image blurring means that the apparent pixel size is recognized larger than the actual pixel size. In fact, the light extraction layer basically causes the image blurring because it increases the light path. Especially, when the out-coupling structure is applied to the bottom emission

type, image blurring becomes more serious. When light extraction is applied to the bottom emission type OLED as shown in Figure 1.8, it is disadvantageous for image blurring due to the long path until the emitted light is extracted to air. On the other hand, the light extraction structure has a potential to be used in display when applied to top emission type, since the top emission type is less blurred due to the short distance of nm scale. However, it is difficult to apply the light extraction structure to the top emission type. Since there is no substrate in the light path, it is rather complicated to form a structure on the emission surface without damage. Therefore, a lot of research is needed for the top emission type light extraction, and the representative light extraction structure for top-emitting OLED is depicted in Figure 1.11.

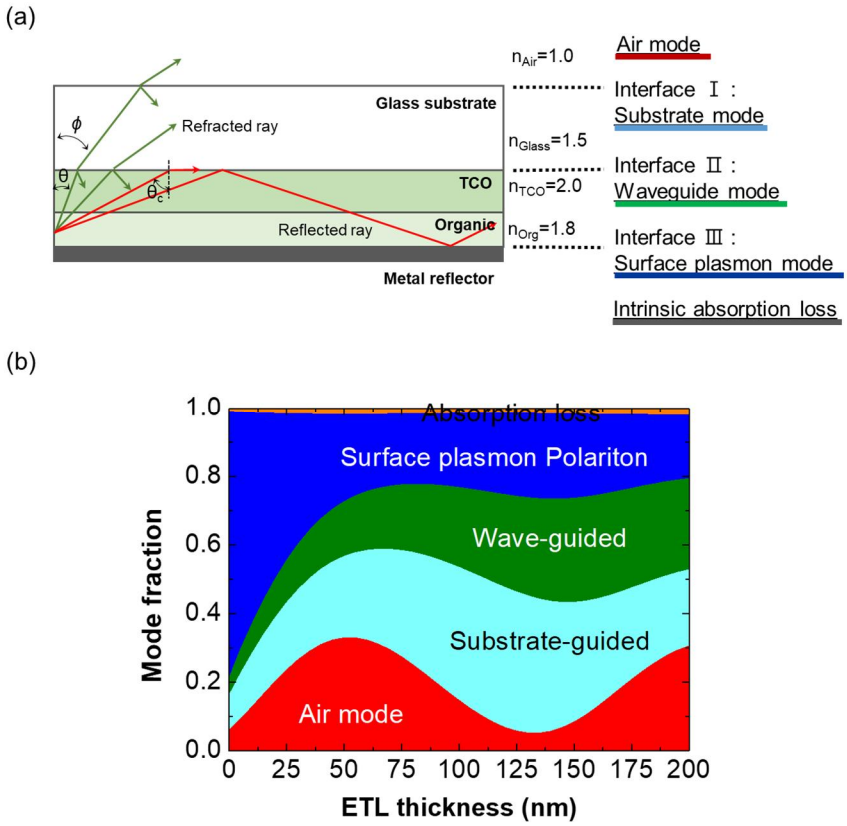

Figure 1.7 (a) Schematic image of the modes exist in OLED structure. (b) Simulated mode fractions as a function of the ETL thickness.

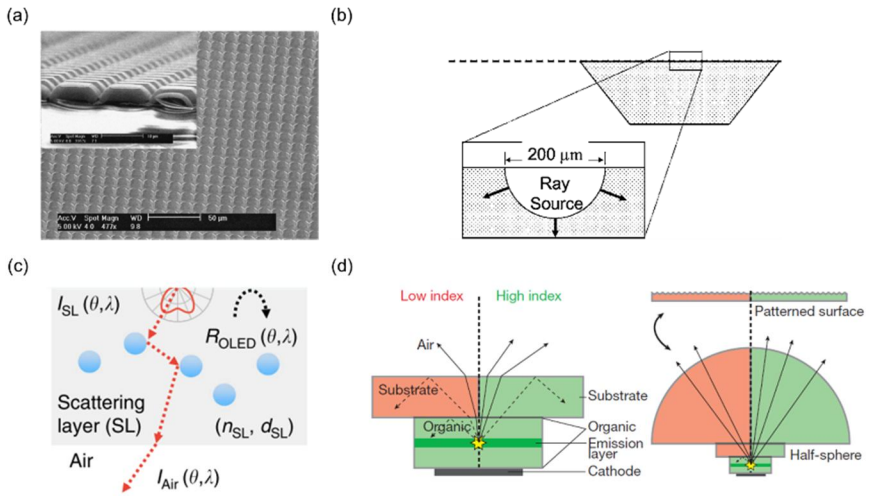

Figure 1.8 Representative external light extraction methods including (a) microlens array (MLA), (b) luminaire, (c) scatter film, and (d) high refractive index substrate.

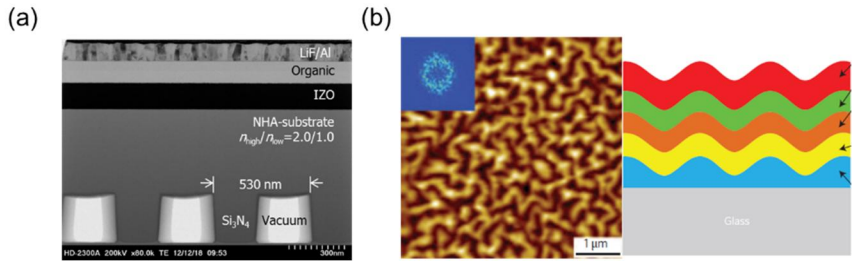

Figure 1.9 Representative internal light extraction methods including (a) photonic crystal embedded high refractive index layer and (b) corrugated device.

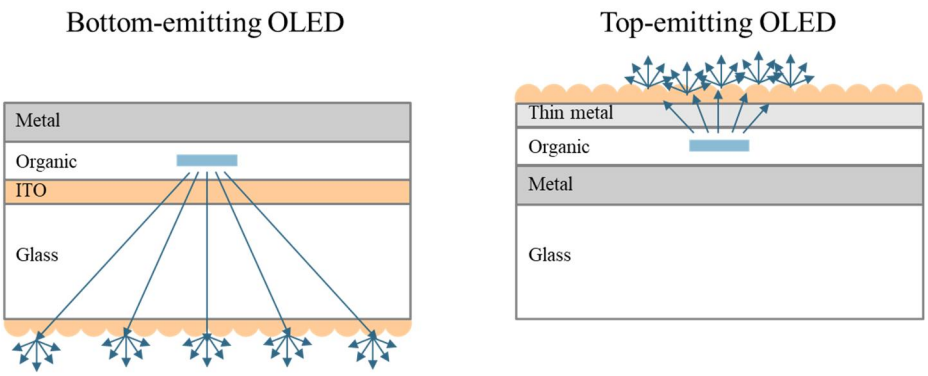

Figure 1.10 Schematic images of the propagating light path depending on the emitting type of OLEDs with light extraction structure.

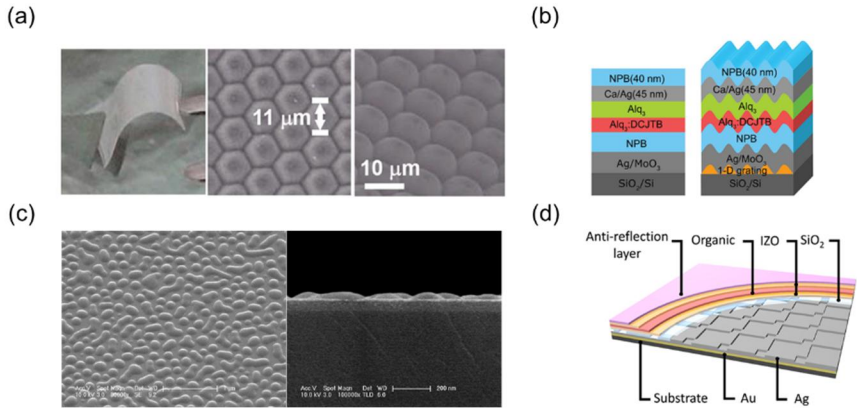

Figure 1.11 Representative light extraction methods for Top-emitting OLED including (a) lamination, (b) corrugated structure, (c) organic nano-lens array by organic vapor phase deposition method (OVPD), (d) planarized corrugated structure.

1.4 Finite difference time domain (FDTD) method

When considering repetitive work and cost, it is important to predict the experimental results through simulation. In addition, prediction through calculation is very important in a light extraction structure design in which an optimized structure is essential. Micro-sized structures can be predicted by ray optics, but nano-sized structures require the use of rigorous methods to solve the solution of the Maxwell equation. Finite difference time domain (FDTD) method is a numerical analysis technique for complex geometries. The space is discretized into cubic-shaped lattices, so-called Yee cell. The electric field is defined at the edge centers of the lattice, and the magnetic field is defined at the face centers of the lattice. The magnetic permeability/magnetic loss is defined at the lattice corners, and the electric permittivity/conductivity is defined at the lattice centers. As FDTD is a time-domain method, it can cover a wide frequency range with a single calculation and handle nonlinear optics in a natural way. However, as the system size increases, the phase error accumulates, so super-fine gride is required when simulating large problems, which consumes a lot of computer cost.

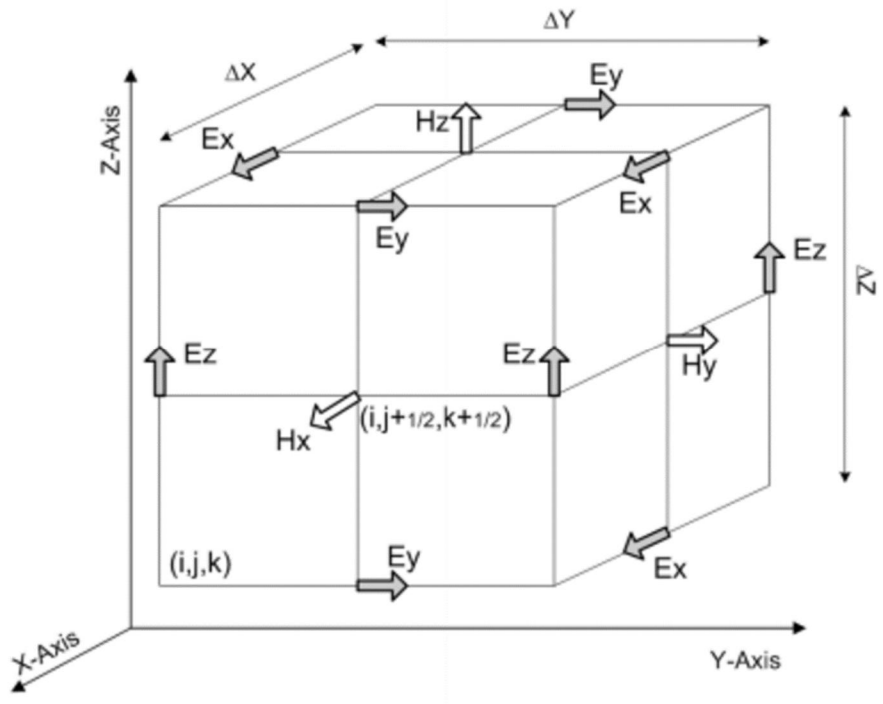

Figure 1.12 Schematic structure of Yee lattice[19]

1.5 Operational stability of OLEDs

Operational stability of OLEDs is an issue that has not yet been resolved. Although a certain level of stability has been achieved through a lot of research and effort, this is only for red and green, and research on blue is still insignificant. There have been many studies on the short operation lifetime of OLEDs, and several mechanisms have been proposed, but there is no concrete description of the origin of degradation.

The study on the lifetime of OLED is difficult because there are both intrinsic and extrinsic factors in the degradation. Extrinsic factors include defects such as particles, temperature changes, moisture, oxygen, sealing, out-gassing and impurities of organic materials. Since these things are difficult to say the properties of materials, these factors should be minimized for studies. However, since it is very tough, it can lead to misinterpretation of the results.

The intrinsic factors are due to the characteristics of the organic material or the device itself, and there are factors like charge balance, charge accumulation at interfaces, diffusion. In 1997, H. Vestwever et al. reported electron migration of mobile ions from Ca and ITO electrodes. In this study, mobile ion changed the internal energy structure of OLED and accompanied decay of luminance and current. After this study, research on the lifetime of OLED has developed into charge and quencher density inside the device. In general, since EML has a bulk heterostructure or bipolar host structure, the hopping rate decreases, and accumulation occurs at the interface between the EML and the transport layer.

High energy is released by annihilation between the accumulated charge, so-called polaron, and exciton of EML, and can cause chemical dissociation or reaction of substances. In addition, since the charge exists as a polaron inside the OLED, the polaron which is in the ionic state is more unstable than the neutral state, which may cause charge induced degradtaion. Also, H. Aziz and G. Xu suggested the degradation mechanism by electron injection electrode and hole injection electrode. They found a decrease in the indium (In) concentration of the anode in the degraded device, as well as an irregular surface of the Al cathode. From these results, it was suggested that electrochemical reaction at interfaces is the cause of degradation. Another study reported morphology changes in organic materials due to moisture and oxygen. Recently, a new mechanism was proposed, and they proposed bond dissociation energy (BDE) as a new degradation mechanismUsing the Density functional theory (DFT) to calculate the bond's BDE, they say that dissociation of a substance by weak bonds such as C-P and C-N causes degradation. However, there is still no concrete model, and several plausible models are proposed.

1.6 Outline of the thesis

In this thesis, we describe the effect of various light extraction structures on OLED efficiency. In addition, we report the effect of lifetime enhancement in OLEDs by doping the orientation polarization molecule.

In order to increase the efficiency of OLED, a light extraction structure is necessary to extract the confined mode. For this reason, numerous light extraction structures have been reported so far, but the microlens array is the most preferred option considering process convenience and cost. Therefore, it is necessary to develop a light extraction structure in the form of a film that is cheaper and has higher efficiency while making it more convenient than MLA. In chapter 2, we report a simple and effective method for the fabrication of random organic nano-textured microstructures for light extraction of blue OLEDs. Donor-acceptor crosslinked microstructures (DACMs) are created by dropping a donor-acceptor-mixed methanol-chloroform solution on a substrate followed by drying the solution under ultraviolet (UV) light. The DACMs are fabricated on an adhesive PET film and attached to a blue phosphorescent OLED for light extraction to get a very high EQE of 44.3%, enhanced by 35% over the planar device. This value is greater than 22% enhancement by the MLA film. In addition to high light extraction efficiency, the extraction method has many advantages for practical use; low cost, large-area processability, insolubility to alkyl halide solvents, and structural controllability without disturbing the inner OLED structure or degrading the device lifetime. (Chap. 2)

Although we developed simple and effective light extraction layer, it is hard to apply to the top-emitting OLED (TEOLED). Since there is no substrate in the light path, it is rather complicated to form or apply a structure on the emission surface without damage. In chapter 3, we report one-step method of fabricating nanowire structures composed of 1,5-diaminoanthraquinone (DAAQ) for light extraction of TEOLED. DAAQ nanowires were formed in the out-of-plane direction on the Ag thin film, and nanowire pitch, height, and diameter were able to be controlled by the deposition conditions. We fabricated DAAQ nanowires on a red phosphorescent TEOLED with a pixel size of 2 × 2 mm for light extraction. It showed 8.6% enhancement for a narrow full width at half maximum (FWHM) device without distorting the emission spectrum, and 10.6% enhancement for a wide FWHM device. The method is suitable for OLED display because it is simple, vacuum-processable and has mild processing conditions without damaging the device. (Chap. 3)

For active matrix OLED (AMOLED) display, each OLED pixel is controlled by thin film transistor (TFT) and it is able to achieve high efficiency and resolution than passive matrix method. For separating OLED and TFT spatially, there is a passivation layer between OLED electrode and TFT drain electrode and they are connected by an electrical channel, which is called via hole. Because internal light extraction layers are usually fabricated beneath OLED electrode, it is necessary to pattern via holes in the internal light extraction layers. In chapter 4, we developed a wet etching process for via hole fabrication

in a random scattering layer (RSL) and demonstrated OLEDs on the patterned out-coupling layer with low leakage current and good light extraction efficiency. (Chap. 4)

Although the efficiency is increased by the light extraction layer, it is necessary to consider the lifetime of the device. As OLED is composed of several layers such as hole transporting layer (HTL) and electron transporting layer (ETL) and the accumulation of irreversible degraded products shorten the lifetime of device, the stability of the materials should be considered. Especially, since ETL requires high electron mobility, high triplet level, and wide energy bandgap characteristics, and it is rather tough to achieve material stability while meeting the above requirements. Therefore, it is important to develop a method to enhance the stability of the ETL. In chapter 5, we discuss how to improve the stability of ETL using spontaneous orientation polarization (SOP). Plus, we investigated the change in the polarization of the device according to the volume ratio of SOP molecules and compared the operational stability of the device. As the polarization increased, the operation lifetime also increased and the applied voltage change decreased. The enhancement in lifetime was only found when the position of the polarized layer was at the EML/ETL interface. This means that hole blocking layer can increase device lifetime when there is a negative surface charge at its interface with EML, and also indicates that the SOP characteristics of the molecule should be considered to improve the lifetime. (Chap. 5)

Chapter 2. Random Organic Nano-textured Microstructures by Photo-Induced Crosslinking for Light Extraction of Blue OLEDs

2.1 Introduction

The efficiency of organic light-emitting diodes (OLEDs) has drastically increased, and OLEDs have become a key technology in displays and lighting. However, more than half of the photons generated in OLEDs are dissipated due to total internal reflection by high-refractive-index organic layers and the substrate.[20–22] Therefore, light extraction technology is required to increase the efficiency and reduce the power consumption of OLEDs. Since displays use numerous small-sized pixels for image clarity, they cannot use light extraction structures that introduce image blurring. Thus, efforts to extract light for displays have attempted to develop a light extraction layer that causes less blurring through patterning processes including photolithographic processes, oblique angle deposition, and imprinting.[23–34] In contrast, light extraction technologies for lighting take into account cost-effectiveness, large area processability, and efficiency improvements, with image blurring being less critical.[16–32] Meanwhile, there is high demand for high-efficiency blue OLEDs both for displays and lighting, because the color quality and the operation lifetime of white OLEDs using two or three emitting units depend largely on blue devices.[52,53] Although significant efforts have been concentrated on light

extraction of blue OLEDs,[27,54–59] the EQEs that have been obtained are much lower than 40% that has been achieved in other color ranges.[26,37,60,61] Attaching commercialized microlens arrays (MLAs) film is a convenient method, but it is less effective. Randomly dispersed metallic oxide compounds have also been used for light-scattering layers, but reliability issues such as surface cracks or agglomeration of inorganic particles can reduce the device efficiency.[62] Organic compounds have been used to form light scatters by vacuum evaporation,[285863–65] but material waste is inevitable in this process.

Here, we report a simple and effective method for the fabrication of random organic nano-textured microstructures for light extraction of blue OLEDs. Donor-acceptor crosslinked microstructures (DACMs) are created by dropping a donor-acceptor-mixed methanol-chloroform solution on a substrate followed by drying the solution under ultraviolet (UV) light. The DACMs are fabricated on an adhesive PET film and attached to a blue phosphorescent OLED for light extraction to get a very high EQE of 44.3%, enhanced by 35% over the planar device. This value is greater than 22% enhancement by the MLA film. In addition to high light extraction efficiency, the extraction method has many advantages for practical use; low cost, large-area processability, insolubility to alkyl halide solvents, and structural controllability without disturbing the inner OLED structure or degrading the device lifetime. Furthermore, we fully discuss on the EQE, enhancement ratio and the efficiency of light extraction structure (ELOS) defined as the ratio of the enhanced EQE to the extractable mode fraction. We show that enhancement ratio and ELOS should be obtained using

the optimized device structure as the reference device to be useful indicators for the effectiveness of a light extraction structure based on the devices with different electron transporting layer (ETL) thicknesses.

2.2 Experimental section

The transmittance of the films was measured using an UV-vis-near infrared spectrophotometer (Cary 5000, Agilent Technologies) in the normal direction. SEM images of the films were taken by a MERLIN Compact microscope (Zeiss) after platinum coating. For fabrication of OLEDs, 70 nm-thick pre-patterned ITO-coated glass substrates were cleaned by dipping in acetone and isopropyl alcohol and boiling in isopropyl alcohol. All of the organic and metal layers were deposited by thermal evaporation at a base pressure of under 5×10^{-7} Torr without breaking the vacuum. For each layer, the total deposition rate was 1 Å/s. mCP, PO-T2T, and FIrpic were purchased from Nichem, and ReO_3 and Rb_2CO_3 were purchased from Sigma Aldrich. The devices were encapsulated with a cover glass in a glovebox using UV-curable resin. Current densities were measured with a programmable source meter (Keithley 2400, Tektronix Inc.), and EL spectra and intensities in the normal direction were measured with a spectrometer (PR-650, Photo Research). The luminance of the OLEDs was calculated using the spectral intensity in the normal direction and the CIE luminosity function. The angle-dependent EL spectra and intensities were measured every 5 degrees with a rotating stage and a fiber optic spectrometer (S2000, Ocean Optics Inc.). The EQEs of the OLEDs without light extraction structures were calculated using the *J-V-L* characteristics and the angle dependent EL spectra and intensities. Detailed method was discussed in our previous reports.[66] The efficiency improvements obtained using the out-

coupling films were measured with a 6-inch integrating sphere (Labsphere) and a monochromator attached to a photomultiplier tube (Acton Research Corp.) by measuring the relative intensities of the devices with light extraction structures against the intensity of the device without the light extraction layers. The out-coupling films were cut and attached to the same size as the substrate. Emitted light of the devices was incident through a port of an integrating sphere having a diameter of 0.75 inches (19 mm), smaller than the size of the substrate (25 × 25 mm) to prevent light the edge of the substrate or films. The MLAs are shaped as half spheres with a radius of 35 μm, and exist in hexagonal arrays with a fill factor of 90%.

2.3 Results and Discussion

Figure 2.1 illustrates the formation process for the DACMs. (1) A methanol-mixed chloroform solution (1:15 volume ratio) containing both 0.005 M 4,4′,4″-tris(carbazol-9-yl)triphenylamine (TCTA) and 0.005 M 4,6-bis(3,5-di(pyridin-4-yl)phenyl)-2-methylpyrimidine (B4PyMPM) was prepared. (2) 0.2 mL of the solution was dropped on a 25 × 25-mm fused silica substrate using a micropipette to cover the substrate. (3) The solution was dried under a UV lamp (λ = 365 nm, 4 W) at room temperature for 3 minutes, resulting in the formation of a light-scattering structure. In addition, DACMs were fabricated on a 100-μm-thick adhesive PET film with a diameter of 100 mm using the same process (Figure 2.2).

Figure 2.3 (a) compares the samples prepared with different solutions and under different light illumination. Haze DACMs covered the glass surface in an irregular pattern (see optical microscope images in Figure 2.4). In contrast, DACMs were not created with solutions containing either only the donor or only the acceptor, or under yellow light. Without the formation of DACMs, some organic molecules formed thin layers on the surface and others precipitated at the edge of the surface. The thin layers and the precipitated powders were removed with a chloroform rinse using a squeeze bottle. However, DACMs were not peeled off by the rinse, although the haziness was reduced. Figure 2.3 (b) shows the fluorescence of the samples under 254 nm wavelength UV illumination. The as-prepared DACMs and the sample dried

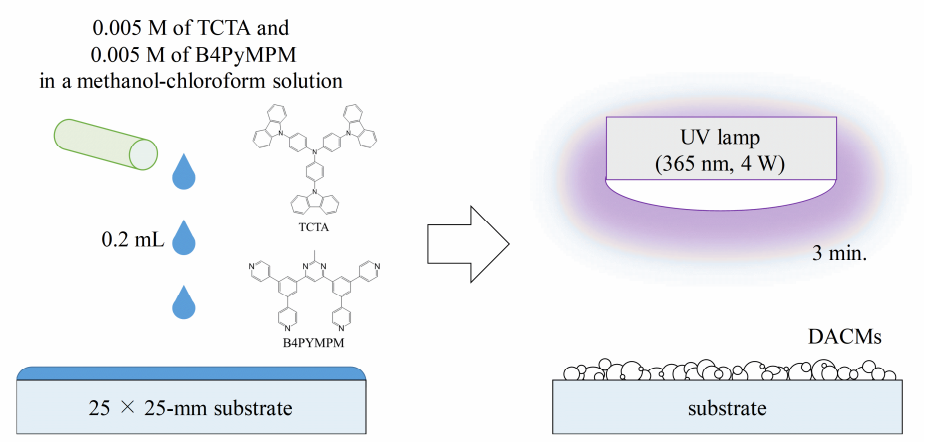

Figure 2.1 Fabrication of donor-acceptor crosslinked microstructures (DACMs). Randomly crumpled microstructures are formed by drying a donor-acceptor dissolved in a methanol–mixed chloroform solution under UV light.

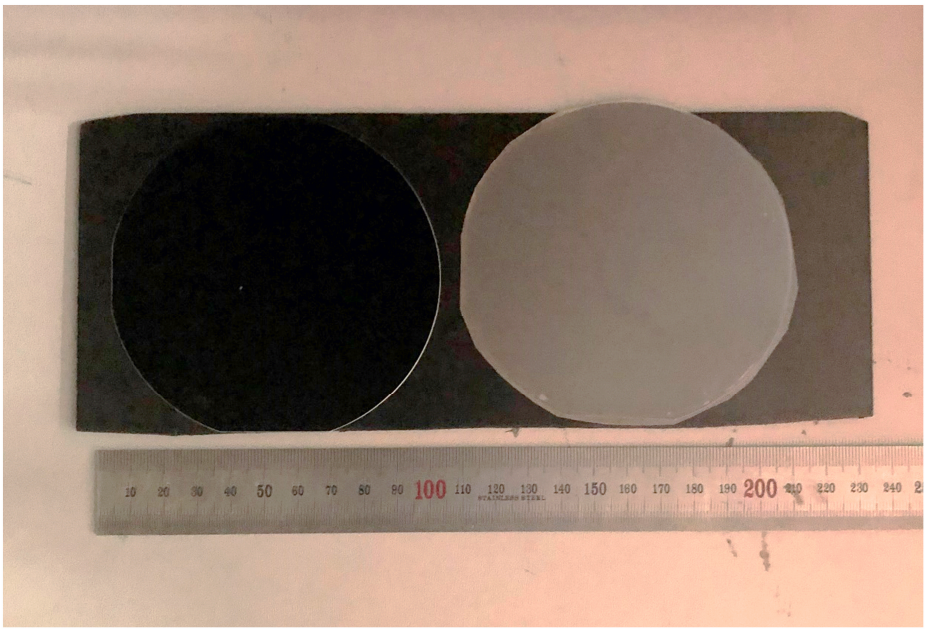

Figure 2.2 DACMs fabricated on a 100-mm-thick PET film attached to a silicon wafer with a diameter of 100 mm (right). Left is a bare silicon wafer.

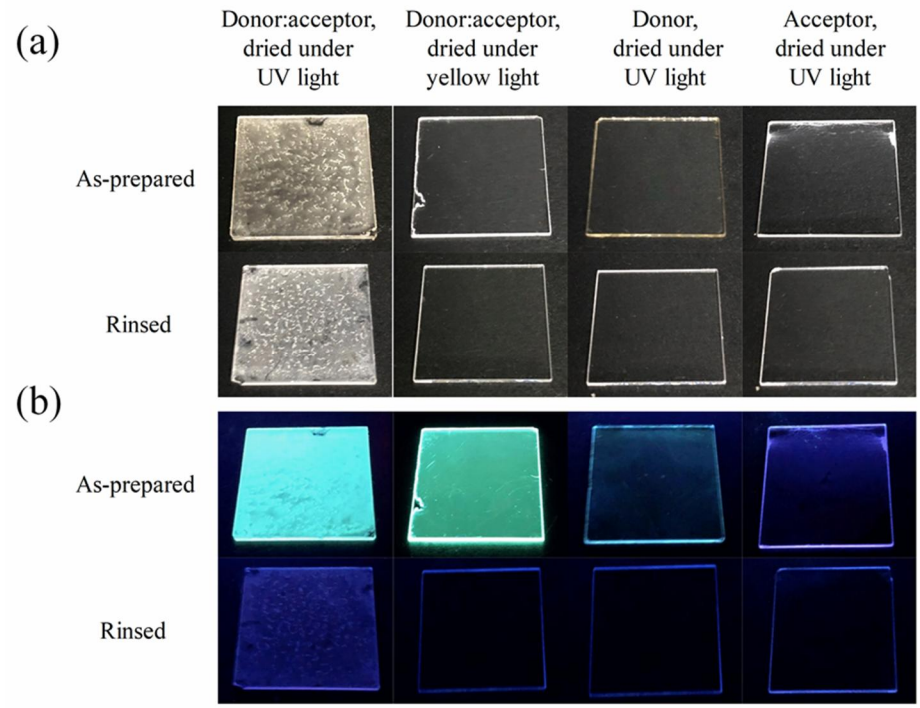

Figure 2.3 Photographs of samples prepared with different solutions and under different drying conditions. (a) Photocrosslinking between TCTA (donor) and B4PyMPM (acceptor) under UV light formed hazy DACMs that are not washed away by chloroform. In contrast, the sample dried under yellow light and the samples prepared using the solutions containing only the donor or the acceptor formed transparent layers instead of DACMs. (b) Green, blue, and violet fluorescence was exhibited by the TCTA:B4PyMPM exciplex, TCTA, and B4PyMPM samples under UV illumination ($\lambda = 254$ nm), respectively. Because the chloroform removed the unreacted monomers, the samples did not show fluorescence. The glow of the DACMs is the scattered violet light from the UV lamp.

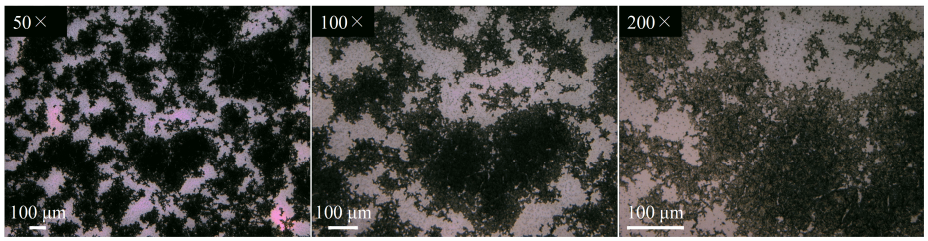

Figure 2.4 Optical microscope images of DACMs at different magnifications: 50× (left), 100× (center), 200× (right). Dark portions are surfaces covered by macromolecules.

under the yellow light emitted green fluorescence corresponding to the TCTA:B4PyMPM exciplex.[67,68] The fluorescence completely disappeared in the both samples after the rinse, at which point the glowing of DACMs is the scattered violet light from the UV lamp (see the spectrum of the lamp in Figure 2.5). The blue and violet fluorescence of the TCTA and B4PyMPM layers, respectively, also disappeared after the rinse. These results indicated the formation of chemically stable macromolecules by photo-crosslinking between TCTA and B4PyMPM. Since the crosslinking was induced by excitation of the monomers in the donor-acceptor mixed solution, the excited state complex between TCTA and B4PyMPM is expected to be the intermediate state of the reaction. The as-prepared DACMs consist of the macromolecules, which are insoluble in chloroform, and the unreacted monomers. The mechanism of the formation of DACM is not clear at this moment and under investigation now. There are many studies on the formation of photo-induced dimer of pyrimidine,[69] but in our results, the DACM was formed by the reaction with TCTA composed of amine and carbazole. Thus, further study is required to clarify the origin(s).

Figures 2.6 (a), (b), and (c) show scanning electron microscope (SEM) images of the as-prepared DACMs, the rinsed DACMs, and the sample dried under yellow light, respectively. The DACMs are clusters of a few micrometers of ball-shaped macromolecules. The clusters cover the surface with irregular patterns. After the rinse, the DACMs have nanopores where the unreacted monomers have been washed away. The size of the macromolecule balls and

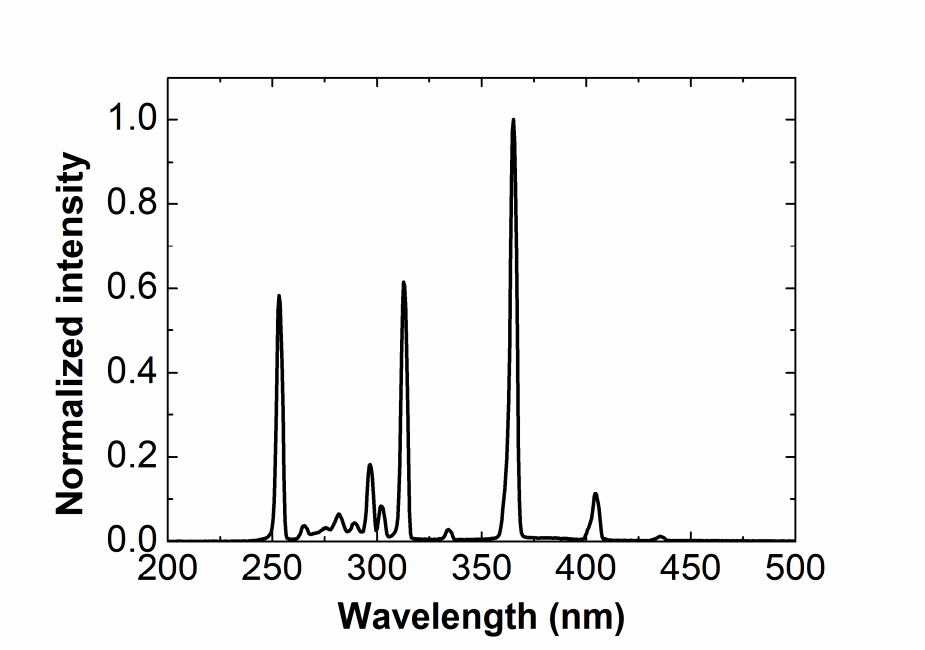

Figure 2.5 Emission spectrum of the UV lamp (λ = 254 nm). The lamp has several peaks from 254 nm to 403 nm.

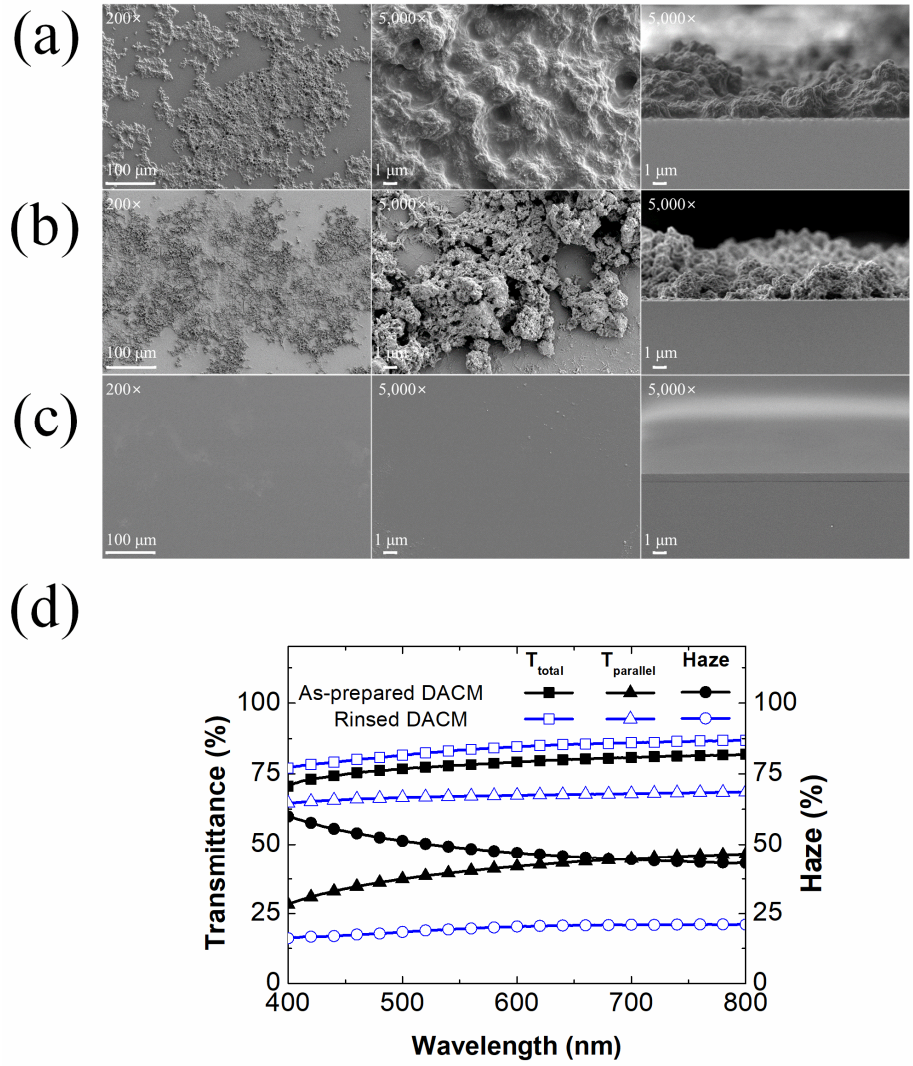

Figure 2.6 Scanning electron microscope (SEM) images of (a) as-prepared DACMs, (b) rinsed DACMs, and (c) a sample dried under yellow light. The first two images are views from the top, and the third image is a view from the side. (d) Total transmittance, specular transmittance, and haze of the as-prepared and rinsed DACMs. The haze was between 40 and 60% for as-prepared DACMs, and between 18 and 20% for rinsed DACMs.

the surface coverage could be controlled by the concentration of the solution and the repeated coating process (Figure 2.7 and 2.8). In contrast, the sample dried under yellow light formed only a micrometer-thick thin layer without a feature of the macromolecules. Figure 2.6 (d) depicts the total transmittance, specular transmittance and haze of the as-prepared and rinsed DACMs, respectively, where haze is calculated using the following equation; Haze = $(T_{total} - T_{specular}) / T_{total}$. The as-prepared DACMs exhibited low specular transmittance between 30 and 50% at a wavelength range between 400 and 800 nm compared to 65 and 70% for the rinsed DACM in the same wavelength range although the total transmittance was similar to that of the rinsed DACMs. As a result, the haze of the DACMs was 53% at the wavelength of 470 nm, which is much higher than the value of 18% after rinsing. Therefore, as-prepared DACMs acted as a better light-scattering structures for visible light than the rinsed one.

For application in light extraction of an OLED, the DACMs-coated PET film was cut and attached to the glass substrate of one of the 2 × 2 mm pixels of a blue phosphorescent OLED with the following structure: ITO(70 nm)/6 wt% ReO_3 doped mCP(40 nm)/mCP(15 nm)/10 wt% FIrpic doped mCP:PO-T2T(1:1, 30 nm)/PO-T2T(20 nm)/4 wt% Rb_2CO_3 doped PO-T2T(30, 50, 70 nm)/Al(100 nm), where mCP represents N , N′-dicarbazolyl-3,5-benzene and PO-T2T represents 1,3,5-triazine-2,4,6-triyl)tris(benzene-3,1-diyl))tris(diphenylphosphine oxide), respectively.[70] A commercial MLA film

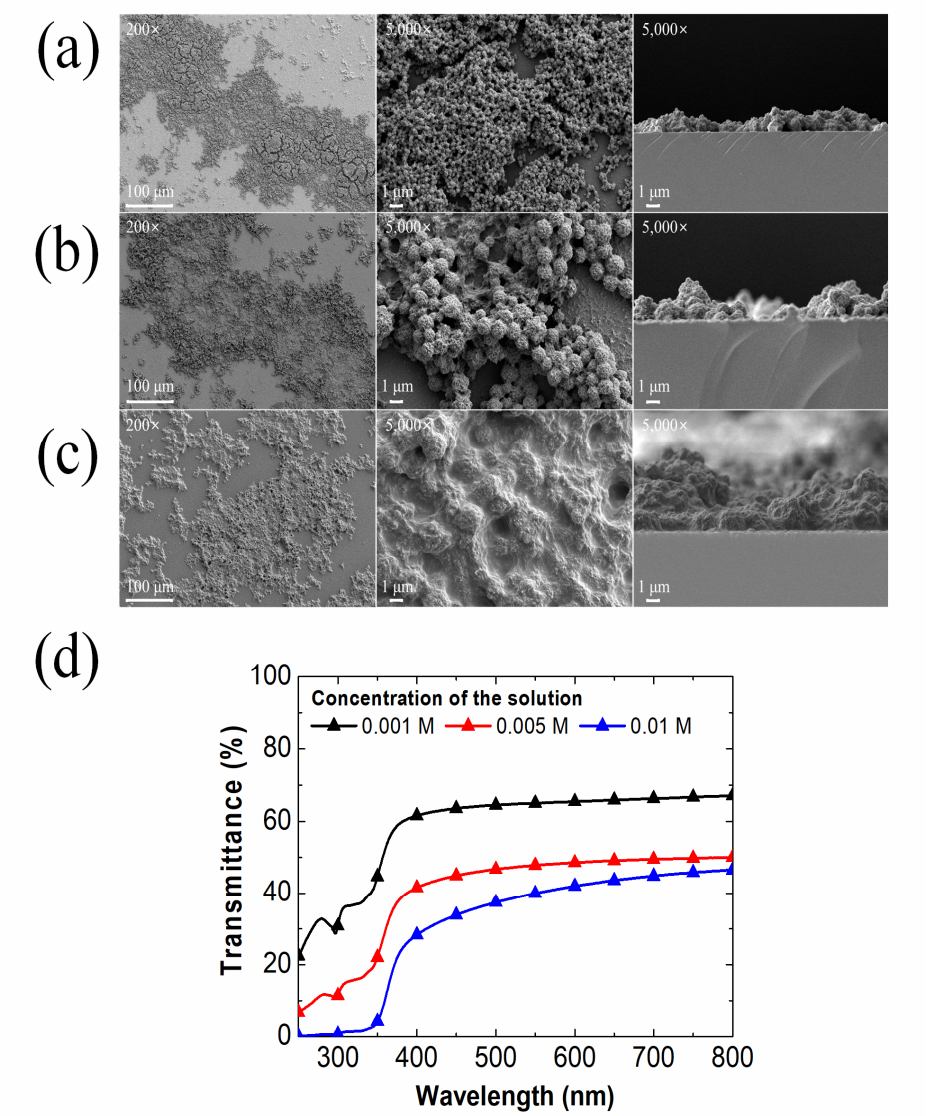

Figure 2.7 Scanning electron microscope (SEM) images of DACMs fabricated by methanol–mixed chloroform solutions with (a) 0.001 M, (b) 0.005 M, or (c) 0.01 M of TCTA and B4PyMPM at a 1:1 molar ratio. As the concentration of the solution was lower, the size of the macromolecule balls was smaller. (d) Transmittance of the DACMs.

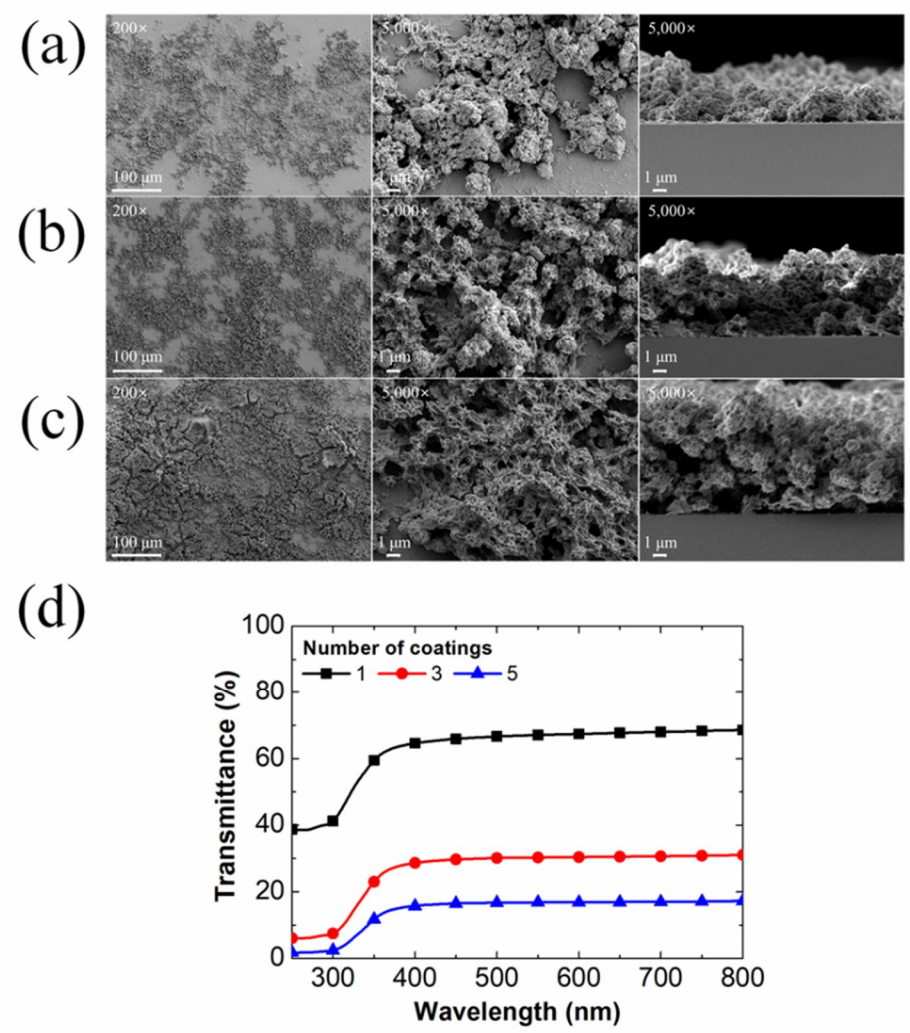

Figure 2.8 SEM images of DACMs prepared with (a) one, (b) three, or (c) five coating-rinse processes. The repeated processes resulted in overlays of DACMs. (d) Transmittance of the DACMs.

(UTE24B, MNtech Co.) was also used as an extraction layer for comparison. Figure 2.9 (a) shows the current density-voltage-luminance characteristics and the electroluminescence images at an applied voltage of 9 V of the reference, DACMs-attached, and MLAs-attached devices with an ETL thickness of 50 nm. The DACMs-attached device showed a lower luminance to the normal direction than the reference and the MLAs-attached devices, and also exhibited blurred electroluminescence images because of the scattering effect. The EL spectra and relative EL intensity of the devices measured at a current density of 3 mA/cm^2 in an integrating sphere are shown in Figure 2.9 (b) and the EQEs of the device with and without the light extraction structures are compared in Figure 2.9 (c) along with the angular emission patterns in the inset. The DACMs-attached device exhibited a wider angular emission pattern than the reference device and the MLAs-attached device. The EQEs were improved by 35% and 22% by attaching the DACM and the MLA films, respectively, compared to the reference device without the extraction layers. As a result, the maximum EQEs were increased to 44.3 and 40.0% by attaching the DACM film and the MLA film, respectively, from the value of 32.8% for the reference device, as shown in Figure 2.9 (c). To the best of our knowledge, 44.3% EQE is the highest efficiency achieved for blue OLEDs with light extraction methods (Table 2.1). The high extraction efficiencies of the DACM film may originate from the coupled nano and microstructures of the light scattering layer as reported before.[49,71] The high haze value of the DACMs, and the blurred electroluminescence image of the DACMs-attached device in Figure 2.9 (a)

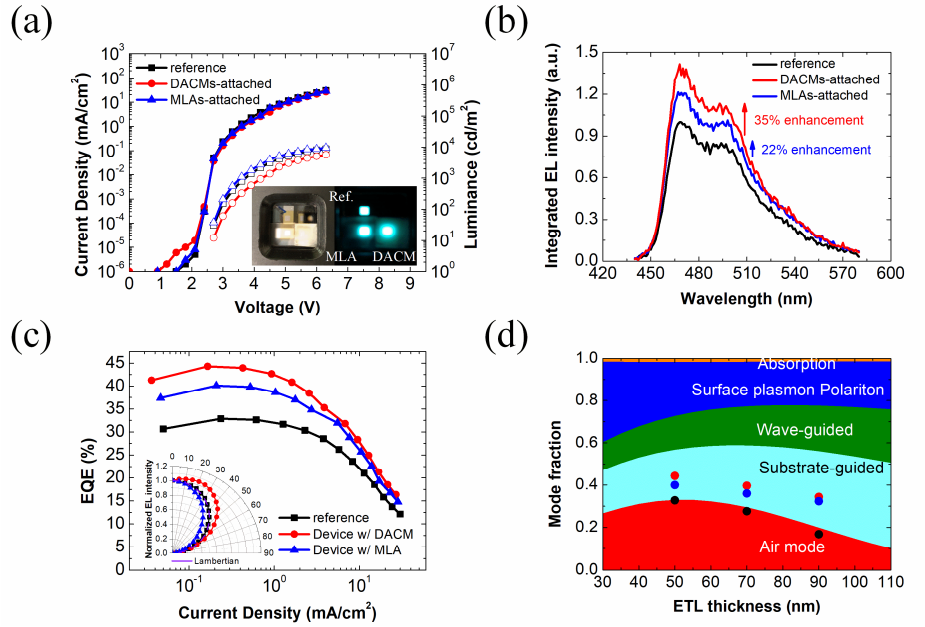

Figure 2.9 (a) *J-V-L* characteristics of reference, DACMs-attached, and MLAs-attached devices. Inset: photographs of electroluminescence of the devices at an applied voltage of 9 V. (b) Relative electroluminescence spectra in an integrating sphere at 3 mA/cm^2. (c) EQEs of the devices as a function of current density. Inset: Angular emission patterns of the devices. (d) Simulated optical mode fractions as a function of the electron transporting layer (ETL) thickness, with black, blue, and red scatters representing the maximum EQEs of the reference, DACMs-attached, and MLAs-attached devices, respectively.

Table 2.1 Characteristics of selected blue OLEDs with light extraction structure.

Light extraction method		Bottom/ top emission	Emitter	Efficiency (reference)[a]	Efficiency with light extraction[a]	Enhancement ratio	Ref.
External structure	Internal structure						
Halographic diffuser	-	Bottom	FIrpic	3.8%	5.5%	1.45	[1]
Moth's eye nanostructure	-	Bottom	FIrpic	12%	20%	1.67	[2]
-	Moth's eye nanostructure	Bottom	FIrpic	12%	19%	1.58	[2]
Moth's eye nanostructure	Moth's eye nanostructure	Bottom	FIrpic	12%	26%	2.17	[2]
Nanostructured PET	-	Bottom	FIrpic	9.1%	12.9%	1.42	[3]
Nanostructured PET with AgNW	-	Bottom	FIrpic	9.1%	34.2%	3.76	[3]
Micro-Nano Nested Structure	-	Bottom	FIrpic	17.2%	27.2%	1.58	[4]
Cicada-wing structure	-	Bottom	FIrpic	11 cd/A	14 cd/A	1.27	[5]
-	Textured surface	Top	FIrpic	11%	16%	1.45	[6]
Organic nanolens array	-	Top	TBPe	4.6 cd/A	7.3 cd/A	1.59	[7]
DACMs	-	Bottom	FIrpic	32.8%	44.3%	1.35	This work
DACMs	-	Bottom	FIrpic	27.7%	39.7%	1.43	This work
DACMs	-	Bottom	FIrpic	16.8%	34.4%	2.05	This work

[a)]Efficiencies are the maximum external quantum efficiencies and the maximal current efficiencies of the devices without and with the light extraction method, respectively.

exhibited the high scattering effect due to irregular nano- and micro-patterns. Thus, the greater efficiency improvement was achieved in the DACM film than the MLA film. The enhancement is nothing to do with the absorption or emission of the DACM because there is no overlap between the emission spectrum of FIrpic and the absorption spectrum of TCTA or B4PyMPM or excitation spectrum of DACM (Figure 2.10 and 2.11).

One needs to note that the enhancement ratio of the OLED efficiency by a light extraction structure depends on the efficiency of a reference device (a device without any light extraction structures) as demonstrated in Figure 2.9 (d), where the efficiencies of the devices with different thicknesses of ETL are compared to theoretical values calculated by an optical simulation using a classical dipole model.[72] PLQY of 100% and the horizontal emitting dipole ratio of 76% were used for the simulation. The device performances are summarized in Table 2.2 and detailed device characteristics are shown in Figure 2.12. The maximum efficiencies of the reference devices were in good agreement with the theoretical values. The simulation indicates that the DACM and MLA films extract 48 and 30% of the light confined in the glass substrate of the optimized reference OLED with the ETL thickness of 50 nm, respectively. As the ETL thickness increased from the optimized one, the EQE of the device with or without the extraction layer was reduced. In contrast, the EQE enhancement ratios were increased from 35% to 43.3% and 105% by attaching the DACM film, and from 22% to 30% and 93% by attaching the MLA film as the thickness of the ETL increased from 50 nm to 70 and 90 nm, respectively.

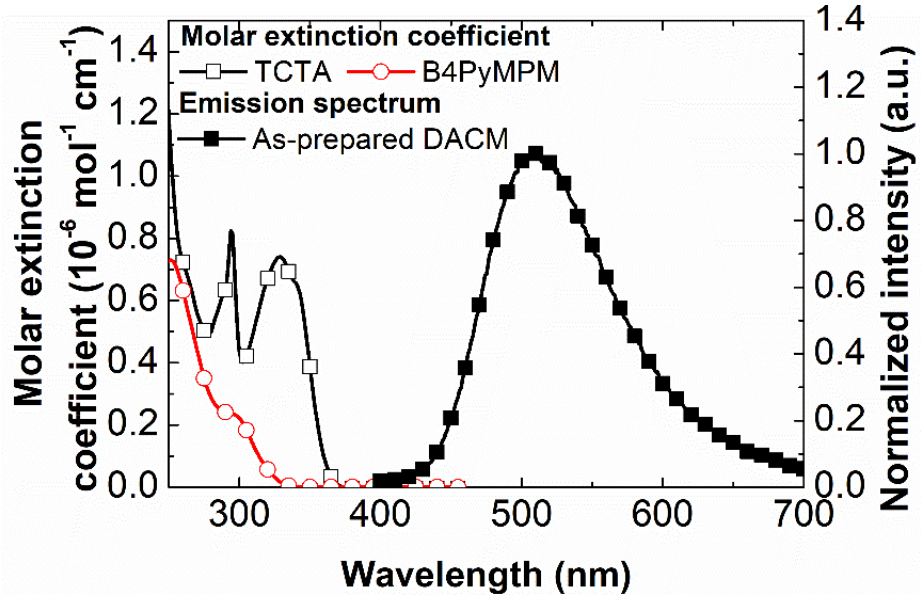

Figure 2.10 Absorption spectra of TCTA and B4PyMPM in methylene chloride (10^{-6} M) and photoluminescence spectrum of the as-prepared DACM.

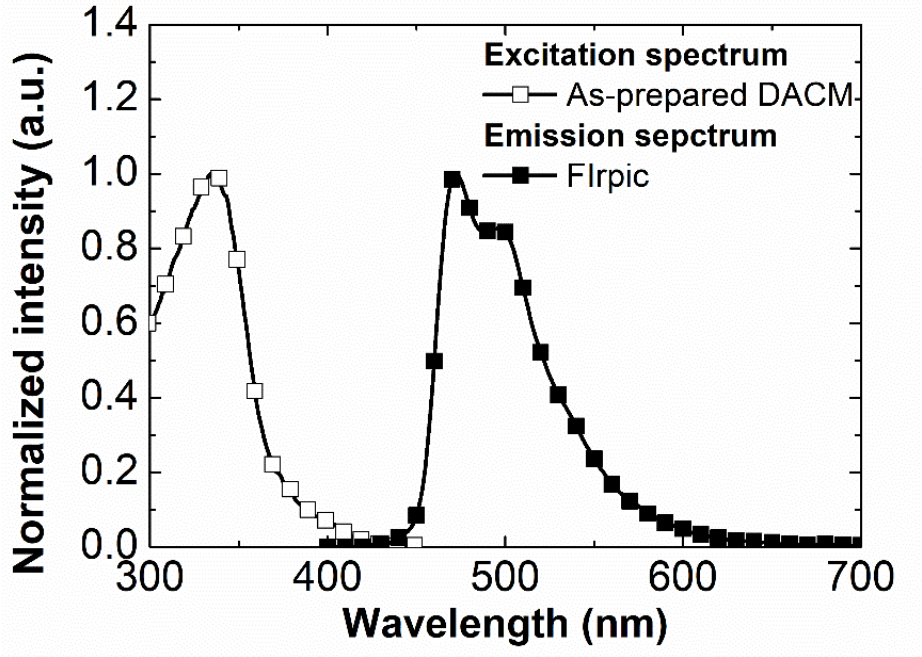

Figure 2.11 Excitation spectrum of as-prepared DACM detected at 550 nm wavelength and photoluminescence spectrum of FIrpic.

Table 2.2 Comparison of quantum efficiency, enhancement ratio, and efficiency of light out-coupling structures (ELOS) for devices with different out-coupling structures.

ETL thickness [nm]	Maximum EQE [%]				Enhancement ratio		ELOS[a] [%]	
	Theoretical (w/o extraction)	Experimental (w/o extraction)	DACMs-attached	MLAs-attached	DACMs-attached	MLAs-attached	DACMs-attached	MLAs-attached
50	32.9	32.8	44.3	40	1.35	1.22	48	30
70	29.4	27.7	39.7	36	1.43	1.30	40	29
90	19.8	16.8	34.4	32.4	2.05	1.93	49	43

[a)]This value was calculated using the following equation; $\eta_{\mathrm{ELOS}} = \frac{\mathrm{EQE}_{\mathrm{extracted}} - \mathrm{EQE}_{\mathrm{reference}}}{\chi_{\mathrm{substrate\text{-}guided}}}$, where $\chi_{\mathrm{substrate\text{-}guided}}$ is the mode fraction confined in the substrate.

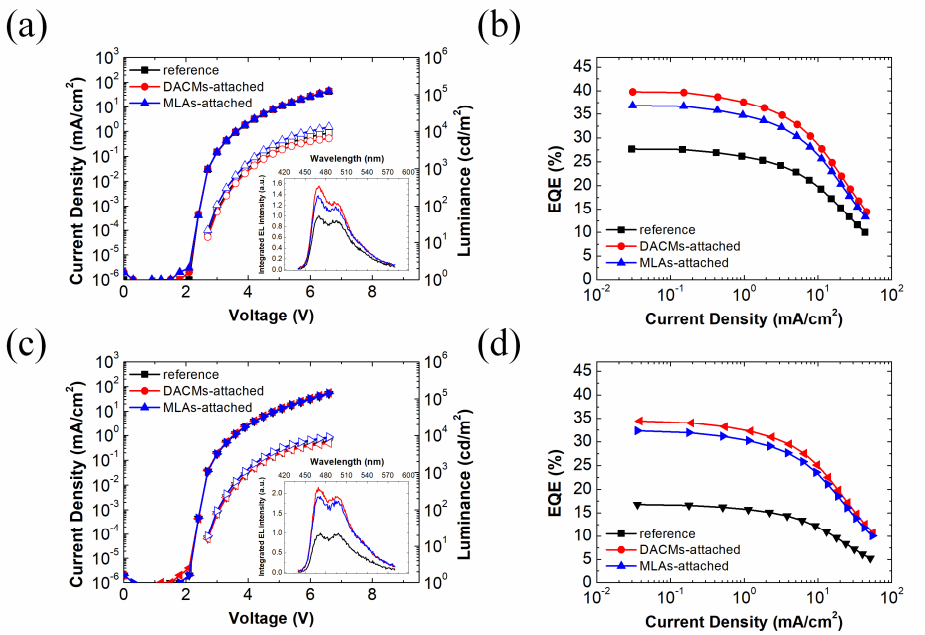

Figure 2.12 (a) *J-V-L* characteristics of reference, DACMs-attached, and MLAs-attached devices at 70 nm ETL thickness. Inset: Relative electroluminescence spectra in an integrating sphere at 3 mA/cm^2. (b) EQEs of the devices as a function of current density at 70 nm ETL thickness. (c) *J-V-L* characteristics of reference, DACMs-attached, and MLAs-attached devices at 90 nm ETL thickness. Inset: Relative electroluminescence spectra in an integrating sphere at 3 mA/cm^2. (d) EQEs of the devices as a function of current density at 90 nm ETL thickness.

These results clearly indicate that the efficiency enhancement ratio does not represent the performance of the extraction layers. Because of the reason, P.-A. Will et al. proposed to use the efficiency of light out-coupling structures (ELOS) defined as the ratio of the enhanced EQE to the extractable mode fraction.[73] The ELOS of the DACM film was 48% for the optimized OLED which is much higher than 30% obtained from the MLA film. Although, the MLA film had the ELOS value of 43% if the OLED structure was not optimized, it does not guarantee high EQE value of the device as demonstrated in this paper. This means that the ELOS value still does not provide a quantitative measure of the effectiveness of the out-coupling structure because the value depends on the device structure. Nevertheless, the ELOS provides a better picture than the enhancement factor as a measure of the quality of the out-coupling structure because its variation depending on the device structure is less than the enhancement factor. In order for the ELOS or the enhancement ratio to have direct connection with achievable EQEs, the OLED structure must be optimized before applying the light extraction structure, which has been done in this paper. In other words, enhancement ratio and ELOS will give a quantitative figure of merit of the light extraction structure under the condition of the optimized reference device structure. Lastly, if the emitting dopant having a higher horizontal dipole ratio is used, the greater enhancement of EQE by light extraction can be achieved due to an increase in the amount of substrate-guided mode (Figure 2.13).

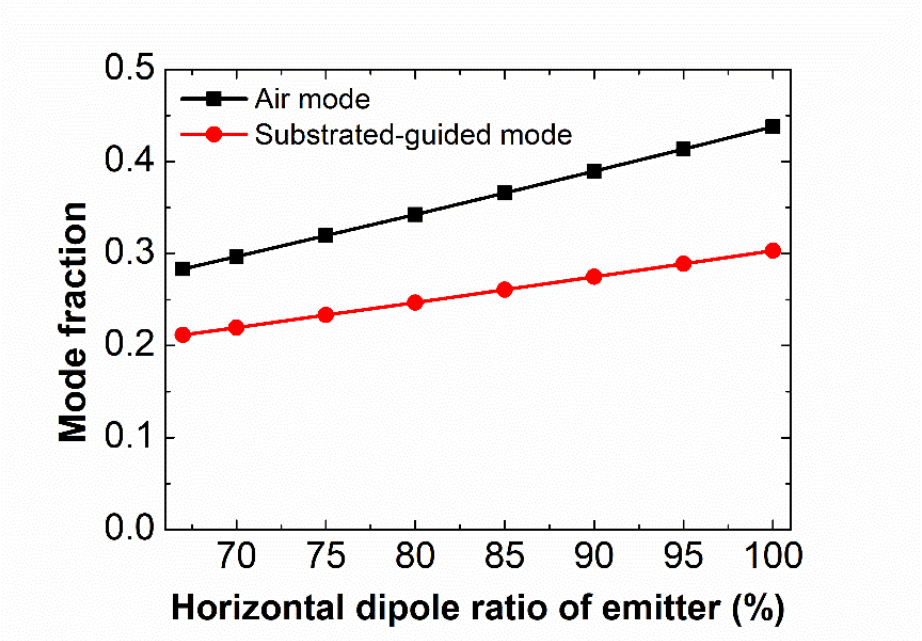

Figure 2.13 Calculated fractions of air and substrate-guided mode as a function of horizontal dipole ratio of emitting dopant. The structure used for the calculation was as follows;

Glass/ITO(70 nm)/hole transporting layer(HTL, 55 nm)/emitting layer(EML, 30 nm)/electron transporting layer(ETL, 50 nm)/Al(100 nm). We assumed the recombination zone was located in the middle of EML and the photoluminescence quantum yield (PLQY) of 100%.

2.4 Conclusion

In summary, a facile and effective method to fabricate random organic nanostructures on microstructures has been developed for efficient light extraction of OLEDs. Simple drop casting of TCTA and B4PyMPM mixed solution followed by UV curing resulted in films with irregular-shaped coupled nano and microstructures (DACMs), ideal for light extraction without diffraction patterns. The microstructures can be fabricated on rigid substrates such as glass, or flexible plastic substrates such as PET films. The DACM film was more effective in light extraction than the MLA film, enhancing the efficiency by 35%, compared to the 22% achieved using an MLA film. Maximum EQE values of 44.3% were obtained by attaching the DACM film to a blue OLED with an EQE of 32.8%. The device with the MLA film attached resulted in an EQE of 40%. This demonstrates good light scattering properties for OLEDs without absorption of visible light. The method is useful for OLED lighting because the fabrication is simple and applicable over a large area on rigid or flexible substrates, material costs are low, the microstructure is insoluble in strong solvents such as chloroform, and the structure can be controlled by a solution process. Furthermore, we have demonstrated that the high EQE enhancements and the ELOS do not guarantee the high EQE values. As the ETL thickness increases from the optimized one, EQE enhancements ratios and ELOS were increased, but the EQEs of the devices with the light extraction layers were decreased. Therefore, in order for the ELOS or the

enhancement ratio to have direct connection with achievable EQEs, the OLED structure must be optimized before applying the light extraction structure.

Chapter 3. Random Nanowire Arrays Spontaneously Formed via Vacuum Deposition for Enhancing Light Extraction from Inverted Top-Emitting Organic Light-Emitting Diodes

3.1 Introduction

Top-emitting organic light-emitting diodes (TEOLEDs) exhibit certain advantages compared to bottom-emitting OLEDs, including unblurred imaging, large aperture ratios and high color purity as a result of the narrow emission spectrum originating from the strong microcavity effect between the metal mirror bottom electrode and the semitransparent thin metal top electrode. Because of the reason, TEOLEDs are widely used, especially in small-sized displays. However, the metal electrodes induce large optical losses due to absorption and surface plasmon polaritons (SPPs). Besides, light is also confined within the OLED stacks because of the high refractive indices of the organic layers. Therefore, light extraction technology for TEOLEDs is required to reduce optical losses and increase efficiency. Despite this demand, it is difficult to apply light extraction technologies to TEOLEDs. Since there is no substrate in the light path, it is rather complicated to form a structure on the emission surface without damage. Thus, lots of efforts have been devoted to reducing damage during the process. One of the proposed methods is to

deposit the OLEDs on a pre-patterned substrate.[32,74–83] Although this method efficiently extracts the confined modes, it is important to ensure electrical uniformity because the device curvature can cause local thickness differences. Another proposed method is to apply optical structures directly to the device via precisely controlled engineering processes such as lamination,[84–89] nano-imprinting,[90] or solution-based processes.[91,92] Such methods minimally affect electrical properties of the device, but are quite challenging in practice because damage to the device can easily occur during the process. Previously, we reported methods of forming organic lens array in vacuum using a micro-sized hole pattern mask[28,64] or the organic vapor phase deposition (OVPD) method.[58,65] In addition, methods of forming nanostructures on the top electrode via crystallization of organic materials have also been utilized. Anthracene, perylene,[93] copper phthalocyanine (CuPC),[94,95] tris(8-hydroxyquinoline)aluminum (Alq3),[96–98] tetracyanoquinodimethane (TCNQ),[99–101] have been reported to form nanostructure through crystallization and 4,4′-bis(1,2,2-triphenylvinyl)biphenyl (BTPE),[63] 4-(4-(1,2,2-triphenylvinyl)phenyl)-7-(5-(4-(1,2,2-triphenylvinyl)phenyl)thiophen-2-yl)benzo[c][1,2,5]thiadiazole (BTPETTD), tetraphenylethene (TPE),[102,103] 4,7-diphenyl-1,10-phenanthroline (Bphen), N,N′-dicarbazolyl-3,5-benzene (mCP), bathocuproine (BCP)[104,105] have served as light extraction layers of OLEDs. However, crystallization of these materials requires annealing or processing time such as storage in vacuum for several hours. Although TPE has been applied as a light extraction layer of TEOLED using its properties

being crystallized at room temperature,[103] it is not possible to control the surface morphology of TPE nanostructure, and needs to evaluate the performance by applying it to a higher efficiency device. It has been reported that 1,5-diaminoanthraquinone (DAAQ) is also crystallized as nanowires without the need for annealing or any other process.[106–108] While the growth mechanism and electrical properties of DAAQ have been reported, few papers have exploited these characteristics to enhance light extraction.

Here, we report one-step method of fabricating nanowire structures composed of DAAQ for light extraction of TEOLED. DAAQ nanowires were formed in the out-of-plane direction on the Ag thin film, and nanowire pitch, height, and diameter were able to be controlled by the deposition conditions. We fabricated DAAQ nanowires on a red phosphorescent TEOLED with a pixel size of 2 × 2 mm for light extraction. It showed 8.6% enhancement for a narrow full width at half maximum (FWHM) device without distorting the emission spectrum, and 10.6% enhancement for a wide FWHM device. The method is suitable for OLED display because it is simple, vacuum-processable and has mild processing conditions without damaging the device.

3.2 Experimental section

Device fabrication

70 nm-thick prepatterned ITO-coated glass substrates were cleaned successively by dipping in acetone and isopropyl alcohol, followed by boiling in the alcohol. Exciplex based red emitting inverted TEOLEDs with the following structure were fabricated on the substrates: Al (70 nm)/Cs_2CO_3 (1 nm)/2 wt% Cs_2CO_3 doped B3PyMPM (20 or 40 nm)/B3PyMPM (10 nm)/5 wt% Ir(mphmq)$_2$tmd doped NPB:B3PyMPM (30 nm)/NPB (5 nm)/TAPC (60 nm)/ReO_3 (1 nm)/Ag (20 nm). B3PyMPM is bis-4,6-(3,5-di-3-pyridylphenyl)-2-methylpyrimidine; NPB is N,N′-di(naphthalen- 1-yl)-N,N′-diphenylbenzidine; and TAPC is 1,1-bis[4-di(p-toluyl)aminophenyl]cyclohexane. All organic and metal layers were deposited via thermal evaporation at a base pressure $< 5 \times 10^{-7}$ Torr without breaking the vacuum. The total deposition rate was 1 Å/s for each layer, with the exception of the DAAQ nanowire array deposited on the top Ag electrode (5 Å/s for a densely packed DAAQ nanowire array and 1 Å/s for a sparsely packed DAAQ nanowire array). B3PyMPM, NPB, and TAPC were purchased from Nichem; ReO_3 and Cs_2CO_3 were from Sigma Aldrich; Ir(mphmq)$_2$tmd was from Lumtec; and DAAQ was from Tokyo Chemical Industry. An ultraviolet (UV)-curable resin was used to encapsulate the devices with cover glasses in an N_2 filled glovebox.

Characterization of devices and films

Electroluminescence (EL) spectra and intensity in the normal direction were measured with a spectrometer (PR-650, Photo Research) and current density was measured with a programmable source meter (Keithley 2400, Tektronix Inc.). External quantum efficiency (EQE) of the device was calibrated with the measured angular emission pattern. Angle-dependent EL spectra were measured at 5° intervals using a customized rotating stage and a fiber optic spectrometer (S2000, Ocean Optics Inc.). Film transmittance in the normal direction was measured using a UV-vis-near infrared spectrophotometer (Cary 5000, Agilent Technologies). Scanning electron microscope (SEM) images of the films were taken by a MERLIN Compact microscope (Zeiss).

Finite-Difference Time-Domain analysis

A commercial software (FDTD solutions, Lumerical Inc.) was used to calculate the optical effect of the DAAQ nanowire array. The distribution of the nanowire arrays in the calculation follows those in the SEM images. The diameter and tilt angle of DAAQ were randomized in the range of 30 to 50 nm and 0 to 10 degrees, respectively. The refractive index of DAAQ was assumed to be 1.7. A perfectly matched layer (PML) was used as the boundary condition in the z-direction, and a periodic condition was used as the horizontal boundary condition. The calculated width was 2000 nm, and the mesh was divided into 5 nm. The plane wave source had a 612 nm peak wavelength and a 40 nm FWHM, and the simulation structure was glass (n = 1.5) / Ag (20 nm) / DAAQ layer (285 nm). The source was placed at 80 nm below the Ag film. The calculated

transmittances at the wavelength of 612 nm were 23% and 28% for the structures with and without the densely packed DAAQ layer. The transmittances are exactly the same as the experimental values in Figure 3.3 (c), demonstrating the reliability of the calculation.

3.3 Results and Discussion

Figure 3.1 (a) illustrates the formation process of the out-coupling structure on the TEOLED. The nanowire array was fabricated via thermal evaporation of DAAQ onto a completed device at room temperature prior to encapsulation. In other words, the DAAQ nanowire array was formed without breaking the vacuum or any extra patterning processes such as substrate heating, imprinting, and crystallization time. It has been reported that intra- and inter-molecular charge transfer between carbonyl and amine group in DAAQ molecule is the reason for forming nanostructure.[106] Density functional theory (DFT) calculation also shows large partial charges of DAAQ molecule, so DAAQ is advantageous for molecular interactions (see Figure 3.2). As the planar morphology of the OLED stacks was not disturbed during the process, the electrical properties of the OLEDs are not affected. In addition, damages during the fabrication of the light extraction structure could be minimized due to the mild fabrication conditions, i.e., thermal evaporation at room temperature in vacuum. Figure 3.1 (b) depicts the molar extinction coefficient of DAAQ in methylene chloride (MC) and the photoluminescence (PL) spectrum of $Ir(mphmq)_2tmd$. The absorption of DAAQ was only up to a wavelength of 540 nm, and barely overlapped with the emission of $Ir(mphmq)_2tmd$. Thus, absorption loss caused by DAAQ can be neglected. Figure 3.3 (a) and (b) exhibit SEM images of DAAQ fabricated at different evaporation rate of 1 Å/s and 5 Å/s onto the surface of a 20 nm Ag thin film,

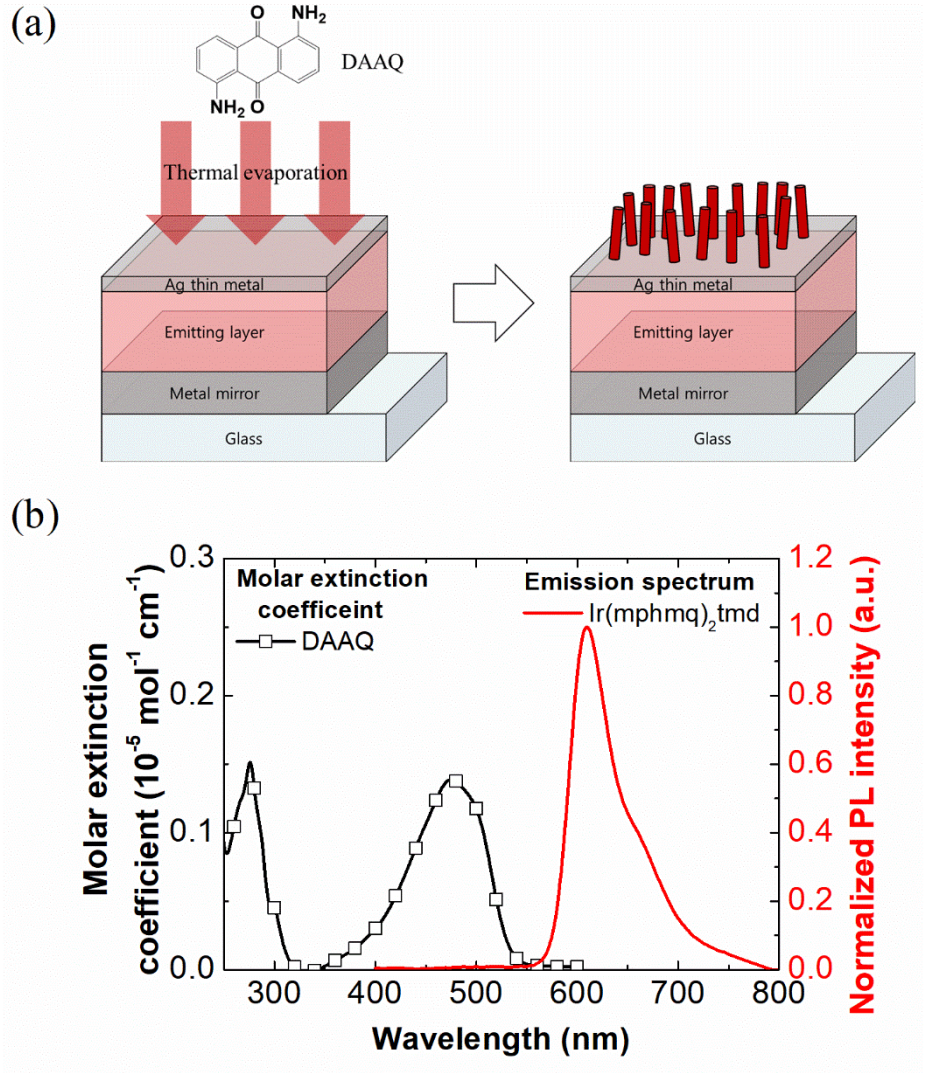

Figure 3.1 (a) Fabrication of 1,5-diaminoanthraquinone (DAAQ) nanowire arrays. The arrays were formed via thermal evaporation of DAAQ onto completed device in vacuum. (b) Absorption spectrum of DAAQ in methylene chloride (10^{-5} M) and photoluminescence spectrum of Ir(mphmq)$_2$tmd red emitting dopant.

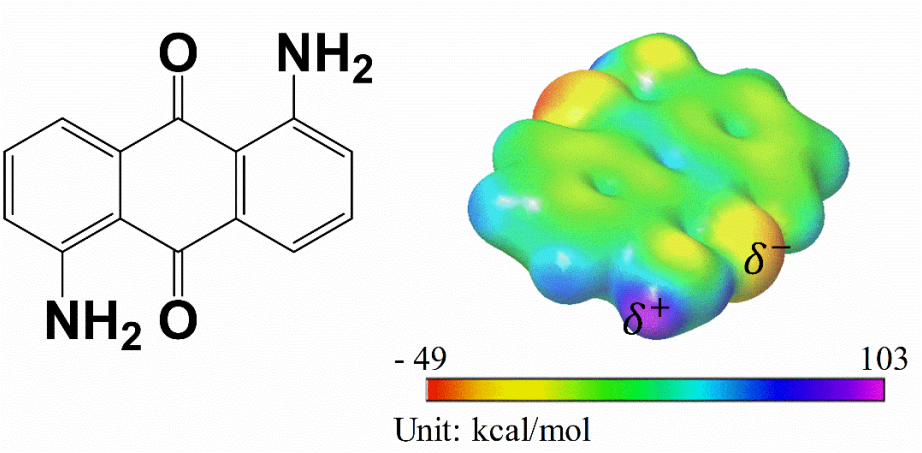

Figure 3.2 Chemical structure and calculated electrostatic potential of DAAQ molecules. Optimization of the molecular structures was demonstrated using B3LYP method and 6-31g** basis set.

respectively. Although the same thicknesses were monitored by a gold-coated thickness sensor, the formed nanowires were different. The nanowire arrays deposited at 1 Å/s were larger in diameter and height than those deposited at 5 Å/s, but the density of nanowires was reduced. The nanowire height was about 500 nm and the radius was in the range of 50-100 nm for 1 Å/s case with a sparsely packed structure. In contrast, 285 nm high wires with a radius of about 30 nm were densely packed when the deposition rate was 5 Å/s. Since DAAQ molecules prefer to grow on initially formed DAAQ seed nanoparticles,[106,107] the evaporation rate is one of the parameters that determines a pitch between nanowires. No further changes were observed to the nanowire arrays as the evaporation rate increased to 9 Å/s (Figure 3.4). Huang et al. reported that the morphology of DAAQ was entangled with the in-plane direction,[107] but in our results, the nanowire with out-of-plane direction was formed. Figure 3.3 (c) is the transmittance of 20-nm-thick Ag films without DAAQ nanowire array, with a sparsely packed DAAQ nanowire array deposited at 1 Å/s, and with a densely packed DAAQ nanowire array deposited at 5 Å/s. The transmittance of the Ag thin film without DAAQ was measured to 25% at 600 nm. The Ag film with the sparsely packed DAAQ nanowire array exhibited a lower transmittance than that of neat Ag film because the nanowire array served as a scattering layer. However, transmittance of the Ag film with the densely packed DAAQ nanowire array was enhanced to 28% around 600 nm wavelength. As DAAQ does not absorb light near 600 nm wavelength, the enhanced transmittance is due to reduced reflection by the DAAQ nanowire

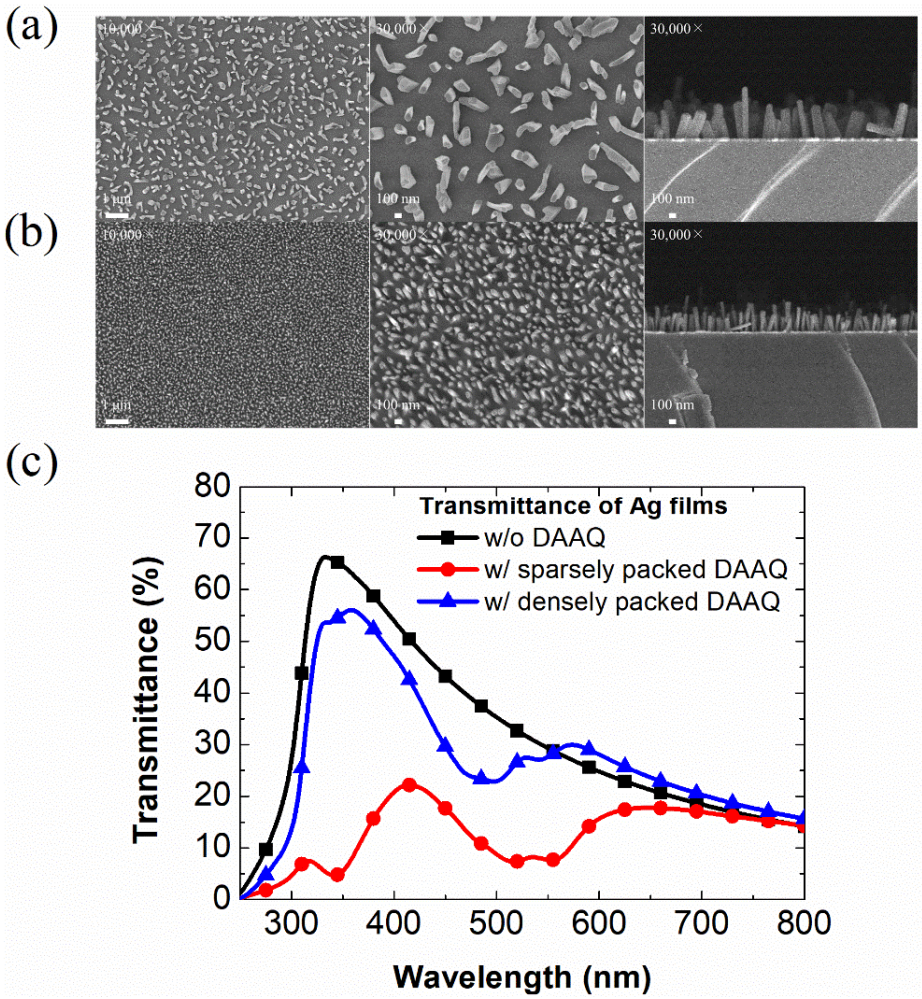

Figure 3.3 Scanning electron microscope (SEM) images of DAAQ nanowire arrays deposited at (a) 1 Å/s and (b) 5 Å/s. The thickness values monitored by quartz thickness sensor were identical. The first two images are top views under different magnification, the third image is a side view. (c) Transmittance of an Ag film without a DAAQ layer, with a layer deposited at 1 Å/s (sparsely packed DAAQ), and with a layer deposited at 5 Å/s (densely packed DAAQ).

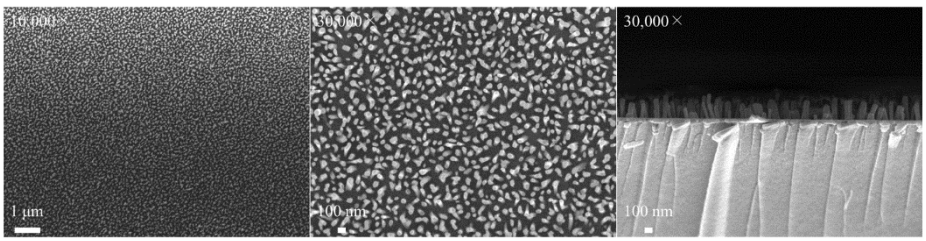

Figure 3.4 Scanning electron microscope (SEM) images of DAAQ fabricated at 9 Å/s at different magnifications: 50× (left), 100× (center), 200× (right).

array. One may consider that the enhancement originates from the effect of the capping layer, i.e., the densely packed DAAQ layer can exhibit the similar optical effects as a planar organic layer due to the effective refractive index by the small pitch between nanowires. To analyze the optical effect of DAAQ layer, the FDTD calculation was performed and the electric field distribution when the planar wave was passing through the layer was simulated. Figure 3.5 depicts the field distribution when a plane wave with a 612 nm peak wavelength and a 40 nm FWHM passes through a 20 nm Ag thin film or a densely packed DAAQ layer, respectively. In the case of Ag thin film, due to the smooth surface, the field distribution was not affected even though the wave passed through the interface, and showed a uniform field distribution. However, in the case of DAAQ, the distribution of the field was influenced by the nanowires and the locally concentrated electric field was observed. Therefore, the working mechanism of DAAQ is different from that of the capping layer. To evaluate its performances in light extraction of the OLED, we fabricated nanowire arrays on a red-emitting TEOLED (Figure 3.6 (a)). The thickness of the electron transporting layer (ETL) was changed to explore the effect of the out-coupling layer according to the electroluminescent (EL) spectrum and angular distribution pattern. DAAQ nanowire arrays were deposited on the semi-transparent Ag electrodes of completed devices by thermal evaporation. The nanowires were fabricated at a deposition rate of 5 Å/s to a height of 285 nm.

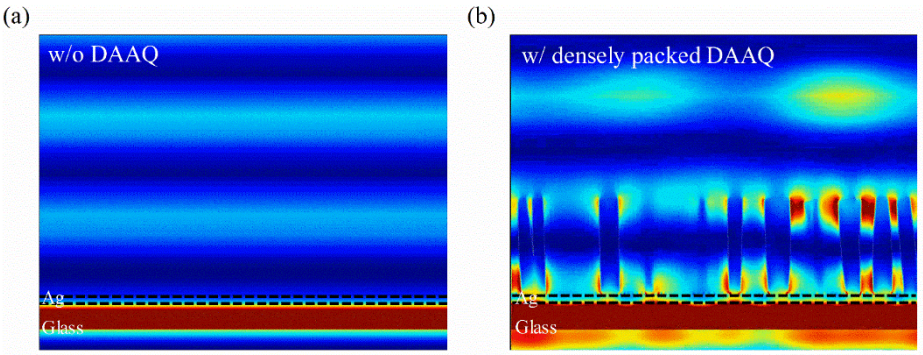

Figure 3.5 Distributions of electric field intensity calculated using the Finite-Difference Time-Domain (FDTD) method. (a) 20 nm-thick Ag film without DAAQ nanowires, (b) 20 nm-thick Ag film with densely packed DAAQ nanowires.

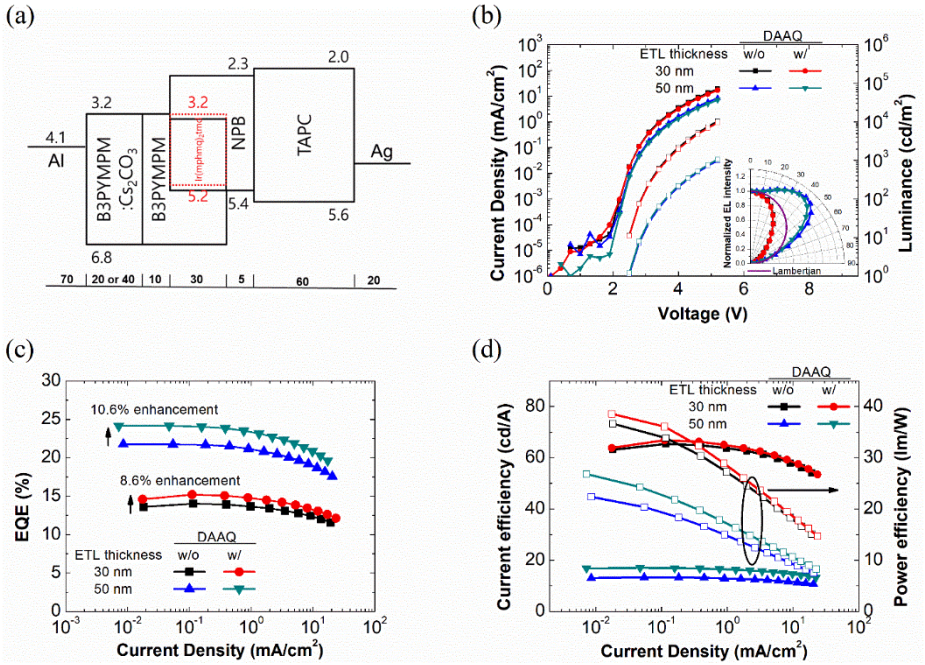

Figure 3.6 (a) Fabricated device structure of exciplex based red emitting inverted TEOLEDs. (b) The current density-voltage-luminance (*J-V-L*) characteristics of devices with and without DAAQ nanowire arrays. Inset: angular emission patterns of the devices. (c) EQEs of the devices as a function of current density. (d) Current efficiency and power efficiency of devices according to the current density.

Figure 3.6 (b) shows the current density-voltage-luminance (*J-V-L*) characteristics and angular distribution of the TEOLEDs with or without the DAAQ nanowire arrays. The DAAQ deposited devices exhibited the same current density as the reference devices, as expected. The nanowire array did not affect the angular distribution of a device with a 30-nm-thick ETL (device A), and only slightly changed the angular distribution of a device with a 50-nm-thick ETL (device B). The maximum EQE of device A increased to 15.2% from 14%, and that of device B increased to 24.1% from 21.8%, as seen in Figure 3.6 (c). The enhancement ratio was 8.6% for device A and 10.6% for device B, respectively. The current efficiencies (CE) and power efficiencies (PE) of the devices as a function of the current density are depicted in Figure 3.6 (d) and the DAAQ deposited devices showed higher efficiencies than the reference devices. When the light extraction layer is applied to the TEOLEDs, there is a change in radiative decay rate and optical interference effect due to the short distance between the out-coupling and emitting layers. This characteristic can be a problem because it may cause unwanted distortion in emission spectrum of the device.[109] Figure 3.7 (a) and (b) show the EL spectra of device A and B by viewing angle, respectively. The peak wavelength and FWHM of the EL spectrum of device A with a DAAQ layer were similar to those of the reference device. The EL intensity was further enhanced above 50 degrees, which improve the EQE of device A with the DAAQ array. On the other hand, for device B, the emission spectra changed significantly according to the viewing angle due to the strong cavity effect.

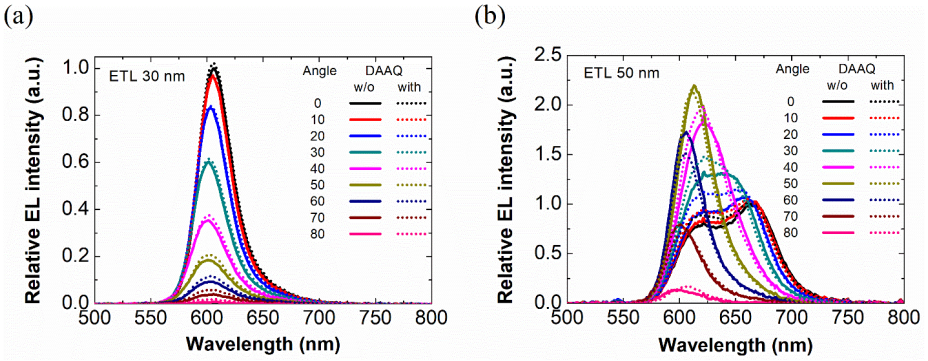

Figure 3.7 Electroluminescence spectra of devices by viewing angle. (a) 30 nm-thick ETL, (b) 50 nm-thick ETL.

In addition, as the DAAQ layer affected the cavity structure of device B, EL intensity increased mildly to around 620 nm wavelength, but the emission spectra were similar to those of the reference device. Since the out-coupling layer was located outside the OLED stack sandwiched between two highly reflective metal electrodes, the emission spectra of the out-coupled device was changed less from those of the reference device. Therefore, DAAQ nanowire array is a light extraction structure that does not distort the emission characteristics of the reference device.

3.4 Conclusion

In summary, we have successfully integrated spontaneously formed organic nanowire arrays to red inverted TEOLEDs to enhance the light extraction efficiency. Thermally evaporated DAAQ crystallized immediately at room temperature and formed nanowire arrays without any need for patterning processes. The density, diameter, and height of nanowire arrays could be controlled by controlling the deposition rate and thickness. The electrical properties of TEOLEDs were not affected by the DAAQ layers. The efficiency of TEOLEDs was improved by 8.6% for narrow FWHM device and 10.6% for wide FWHM device by the light extraction layer, respectively. In addition, the layer did not distort emission properties of the reference device. This method is useful for OLED displays because it is simple, vacuum-processable, and does not compromise device lifetime or the emission spectrum.

Chapter 4. Via Hole Patterning of Light Extraction Layer for Electrical Connection

4.1 Introduction

Organic light-emitting diode (OLED) displays have a potential of excellent color quality, flexibility and power efficiency compared to LCDs. The efficiency of OLEDs has significantly improved during the past few decades, reaching an external quantum efficiency (EQE) of over 30% in recent years without any extra light extraction layers.[12,22,66,110–117] However, over 60% of generated light is still confined in OLEDs as substrate modes, waveguide modes in indium tin oxide (ITO) and organic layers, and surface plasmon polariton (SPP) modes. Various external structures, such as micro-lens arrays[35,84,118], roughed surfaces[119], and internal structures such as low index layers[120,121], photonic crystals[122,123], high refractive index substrates[36,124], Bragg gratings[44,74,125], randomly dispersed nano-pillar arrays[30,126], nanoparticles with a thin electrode[127], moth-eye structures[55,128] and metal nanoclusters[129], have been integrated with OLEDs to extract confined light.

For active matrix OLED (AMOLED) display, each OLED pixel is controlled by thin film transistor (TFT) and it is able to achieve high efficiency and resolution than passive matrix method. For separating OLED and TFT spatially, there is a passivation layer between OLED electrode and TFT drain electrode and they are connected by an electrical channel, which is called via hole. The

via hole is formed by etching method, like dry or wet etch. Because internal light extraction layers are usually fabricated beneath OLED electrode, it is necessary to pattern via holes in the internal light extraction layers to connect the electrode of OLED with that of TFT on the backplane for practical application. Therefore, the degree of being patterned, which is called the patternability, is a critical issue for the light extraction layer. Generally, the internal light extraction layers consist of two materials with different refractive indices, so good patternability of the layers is not guaranteed with matched etch selectivities. To the best of our knowledge, there have been no reports on concerning the patternability issue of the light extraction layer.

In this report, we developed a wet etching process for via hole fabrication in a random scattering layer (RSL) and demonstrated OLEDs on the patterned out-coupling layer with low leakage current and good light extraction efficiency.

4.2 Experimental section

Figure 4.1 shows the fabrication process for via holes and the OLED device structure developed to demonstrate the patternability of the RSL. The device structure is a simplification of a display panel structure. The OLEDs obtain their electrical signal from a back plane consisting of TFTs and capacitors through the via hole. The pad ITO electrode with a thickness of 150 nm on a glass substrate represents the drain part of the TFT. The RSL and OLEDs were fabricated sequentially on the pad ITO electrode. The RSL was composed of SiO_x randomly dispersed nano pillars (50–700 nm in diameter and about 350 nm in height), called random nano scatter (RNS) in a TiO_2 layer (refractive index n = 2.0). The thickness of the RSL was about 700 nm, with a surface roughness of ~1 nm. A detailed fabrication process for the RSL layer is described in reference[130].

Photolithography was used to fabricate via holes in the RSL on the ITO electrode. First, photoresist solution was coated on the RSL and the via hole pattern was photolithographically defined using a MA6 mask aligner (Karl Suss). After developing the pattern, a circular via hole pattern of the photoresist which had the diameter of 100 μm was formed, and the photoresist pattern was used as the etch mask for the RSL. Various etchants were tested for patterning the via holes under room temperature. After these steps, the photoresist was removed using a photoresist stripper and the substrate including the via hole patterns in the RSL was cleaned with acetone and isopropanol.

On the prepared substrates, OLED devices, composed of IZO (150 nm)/TAPC (40 nm)/HAT-CN (5 nm)/TAPC (40 nm)/HAT-CN (5 nm)/TAPC (40 nm)/HAT-CN (5 nm)/TAPC (40 nm)/TCTA (10 nm)/TCTA:B3PYMPM:$Ir(ppy)_2acac$ (0.46:0.46:0.08 in weight ratio, 30 nm)/B3PYMPM (50 nm)/LiF(0.7 nm)/Al (115 nm), were fabricated, where TAPC, HAT-CN, TCTA, B3PYMPM, and $Ir(ppy)_2acac$ stand for 1,1-bis-(4-bis(4- methyl-phenyl)-amino-phenyl)-cyclohexane (TAPC), 1,4,5,8,9,11-hexaazatriphenylene hexacarbonitrile (HAT-CN), 4,4',4''-tris(N-carbazolyl)-triphenylamine (TCTA), bis-4,6-(3,5-di-3-pyridyl- phenyl)-2-methylpyrimidine (B3PYMPM), and bis(2-phenylpyridyl) iridium(III) acetyl- acetonate ($Ir(ppy)_2acac$), respectively. A multi-hole injection layer was used for stabilizing current injection. The current density–voltage–luminance (*J–V–L*) characteristics of the devices were measured using a Keithley 2400 semiconductor parameter analyzer and a Photo Research PR-650 spectrophotometer. The angle-dependent electroluminescence (EL) intensity was recorded using a silicon photodiode (Ocean Optics) and the out-coupling efficiency was calibrated using a 6-inch integrating sphere (Labsphere) at 1 mA/cm^2 current density.

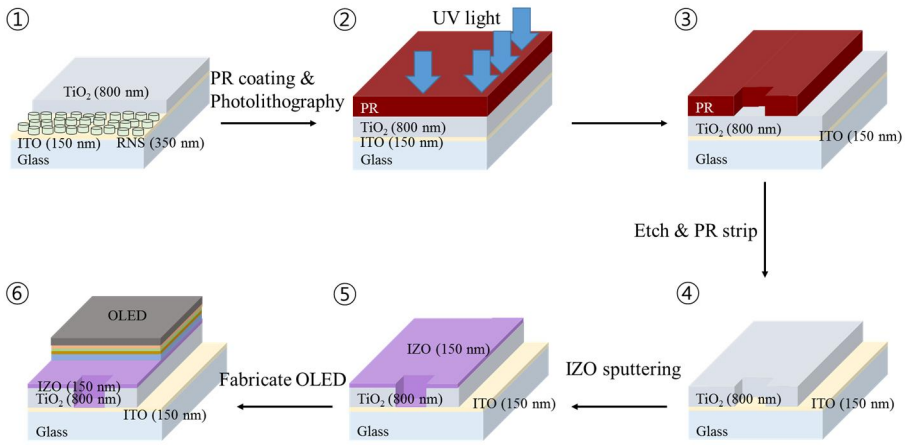

Figure 4.1 Steps for fabrication of an OLED device including the RSL with via holes: (1) fabricating a random scattering layer (RSL) on a 150 nm indium tin oxide (ITO) substrate, (2) depositing photoresist on RSL by spin coating, (3) and (4) making via hole patterns by photolithography and etching, (5) electrical contact between the pad ITO electrode and upper layer using sputtered indium zinc oxide (IZO), (6) fabricating organic light emitting diode (OLED) on IZO.

4.3 Results and Discussion

One of the most important fabrication steps for via holes is to find a proper etchant showing similar etching selectivity of two different materials (in this case, SiO_x and TiO_2, of which the RSL is composed). There is a previous report that the layer which is composed of SiO_2/TiO_2, has an undercut problem when it is etched by wet etchant,[131] and it is hard to find the proper etchant in our knowledge. So, it is necessary to develop a new etchant which has similar etching selectivity to above two materials. Hydrofluoric acid (HF) is a good etchant for SiO_x and TiO_2, and hence was a natural choice for the first trial. However, 49% HF solution could not be used because the undercut problem was shown at etched samples (Figure 4.2 (a)). No matter how etchant was diluted, the undercut was appeared, and after stripping process, the pattern was formed which was about 30 ㎛ larger than photolithographically defined area (Figure 4.2 (b)). The result is caused by the etching rate of TiO_2 by HF is much lower than that of SiO_x. H_2SO_4 or H_3PO_4 added BOE was tested to get a balanced etching rate between SiO_x and TiO_2 by enhancing the etching rate of TiO_2.[132] The H_2SO_4 mixed BOE turned out to have too high a reactivity to dissolve out the photoresist. In contrast, the H_3PO_4 mixed BOE etchant showed drastically improved etching characteristics, resulting in smooth etched patterns without etched gaps between the TiO_2 planarization layer and the pad ITO electrode (Figure 4.3). The mixing ratio of BOE and H_3PO_4 was further

optimized to obtain smooth via holes with a proper slope for good electrical connection.

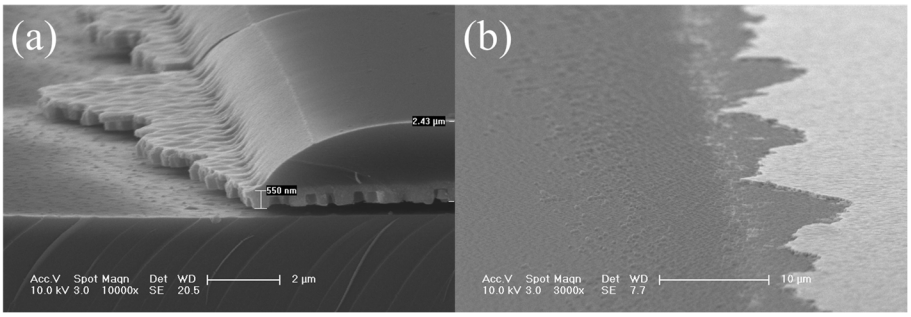

Figure 4.2 Scanning electron microscopy (SEM) images of the etched surface under 49% HF solution. The undercut is observed at (a) before PR stripping. (b) After PR stripping, the undercut area is also stripped away and non-linear edge is formed. ((a) : $\times \mathbf{10000}$; (b) : $\times \mathbf{3000}$).

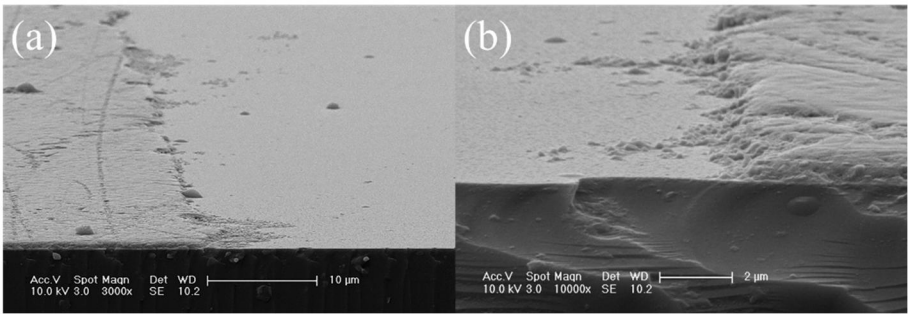

Figure 4.3 SEM images of the etched surface under a 0.5 volume ratio of H_3PO_4 to BOE for 1 min with different scales. Upper layer is the planarization layer and bottom layer is the pad ITO electrode ((a) : $\times \mathbf{3000}$; (b) : $\times \mathbf{10000}$).

The etching height change depending on the H_3PO_4 ratio is shown in Figure 4.4. The RSL was insufficiently etched by pure BOE even after 2 min dipping because the etching rate of TiO_2 was too low. As the volume percentage of H_3PO_4 was increased, the overall etch rate also increased, and 2 min were required to etch the 800 nm-thick RSL with a 0.3 volume ratio of H_3PO_4. The best conditions for formation of a smooth etch surface and a gentle slope were a 0.5 volume ratio of H_3PO_4 to BOE (0.5 etchant). When the volume ratio of H_3PO_4 was over 0.5, the slope of the etch slope was too steep to form an electrical connection between the upper and lower layers. Because H_3PO_4 etch TiO_2 very slowly is reported (1.5 nm/min at 80 °C)[133] and that phenomenon coincides with our experiment, it is hard to say that the undercut problem is solved by matching etch rate. However, as ratio of H_3PO_4 goes higher, enhanced total etching rate is observed clearly. In an aspect of the viscosity of mixed solution, it was more viscous depending on the percentage of H_3PO_4, and a viscous etchant might reduce undercutting. There needs more study on the mechanism of improved undercut when added H_3PO_4 to BOE.

Via hole patterning was performed by using previously developed etchant. Figure 4.5 shows scanning electron microscopy (SEM) images of a via hole fabricated using the 0.5 etchant with a diameter of 100 μm after sputter deposition of a 150 nm-thick IZO layer. As the etched surface didn't look like a steep but a smooth hill, the sputtered IZO was able to follow up the surface without being torn. It means that the via hole will work normally when the electrical signal is injected to bottom pad ITO.

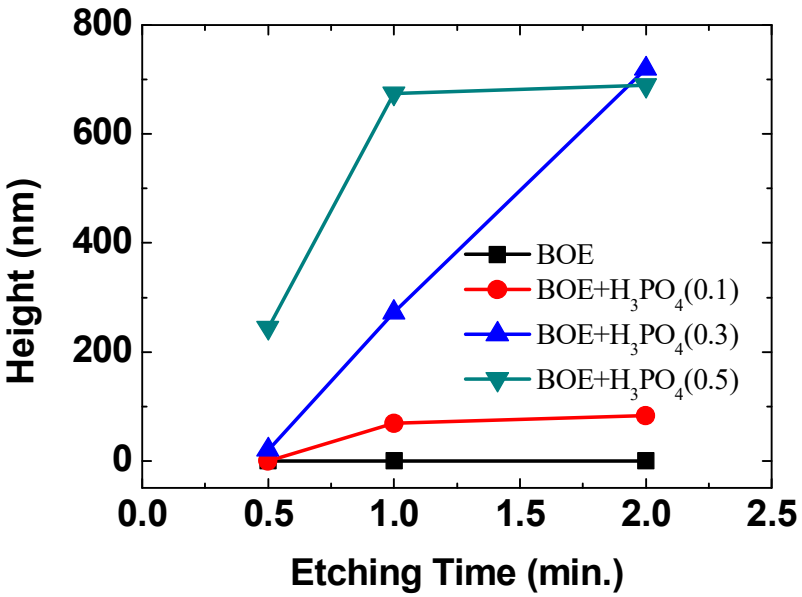

Figure 4.4 Etch height of the RSL depending on the volume ratio of H_3PO_4 to BOE.

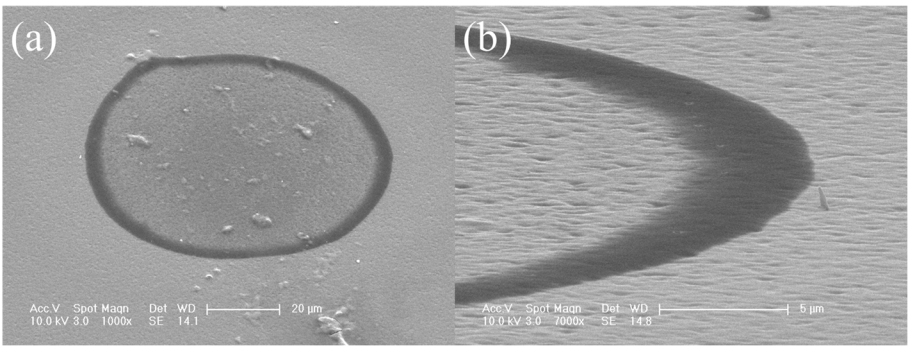

Figure 4.5 SEM images of via hole with 150 nm sputtered indium zinc oxide (IZO). The via hole has a diameter of 100 **µm** and is formed under a 0.5 volume ratio of H_3PO_4 to BOE conditions over 1 min with different scales ((a) : $\times$ **1000**; (b) : $\times$ **7000**).

For evaluating electrical operation, we fabricated OLED devices on the RSL substrate with the via hole. The thicknesses of the organic layers were optimized to maximize the air mode of OLEDs without the out-coupling layer. Figure 4.6 (a) shows the *J–V–L* characteristics of the OLEDs. The device with the patterned RSL showed a similar *J–V* curve, with low leakage current, to the device without the RSL, indicating that the processes used for patterning the via hole maintained smooth surfaces. In addition, both devices were turned on at the same voltage, 2.4 V, demonstrating that no electrical variation was induced by the via hole patterning. Figure 4.6 (b) shows external quantum efficiencies (EQEs) of the OLED devices. The maximum EQE of the OLED without the RSL layer was 21.7%, very close to the theoretically calculated maximum achievable EQE of 22%; this indicates that the charge balance in the OLEDs was good. The EQE of the OLED with the patterned RSL was 32.7% measured using the integrating sphere at 1 mA/cm^2, corresponding to an enhancement of 50.7% (Figure 4.6 (c)). We reported the experimental results for light extraction effects of the RSL without the via hole[31], and the EQE enhancement of the previous study was similar to that of the present study. This indicates that overall processes for fabricating the via hole were not damaging to the optical characteristics of the RSL. The current efficiencies and the power efficiencies of the device with the RSL were also enhanced by 31.2% and 56.7%, respectively (current efficiencies; from 74.3 cd/A to 97.5 cd/A and power efficiencies; from 89.0 lm/W to 139.5 lm/W, figure 4.6 (d)).

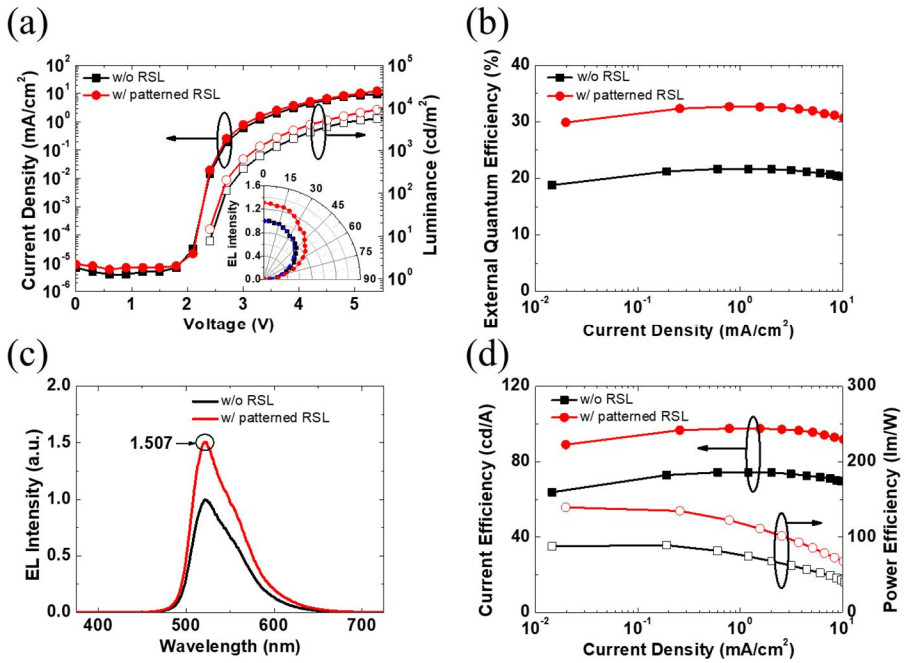

Figure 4.6 (a) Current density–voltage–luminance (*J–V–L*) characteristics of the devices. The black line shows the device without the RSL and the red line indicates the device with the RSL; inset shows angular electroluminescence (EL) measurements (The blue line is the Lambertian pattern.). (b) External quantum efficiencies (EQEs) against current density of the device without the RSL and the device with the RSL. (c) Electroluminescence (EL) spectra of OLEDs measured in the integrating sphere at 1mA/cm^2. (d) Current efficiencies (left) and power efficiencies (right) against current density of the device without the RSL and the device with the RSL.

4.4 Conclusion

A suitable etchant for an internal light extraction layer composed of SiO_x and TiO_2 was developed to fabricate via holes for application in OLED displays. The via holes fabricated using a 0.5 volume ratio of H_3PO_4 to BOE showed excellent characteristics for the OLEDs with them. The low leakage current level and similar *J-V* characteristics to the reference device were shown on the via hole patterned devices, indicating that electrical characteristics were not affected by the fabrication of the via hole. In addition, the out-coupling efficiency of the RSL and via hole OLED device was enhanced by 50% compared to that of the OLED without the RSL. These results are very close to those reported in the previous study[130], indicating that the overall processes do not damage to the electrical and optical characteristics of the RSL.

Chapter 5. Improving Operation Lifetime of OLEDs using Spontaneous Orientation Polarization

5.1 Introduction

Organic light-emitting diodes (OLEDs) are used in a wide range of fields from displays to potentially lightings due to its luminous properties and thin panel thickness. However, despite the numerous advantages of OLEDs, the operation lifetime issue is still being raised. Even now, efforts are being made to increase the lifetime of OLEDs, and the methods of controlling exciton-polaron interaction inside the emitting layer (EML) such as bipolar host,[134–139] hole transporting management,[140] quenching layer,[141] interlayer reducing deep traps,[142] graded doping concentration,[143] high doping concentration,[144] hot excited state management,[145] radical ion management[146] have successfully extended the lifetime of the device. Among these approaches, in particular, mixed-host system such as exciplex was considered as a conducive way to increase the lifetime of the device due to broad recombination zone and reduced polaron-induced quenching. However, even in exciplex host system, the recombination zone was reported to be split at each interfaces,[147] and this effect promotes local degradation of EML. Thus, the lifetime of the device can be further improved if the distribution of excitons in EML can be controlled. In addition, as OLED is composed of several layers such as hole transporting layer

(HTL) and electron transporting layer (ETL) and the accumulation of irreversible degraded products of these layer shorten the lifetime of device,[148–150] stability of organic materials is also one of the factors related to the device lifetime.[139,151] Especially, since ETL requires conflicting characteristics such as high electron mobility and high triplet level,[152] it is rather tough to achieve material stability while meeting the above requirements. Therefore, it is important to develop a method that manipulates the exciton distribution and improves the stability of ETL in terms of the device structure, not the modification of materials.

Meanwhile, after it was revealed that an interfacial charge exists at the interface of NPB/Alq3 in a bilayer device,[153] several electron transporting materials (ETMs) were found to have spontaneous orientation polarization (SOP) properties.[154] In addition, it was observed that the direction of polarization was different for each materials, and the charge injection characteristics were changed according to the polarization direction.[155] Kinjo et al. reported that vacuum level shift occurs due to the interfacial charge of the SOP molecule, and this property affects the charge injection from the electrode to the transporting layer.[156–158] Besides, the PDM alignment also appeared in the host-guest system, and Jäger et al. demonstrated that SOP properties of Alq_3 appeared even when Alq_3 was doped into the NPB host.[159] Additionally, the density of the interfacial charges varied with the doping ratio, and larger polarity was observed than that of the neat Alq_3 film. Thus, the interfacial

charge density can be controlled by the ratio of SOP molecules to host molecules. Although the effects of polarization on electrical properties of the device have been reported, there are few reports on the effects of polarization on operation lifetime of device.

In this report, we demonstrated that the operation lifetime of the device and the stability of the ETL can be enhanced by the introduction of polarization. We co-deposited bis(2-methyl-8-quinolinolato)(4-phenylphenolato)aluminum (BAlq), which was reported to have the property of orientation polarization,[154,160] and (1,3,5-triazine-2,4,6-triyl)tris(benzene-3,1-diyl)tris(diphenylphosphine oxide) (PO-T2T) to the electron transporting layer (ETL) of a red exciplex based OLED.[161] The degree of polarization was changed according to the volume ratio of BAlq, and the largest polarization was exhibited when BAlq was mixed at 50% by volume in ETL. In addition, the 50 vol.% BAlq doped device exhibited 3.5 times enhanced LT_{90} lifetime at 5,000 cd/m^2 and lower variation in applied voltage than the reference. As BAlq does not absorb the emission of the exciplex host or the emitting dopant and does not form any complex with them, this effect is not due to the effect of the additional quenching layer. Besides, the enhanced lifetime is not also due to the stability of BAlq since BAlq has weak bond dissociation energy in the cation state (1.78 eV) and has shallow HOMO level (5.9 eV) than PO-T2T (7.5 eV). Also, we observed the changes in device characteristics depending on the position of the BAlq mixed layer, and the operation stability was greatly

improved only when the polarized layer existed between the EML and ETL. To investigate the origin of this effect, the photoluminescence (PL) intensity of the degraded device's EML was measured, and the degree of electroluminescence (EL) degradation and PL degradation was different in the reference device, while it was same in the BAlq doped device. This means that the EML was uniformly degraded in the BAlq doped device and it is postulated the repulsive force by negative interfacial charge broaden the recombination zone in EML. Furthermore, the electric field is less applied to the ETL because of the interfacial charge. As a results, it suppresses the hole injection to ETL through tunneling, thereby lowering the variation in applied voltage. This method is very useful because there is no need to modify the structure of device for enhancing the operation stability.

5.2 Experimental section

100 nm-thick prepatterned ITO-coated glass substrates were cleaned successively by dipping in acetone and isopropyl alcohol, followed by boiling in the alcohol. Before deposition, the ITO substrate was treated by UV-O_3 treatment for surface cleaning and better hole injection. Exciplex based red emitting OLED were fabricated with the following structure: 1wt% MoO3 doped TAPC (40 nm)/TAPC (30 nm)/NPB (10 nm)/7 wt% Ir(mphmq)2tmd doped NPB:PO-T2T (5:5 in molar ratio, 30 nm)/electron transporting layer (60 nm)/LiF (0.5 nm)/Al (100 nm). PO-T2T is (1,3,5-triazine-2,4,6-triyl)tris(benzene-3,1-diyl))tris(diphenylphosphine oxide); NPB is N,N′-di(naphthalen- 1-yl)-N,N′-diphenylbenzidine; and TAPC is 1,1-bis[4-di(p-toluyl)aminophenyl]cyclohexane. All layers were deposited via thermal evaporation at a base pressure $< 5 \times 10^{-7}$ Torr without breaking the vacuum and the total deposition rate was 1 Å/s for each layer. PO-T2T and TAPC were purchased from Shine Materials; MoO3 and Ir(mphmq)$_2$tmd were from Lumtec; and NPB was from Nichem. An ultraviolet (UV)-curable resin was used to encapsulate the devices with getter attached cover glasses in an N_2 filled glovebox. Electroluminescence (EL) spectra and intensity in the normal direction were measured with a spectrometer (PR-650, Photo Research) and current density was measured with a programmable source meter (Keithley 2400, Tektronix Inc.). The capacitance of the device was measure by impedance spectroscope (Analytical moduLab XM, Solartron). The operational

stability was measured by lifetime measurement system with constant temperature and humidity (Polaronix M6000T). The bond dissociation energy was calculated using the LACV3P** basis set and B3LYP functional by Schrödinger Materials Science suite.

5.3 Results and Discussion

Figure 5.1 (a) and (b) show the band structure of OLED without and with polarization of ETL, respectively. If there is no interfacial surface potential in any layer, charges are injected and recombined at the voltage above the built-in voltage (V_{bi}). On the other hand, if there is a negative surface potential between ETL and EML, injection of holes occurs at the voltage before V_{bi} due to the vacuum level shift. As predicted in the band diagram, we speculated that the field applied to the ETL would be reduced in the polarized ETL case, and this effect would suppress hole injection to the ETL through tunneling. In addition, the presence of surface charges can induce modifications in the recombination zone due to the coulomb interaction with charge carriers. By the above changes, the operation stability of device can be improved.

In order to demonstrate the concept, SOP molecule was doped into ETL of exciplex-based red emitting OLED. Figure 5.2 (a) exhibits schematic diagrams of the device structure and the chemical structures of organic materials used in this report. Several ETMs such as Alq_3,[155] BCP, TPBi, OXD-7,[162] Bpy-OXD, and Bphen[160] have been reported to have SOP properties, but we used BAlq as a SOP molecule because BAlq has a higher LUMO level than PO-T2T, which does not act as an electron trap and does not form a complex with EML components. Figure 5.2 (b) depicts the absorbance of BAlq film and the PL spectra of exciplex host and red dopant. The absorbance of BAlq did not overlapped with the emission of exciplex and

emitting dopant. Therefore, as energy transfer between EML and BAlq is difficult to occur, the effect of polarization can be considered as a major origin for variations in device stability.

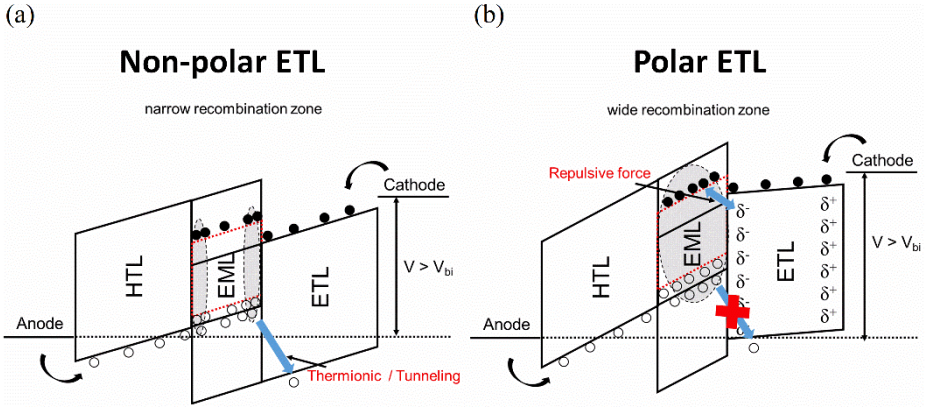

Figure 5.1 Schematic band diagrams of exciplex-based OLEDs used in this report according to the polarity of electron transporting layer (ETL). (a) is non-polar ETL case, and (b) is polar ETL case. Hole transporting layer (HTL) and emitting layer (EML) are assumed to have no polarity.

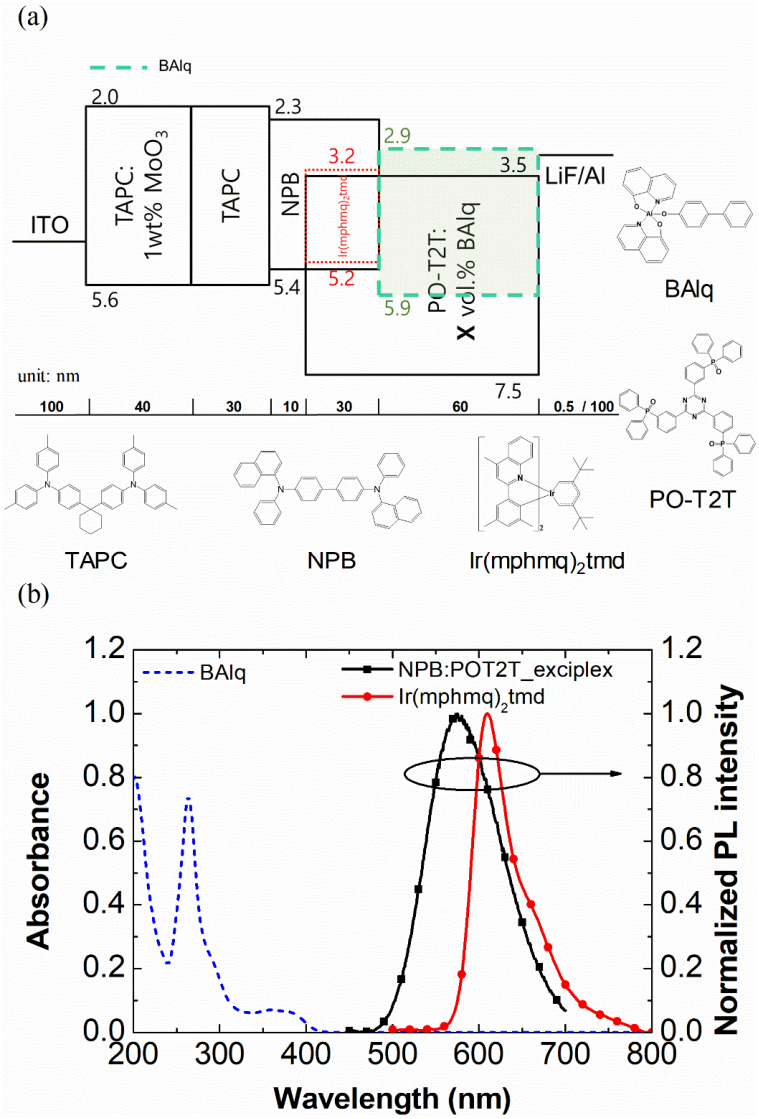

Figure 5.2 (a) Fabricated device structure of exciplex based OLEDs, and chemical structures of molecules. (b) Absorbance of BAlq thin film and photoluminescence spectra of NPB:POT2T exciplex and Ir(mphmq)$_2$tmd red emitting dopant.

Figure 5.3 (a) shows the current density-voltage-luminance (*J-V-L*) characteristics of the devices with different volume ratio of BAlq. As the volume ratio of BAlq increased, current density and luminance of the device decreased, and neat BAlq ETL device (100 vol.%) showed the lowest value. Since BAlq has low electron mobility (5×10^{-6} $cm^2/V \cdot s$)[163,164] than that of PO-T2T (1×10^{-4} $cm^2/V \cdot s$),[165] reduced current density is due to the difference in electron mobility between BAlq and PO-T2T. Figure 5.3 (b) exhibits the external quantum efficiencies (EQEs) of the BAlq mixed devices and the EQEs decreased as the ratio of BAlq increased. This is also due to the decreased electron mobility of the mixed ETL. As the mobility of the mixed ETL decreases, the position of the recombination zone will gradually be located toward the ETL. The optical simulation using a classical dipole model[72] exhibits that the efficiency decreases as the recombination zone is placed toward the ETL (Figure 5.4). Although the EQE was decreased by BAlq doping, the decrement was not large, from 22.9% (0 vol.%) to 20.0% (60 vol.%) at 1000 cd/m^2. It means that no additional quenching path is formed by BAlq doping. No other emission was observed except for the red emitting dopant at 5,000 cd/m^2 (Figure 5.5) and therefore, unintended energy transfers or recombination at BAlq did not occur. Figure 5.3 (c) is the capacitance-voltage (C-V) characteristics of the devices. There were two plateau on the C-V curve due to polarization. The transition voltage (V_{tr}) where the hole injection occurred was changed according to the composition of ETL. According to the equation introduced by Brütting et al., the interfacial

charge density between EML and ETL can be obtained by the following equation: $\sigma_{if} = \frac{C_{ETL}}{A}(V_{tr} - V_{bi})$.[166] Here, σ_{if} is interfacial charge density, C_{ETL} is capacitance of the ETL, A is the pixel area, and V_{bi} is the built-in voltage. Since the pixel area (4 mm^2), thickness of ETL, and V_{bi} of the devices are the same, the interfacial surface charge density can be expressed by V_{tr}. Therefore, it has a global maximum interfacial charge density at 50 vol.% and this value is larger than that of neat PO-T2T ETL device and neat BAlq ETL device. The origin of this phenomenon is postulated to have the preferred direction of PDM due to the dipole-dipole interaction between SOP molecules and the interaction with the surface molecules of the sublayer.[159] To evaluate the correlation between the polarization of the ETL and the lifetime of the device, the normalized EL decay curves as a function of operating time was measured at 5,000 cd/m^2 (figure 5.3 (d)). Since only the ETL side was modified, the variation in device lifetime can be interpreted as a result of modified ETL. As the ratio of BAlq increased, the operating lifetime using LT_{90} was also enhanced, increasing from 61 hours (0 vol.%) to 218 hours (50 vol.%), and the mixed ETL devices were found to be stable compared to the neat PO-T2T ETL (0 vol.%) and neat BAlq ETL (100 vol.%) devices. In addition, the variations in applied voltage (ΔV) were also reduced in the case of mixed ETL, which means that the material degradation of the ETL was suppressed effectively. This increased stability does not come from

the material stability or hole blocking property of BAlq since BAlq has weak bond dissociation energy in the cation state (1.78 eV) and has shallow HOMO level (5.9 eV) than PO-T2T (7.5 eV). The enhanced stability is supposed that the reduced electric field of ETL by polarization suppress the hole injection through tunneling. Therefore, the interfacial charge existing in the ETL can improve hole blocking properties. However, the 60 vol.% device had the largest variation in applied voltage, and had the shorter operation lifetime than that of the 50 vol.% device. It is due to the position of recombination zone and the weak hole blocking characteristics of BAlq. As the ratio of BAlq increases, it is obvious that recombination will mainly occur in the vicinity of ETL because of the BAlq's low electron mobility. In addition, BAlq also has a shallow HOMO level compared to PO-T2T, which weakens the hole blocking properties of the ETL by thermionic injection. As a result, the degradation of the EML/ETL interface was promoted, shortening the operation lifetime and increasing the applied voltage. However, even in 60 vol.% BAlq doped device, it still shows a longer lifetime than neat PO-T2T and neat BAlq cases, suggesting that there are additional factors to enhance the stability.

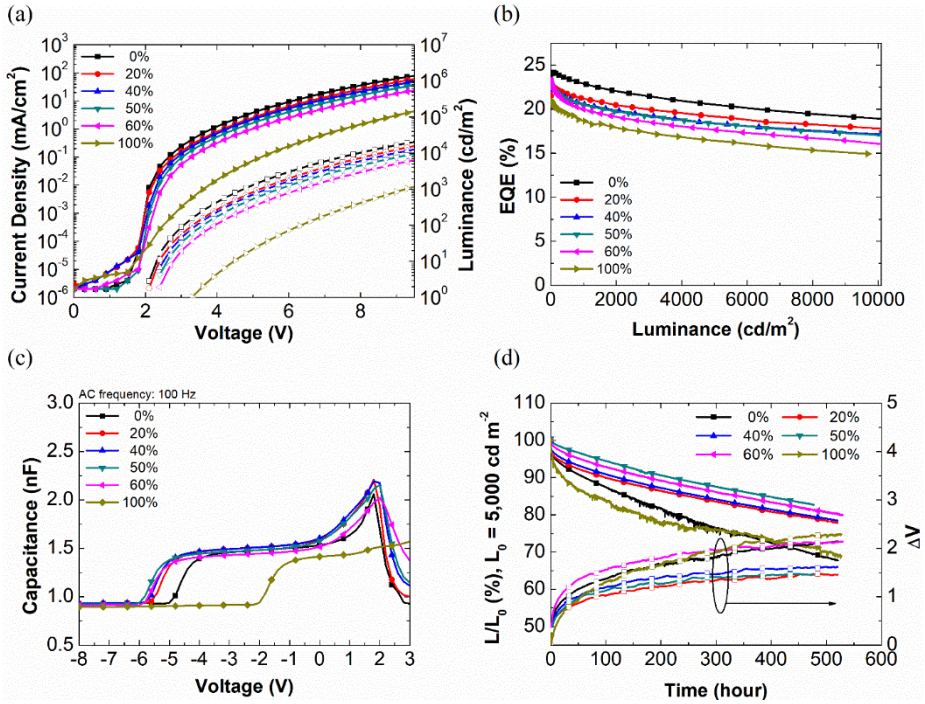

Figure 5.3 (a) The current density-voltage-luminance (*J-V-L*) characteristics of devices according to vol.% BAlq of ETL. (b) EQEs of the devices as a function of luminance. (c) Capacitances of the devices as a function of voltage. (d) EL decay curves of the BAlq mixed OLEDs as a function of operational time at an initial luminance (L_0) of 5,000 cd/m^2.

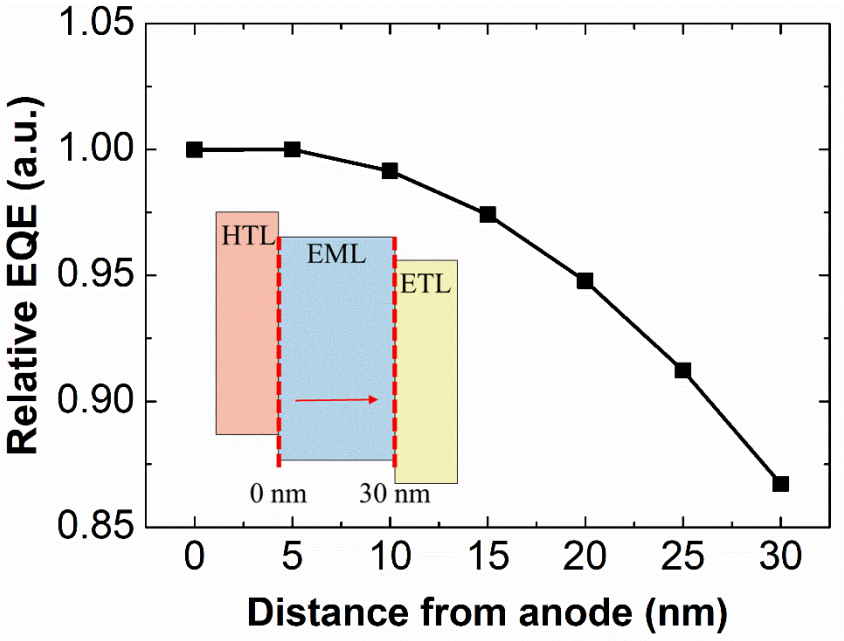

Figure 5.4 Calculated EQEs as a function of the position of recombination zone in emitting layer (EML). As the position of the recombination zone gradually move toward the ETL, the calculated results exhibit that the efficiency decreases.

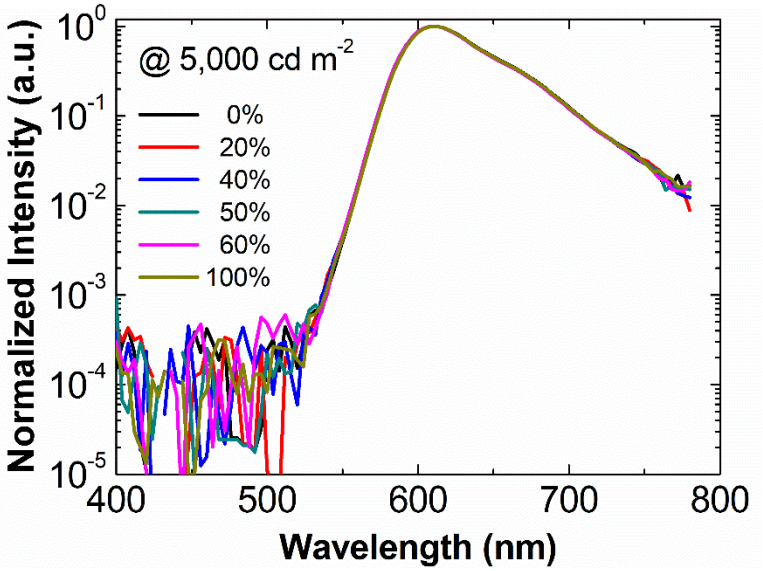

Figure 5.5 Electroluminescence (EL) spectrum of the devices at 5,000 cd/m^2.

No other emission was observed except for the red emitting dopant.

To verify the additional factor, variations in efficiency roll-off, EL spectrum, and transient EL decay between fresh and degraded device were observed depending on the ETL conditions (Figure 5.6). The degraded device exhibited reduced roll-off tendency, same EL spectrum peak, and same exciton lifetime compared to the fresh device. These results showed the absence of additional quenching paths such as exciton-exciton annihilation, exciton-polaron quenching, and implied that the decreased luminance of device is caused by reduced quantum yield of emitter. Figure 5.7 showed the PL intensities of EML between fresh device and degraded device depending on the ETL conditions. The EML was excited using a 405 nm peak wavelength laser which is not absorbed by the transporting layers, and the volume ratio of BAlq was 50 vol.%, which is the condition with the longest lifetime. The ratio of degraded device's EL intensity was 59% compared to the fresh device in case of neat PO-T2T ETL condition (0%). However, PL intensity of the degraded device showed 84% compared to the fresh device, which was less than the deviation of EL intensity. On the other hand, in case of the 50 vol.% BAlq mixed device, EL intensity of degraded device compared to the fresh one was 84%, which was same as the variation ratio in PL case. Considering that photons are emitted from the entire EML area by photoexcitation, the difference means that BAlq induces uniform EML degradation, i.e., a wide recombination zone. It is estimated that the repulsive coulomb force by negative interfacial charge forms a wide recombination zone in the EML. Therefore, the surface charge of the interface between EML and ETL can

enhance the stability of device by reducing the electric field applied to the ETL and controlling the width of recombination zone.

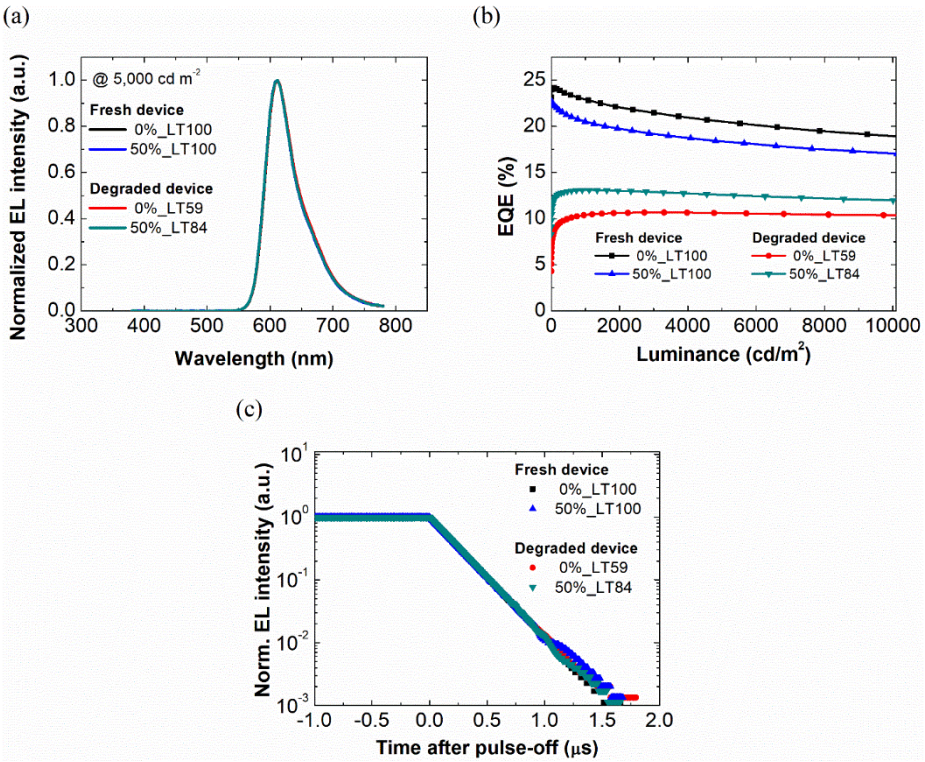

Figure 5.6 (a) Electroluminescence (EL) spectrum of the reference and BAlq doped devices at 5,000 cd/m^2, (b) EQEs of the devices as a function of luminance, (c) transient EL decay curves of the deivces depending on the degraded conditions.

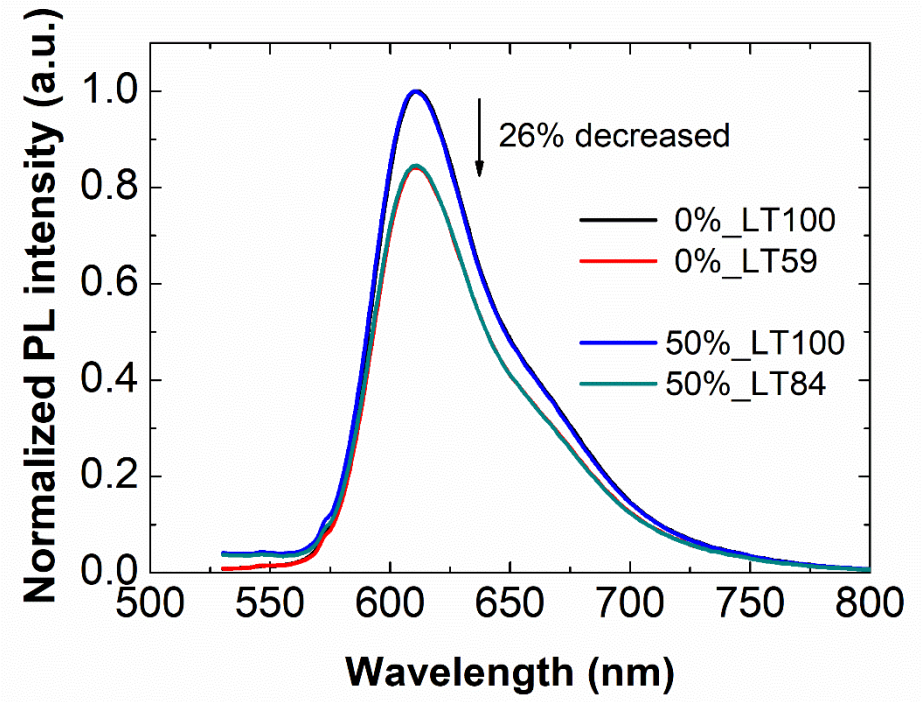

Figure 5.7 PL intensities of EML between fresh device and degraded device depending on the ETL conditions. The EML was excited using a 405 nm peak wavelength laser which is not absorbed by the transporting layers, and the volume ratio of BAlq was 50 vol.%. The degree of EL degradation and PL degradation was different in the reference device, while it was same in the BAlq doped device.

Although the stability of the device was increased by the SOP molecule, it was necessary to optimize the most effective position and thickness of the polarized layer because of the decrease of current density in the mixed ETL. To verify the position dependency of the mixed ETL, four devices were fabricated with modified ETL structures and figure 5.8 (a) is a schematic image of the devices. The thicknesses and materials of all the layers except ETL corresponded to figure 5.2 (a), and the volume ratio of BAlq was fixed as 50 vol.%. The structure of ETL is as follows; Device 1 (60 nm PO-T2T), Device 2 (30 nm PO-T2T + 30 nm mixed ETL), Device 3 (30 nm mixed ETL + 30 nm PO-T2T), Device 4 (60 nm mixed ETL). Figure 5.8 (b) shows *J-V-L* characteristics of the devices with different ETL structures. Compared to Device 1, the current density and luminance decreased in the rest of the cases, but the deviation was very different. When the interface between the cathode and the mixed layer existed, as in Device 2 and Device 4, there was a relatively large decrease in current density. In addition, interestingly, Device 4 had better electron injection properties than Device 2. On the other hand, when the mixed layer was located between EML and ETL as Device 3, the decrease in current density was suppressed effectively. Figure 5.8 (c) exhibits the EQEs as a function of luminance. Although Device 1 showed the highest EQE among them, the rest showed similar EQEs with Device 1. Figure 5.8 (d) shows the C-V curve of the devices. In the case of Device 4, the polarization of ETL was the largest, and the smallest in Device 1. In particular, the polarization properties of Device 2 and 3 were different despite the same thickness of polarized layer and further research on this origin

is needed. Currently, it is speculated that the orientation of PDM of BAlq varies depending on the interaction with the initial surface of the sublayer. Figure 5(e) shows the EL intensity decay curve measured at an initial luminance of 5,000 cd/m^2. Device 2 showed the fastest decay and largest voltage change. Differently, Device 4, which had the same cathode/ETL interface as Device 2, showed a large improvement in operation lifetime and small changes in applied voltage. Device 3, which had the same cathode/ETL interface as Device 1, showed the improved stability and the lowest variation in applied voltage. In other word, only the polarized layer adjacent to the EML interface mainly contributes to improving the stability of the device. Even if the polarized layer was only 5 nm away from the EML, there was no effect of increasing the lifetime. This result is because exciton distribution and hole blocking characteristics can be affected effectively only when the interfacial charge is existed at the interface. Thus, the SOP characteristics of the layer adjacent to the EML can influence the degradation of the device, and in order to design a stable device structure, the material's SOP property should also be considered.

Table 5.1 Comparison of applied voltage, EQE, and lifetime of the devices with different vol.% of BAlq in ETL.

Vol.% of BAlq	**1,000 nitt. voltage**	**1,000 nitt. EQE**	**LT_{90} (5,000 cd/m^2)**	**LT_{80} (5,000 cd/m^2)**
0%	4.8 V	22.9%	61	228
20%	5.2 V	21.2%	100	436
40%	5.4 V	20.6%	122	458
50%	5.7 V	20.5%	218	-
60%	6.3 V	20.0%	178	529
100%	9.3 V	18.7%	24	161

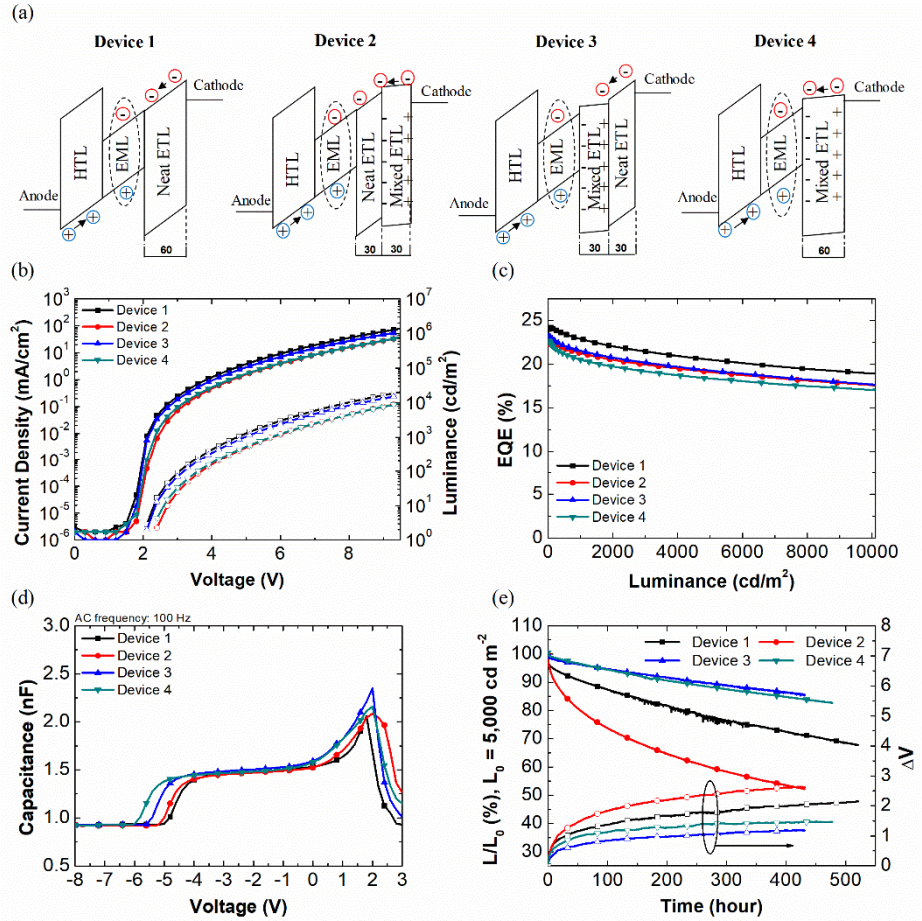

Figure 5.8 (a) Schematic band diagrams of exciplex-based OLEDs with different ETL conditions. (b) The current density-voltage-luminance (*J-V-L*) characteristics of the devices. (c) EQEs of the devices as a function of luminance. (c) Capacitances of the devices as a function of voltage. (d) EL decay curves of the devices as a function of operational time at an initial luminance (L_0) of 5,000 cd/m^2.

Another SOP molecule, Alq3, was also found to improve the lifetime of OLEDs. (Figure 5.9, 5.10, 5.11) However, there was a significant efficiency drop compared to that of BAlq, due to the emission of Alq_3. In addition, due to the improved efficiency by reduced Alq_3 emission, overshoot occurred during the lifetime measurement. (Figure 5.12) As in the case of BAlq, the lifetime increased only when there was a polarized layer at the interface with EML (Figure 5.13), and this also shows that the negative surface charge of HBL can increase the stability of OLEDs.

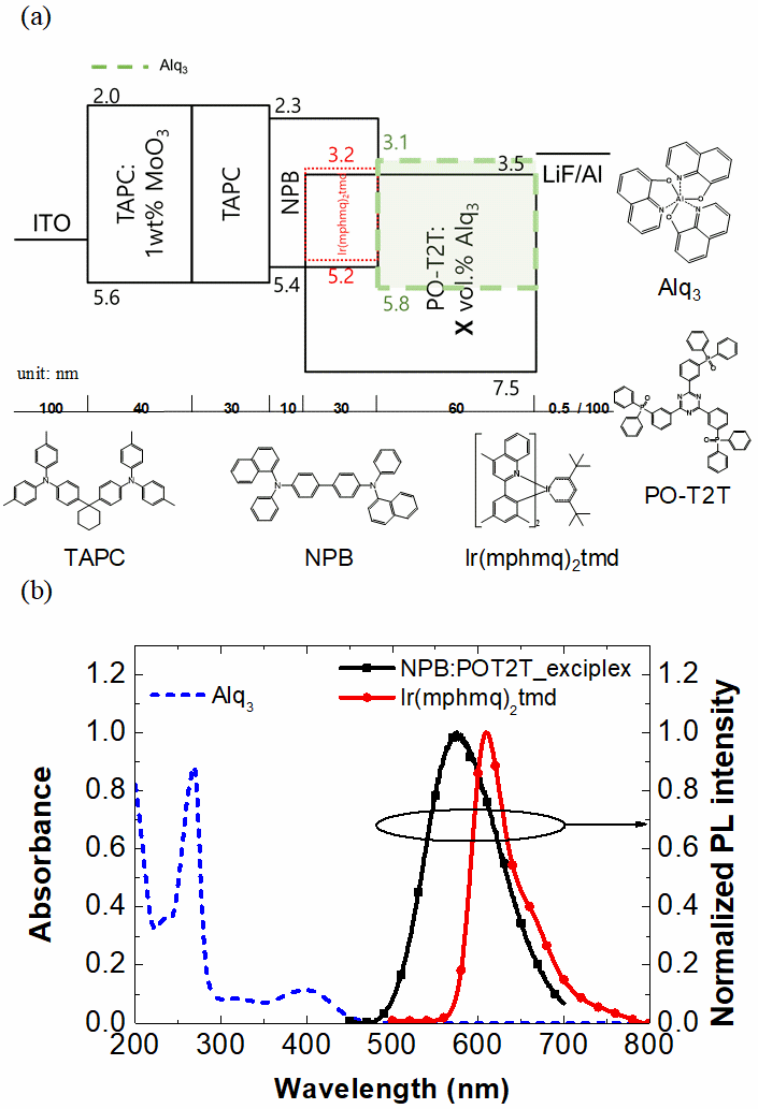

Figure 5.9 (a) Fabricated device structure of exciplex based OLEDs, and chemical structures of molecules. (b) Absorbance of Alq_3 thin film and photoluminescence spectra of NPB:POT2T exciplex and $Ir(mphmq)_2tmd$ red emitting dopant.

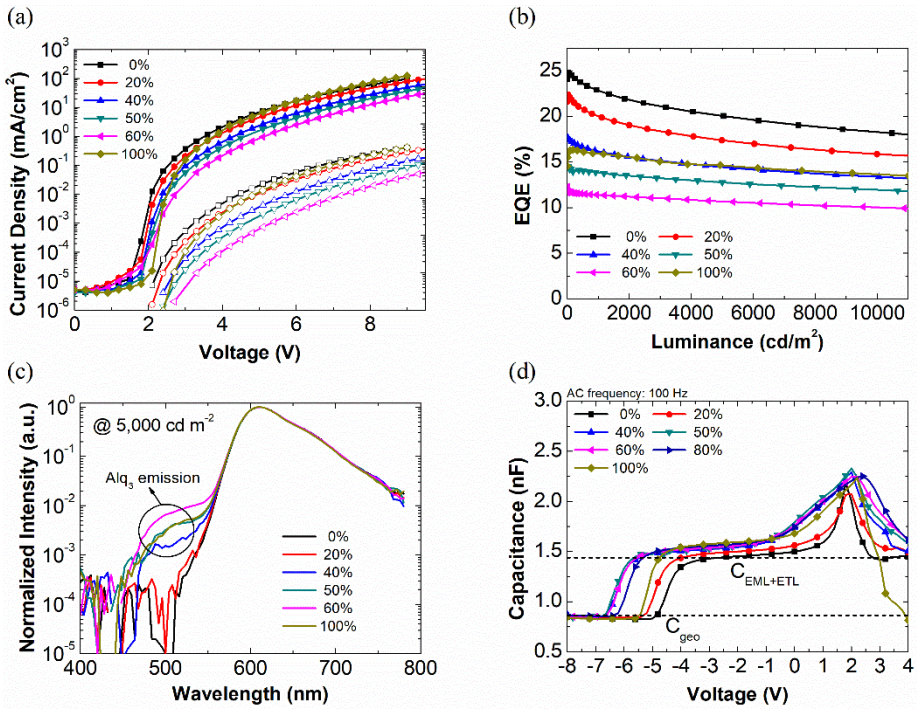

Figure 5.10 (a) The current density-voltage-luminance (*J-V-L*) characteristics of devices according to vol.% Alq_3 of ETL. (c) EQEs of the devices as a function of luminance. (c) Electroluminescence (EL) spectrum of the devices at 5,000 cd/m^2. (d) Capacitances of the devices as a function of voltage.

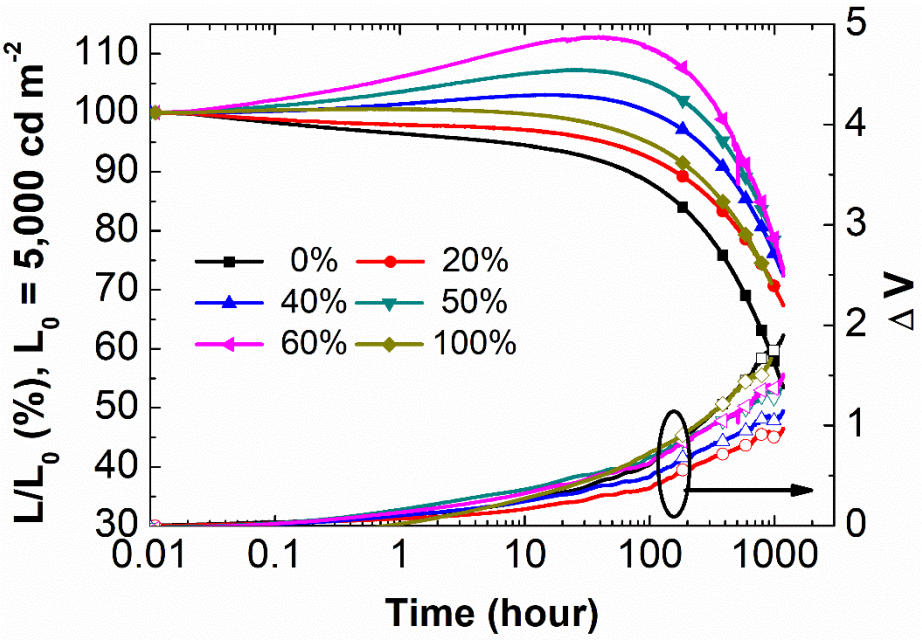

Figure 5.11 EL decay curves of the Alq_3 mixed OLEDs as a function of operational time at an initial luminance (L_0) of 5,000 cd/m^2.

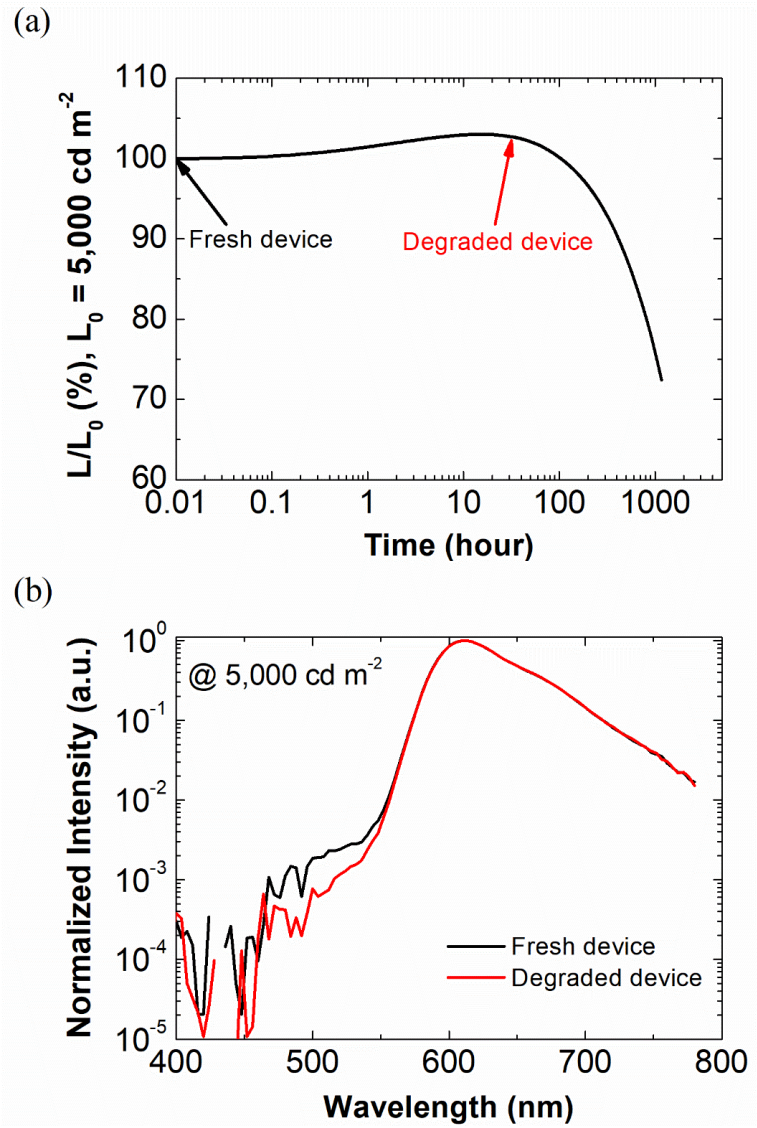

Figure 5.12 (a) EL decay curve of the 40 vol.% Alq_3 mixed OLED as a function of operational time at an initial luminance (L_0) of 5,000 cd/m^2. (b) EL spectrum of the 40 vol.% Alq_3 mixed OLED at the condition of fresh (black line) and degradation (red line).

Table 5.2 Comparison of applied voltage, EQE, and lifetime of the devices with different vol.% of Alq_3 in ETL.

Vol.% of Alq_3	**1,000 nitt. voltage**	**1,000 nitt. EQE**	**LT_{90} (5,000 cd/m^2)**	**LT_{80} (5,000 cd/m^2)**
0%	4.2 V	22.8%	69	277
20%	4.7 V	20.0%	161	520
40%	5.6 V	16.0%	415	814
50%	6.2 V	13.8%	556	928
60%	2.7 V	11.4%	622	937
100%	7.0 V	15.9%	225	622

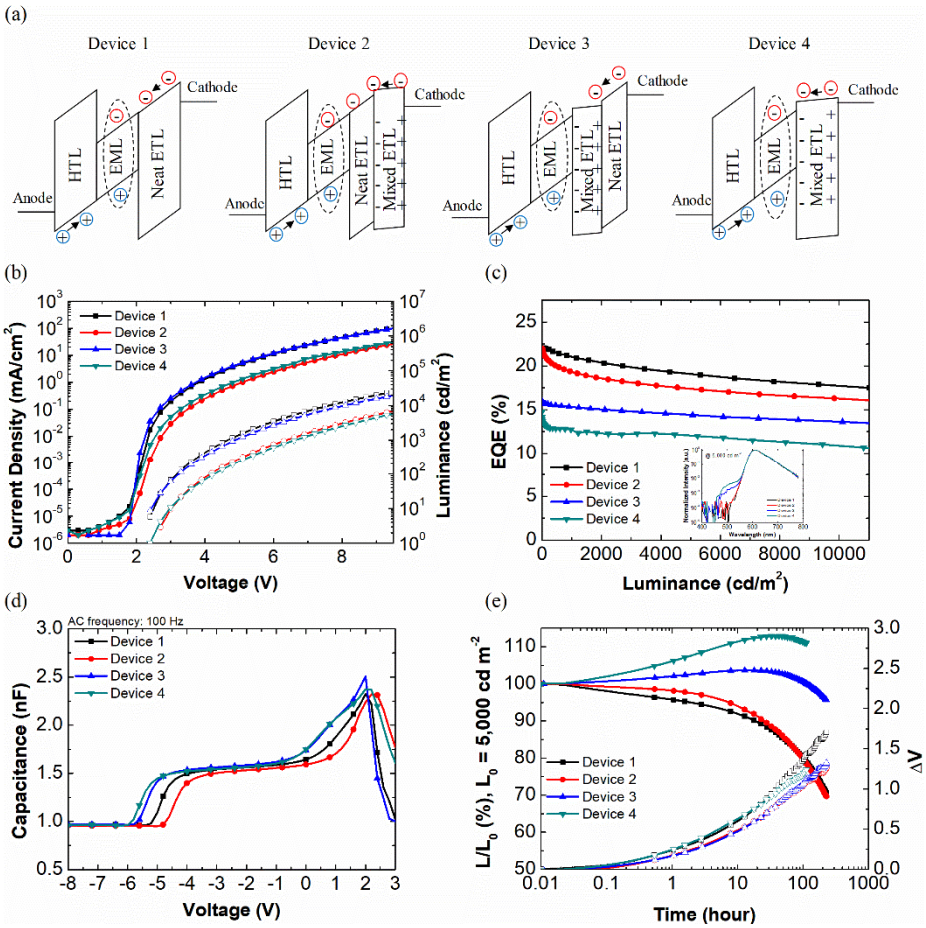

Figure 5.13 (a) Schematic band diagrams of exciplex-based OLEDs with different ETL conditions. (b) The current density-voltage-luminance (*J-V-L*) characteristics of the devices. Inset: EL spectra of the devices at 5,000 cd/m^2. (c) EQEs of the devices as a function of luminance. (c) Capacitances of the devices as a function of voltage. (d) EL decay curves of the devices as a function of operational time at an initial luminance (L_0) of 5,000 cd/m^2.

5.4 Conclusion

In summary, we improved the stability of the ETL by utilizing the SOP characteristics of BAlq. According to the volume ratio of BAlq, the polarization characteristics of the doped device were changed, and the operation stability of the devices increased. In addition, the enhancement in lifetime was only found when the position of the polarized layer was at the EML/ETL interface. This means that HBL can increase device lifetime when there is a negative surface charge at its interface with EML, and also indicates that the SOP characteristics of the molecule should be considered to improve the lifetime.

Chapter 6. Summary and Conclusion

OLED is no longer a prototype product, but can be easily found around us. However, high efficiency and long operating lifetime are still required in OLED, and if these problems are solved, the application of OLED can be further expanded. In this respect, this thesis contains information on the structure of light extraction to improve efficiency and how to increase operational stability.

In chapter 2, we developed a facile and effective two-step method for fabricating random organic microstructures for efficient light extraction from blue OLEDs is presented. An external quantum efficiency (EQE) of 44.3% is realized by attaching DACMs film and the efficiency is improved by 35% compared to a planar device without the light extraction layer, greater than the 22% improvement obtained by using microlens arrays (MLAs). The method is useful for OLED lighting and potentially in displays because of the simple fabrication method that is applicable to a large area on rigid or flexible substrates, the low material cost, the insolubility of the microstructure in alkyl halide solvents such as chloroform, and the controllability of the structure through the solution process.

In chapter 3, we show the damageless light extraction structure for top-emittng organic light-emitting diodes (TEOLEDs) by thermal evaporation of 1,5-diaminoanthraquinone (DAAQ). DAAQ nanowire arrays were applied to a red phosphorescent inverted TEOLED, enhancing the external quantum efficiency

(EQE) by 8.6% in a narrow full-width-at-half-maximum (FWHM) device, and by 10.6% in a wide FWHM device with same electrical properties. The method is useful for OLED displays because it is simple, vacuum-processable, and does not compromise device lifetime or the emission spectrum.

In chapter 4, we suggest the importance of patternability of internal light extraction layer. Integration of internal light extraction layers in OLED displays requires electrical connection between driving circuits in the backplane and an OLED electrode. We discussed the patternability of light extraction layers demonstrated it experimentally. The OLEDs fabricated on this patterned substrate showed similar current density-voltage (*J-V*) characteristics to OLEDs on a glass substrate with low leakage levels. The device showed over 50% enhancement of external quantum efficiency (EQE; from 21.7% to 32.7%), similar to the device without via holes.

In chapter 5, we proposed a method for improving the stability of electron transporting layer. We observed the SOP characteristics and the change in the lifetime of device when BAlq was doped in PO-T2T with different volume ratios. As the polarization increased, the operation lifetime also increased and the applied voltage change decreased. In addition, the lifetime enhancement was only observed when there was a polarized layer at the interface with the emtting layer (EML). This shows that hole blocking layer (HBL) can enhance the lifetime when it has a negative surface charge at the interface with EML,

and also indicates that the SOP characteristics of the molecule should be considered for improving the lifetime.

We believe that the developed light extraction structure and lifetime enhancing method providing a new insight for achieving highly efficient and stable OLEDs.

Bibliography

1. Akamatu, H. & Inokuchi, H. On the electrical conductivity of violanthrone, iso-violanthrone, and pyranthrone. *J. Chem. Phys.* **18**, 810–811 (1950).

2. Pope, M., Kallmann, H. P. & Magnante, P. Electroluminescence in organic crystals. *J. Chem. Phys.* **38**, 2042–2043 (1963).

3. Partridge, R. H. Electroluminescence from polyvinylcarbazole films: 3. Electroluminescent devices. *Polymer (Guildf).* **24**, 748–754 (1983).

4. Hayashi, S., Etoh, H. & Saito, S. Electroluminescence of perylene films with a conducting polymer as an anode. *Jpn. J. Appl. Phys.* **25**, L773–L775 (1986).

5. Tang, C. W. & Vanslyke, S. A. Organic electroluminescent diodes. *Appl. Phys. Lett.* **51**, 913–915 (1987).

6. Tang, C. W., Vanslyke, S. A. & Chen, C. H. Electroluminescence of doped organic thin films. *J. Appl. Phys.* **65**, 3610–3616 (1989).

7. Baldo, M. A. *et al.* Highly efficient phosphorescent emission from organic electroluminescent devices. *Nature* **395**, 151 (1998).

8. Uoyama, H., Goushi, K., Shizu, K., Nomura, H. & Adachi, C. Highly efficient organic light-emitting diodes from delayed fluorescence. *Nature* **492**, 234–238 (2012).

9. Goushi, K., Yoshida, K., Sato, K. & Adachi, C. Organic light-emitting diodes employing efficient reverse intersystem crossing for triplet-to-singlet state conversion. *Nat. Photonics* **6**, 253–258 (2012).

10. Park, Y. S., Kim, K. H. & Kim, J. J. Efficient triplet harvesting by fluorescent molecules through exciplexes for high efficiency organic light-emitting diodes. *Appl. Phys. Lett.* **102**, 1–6 (2013).

11. Park, Y. S., Jeong, W. I. & Kim, J. J. Energy transfer from exciplexes to dopants and its effect on efficiency of organic light-emitting diodes. *J. Appl. Phys.* **110**, (2011).

12. Sun, J. W. *et al.* A fluorescent organic light-emitting diode with 30% external quantum efficiency. *Adv. Mater.* **26**, 5684–5688 (2014).

13. Moon, C. K. *et al.* Combined Inter- and Intramolecular Charge-Transfer Processes for Highly Efficient Fluorescent Organic Light-Emitting Diodes with Reduced Triplet Exciton Quenching. *Adv. Mater.* **29**, 1–5 (2017).

14. Nakanotani, H. *et al.* High-efficiency organic light-emitting diodes with fluorescent emitters. *Nat. Commun.* **5**, 1–7 (2014).

15. Kim, H. G., Kim, K. H., Moon, C. K. & Kim, J. J. Harnessing Triplet Excited States by Fluorescent Dopant Utilizing Codoped Phosphorescent Dopant in Exciplex Host for Efficient Fluorescent Organic Light Emitting Diodes. *Adv. Opt. Mater.* **5**, 2–7 (2017).

16. Kim, H. G., Kim, K. H. & Kim, J. J. Highly Efficient, Conventional, Fluorescent Organic Light-Emitting Diodes with Extended Lifetime. *Adv. Mater.* **29**, 2–7 (2017).

17. Kim, H. G. *et al.* Triplet Harvesting by a Fluorescent Emitter Using a Phosphorescent Sensitizer for Blue Organic-Light-Emitting Diodes. *ACS Appl. Mater. Interfaces* **11**, 26–30 (2019).

18. Purcell, E. M. Resonance Absorption by Nuclear Magnetic Moments in a Solid. *Phys. Rev* **69**, (1946).

19. Chen, W., Kosmas, P., Leeser, M. & Rappaport, C. An FPGA Implementation of the Two-Dimensional Finite-Difference Time-Domain (FDTD) Algorithm Categories and Subject Descriptors. *ACM Trans. Des. Autom. Electron. Syst.* 213–222 (2004).

20. Neyts, K. A. Simulation of light emission from thin-film microcavities. *J. Opt. Soc. Am. A* **15**, 962 (1998).

21. Furno, M., Meerheim, R., Hofmann, S., Lüssem, B. & Leo, K. Efficiency and rate of spontaneous emission in organic electroluminescent devices. *Phys. Rev. B - Condens. Matter Mater. Phys.* **85**, 115205 (2012).

22. Kim, S. Y. *et al.* Organic light-emitting diodes with 30% external quantum efficiency based on a horizontally oriented emitter. *Adv. Funct. Mater.* **23**, 3896–3900 (2013).

23. Choi, C. S. *et al.* Blur-free outcoupling enhancement in transparent organic light emitting diodes: A nanostructure extracting surface plasmon modes. *Adv. Opt. Mater.* **1**, 687–691 (2013).

24. Kim, Y. D. *et al.* Enhanced light extraction efficiency in organic light-emitting diode with randomly dispersed nanopattern. *Opt. Lett.* **40**, 5838 (2015).

25. Zhou, L. *et al.* Light beam shaping for collimated emission from white organic light-emitting diodes using customized lenticular microlens arrays structure. *Appl. Phys. Lett.* **112**, 201902 (2018).

26. Qu, Y., Kim, J., Coburn, C. & Forrest, S. R. Efficient, Nonintrusive Outcoupling in Organic Light Emitting Devices Using Embedded

Microlens Arrays. *ACS Photonics* **5**, 2453–2458 (2018).

27. Zhou, L. *et al.* Multiscale micro-nano nested structures: Engineered surface morphology for efficient light escaping in organic light-emitting diodes. *ACS Appl. Mater. Interfaces* **7**, 26989–26998 (2015).

28. Kim, J. B., Lee, J. H., Moon, C. K., Kim, K. H. & Kim, J. J. Highly enhanced light extraction from organic light emitting diodes with little image blurring and good color stability. *Org. Electron.* **17**, 115–120 (2015).

29. Hwang, J. H. *et al.* Enhanced light out-coupling efficiency of organic light-emitting diodes with an extremely low haze by plasma treated nanoscale corrugation. *Nanoscale* **7**, 2723–2728 (2015).

30. Lee, C., Han, K.-H., Kim, K.-H. & Kim, J.-J. Direct formation of nano-pillar arrays by phase separation of polymer blend for the enhanced out-coupling of organic light emitting diodes with low pixel blurring. *Opt. Express* **24**, A488 (2016).

31. Suh, M. C., Pyo, B., Lim, B. W. & Kim, N. S. Preparation of randomly distributed micro-lens arrays fabricated from porous polymer film and their application as a light extraction component. *Org. Electron.* **38**, 316–322 (2016).

32. Qu, Y., Coburn, C., Fan, D. & Forrest, S. R. Elimination of Plasmon Losses and Enhanced Light Extraction of Top-Emitting Organic Light-Emitting Devices Using a Reflective Subelectrode Grid. *ACS Photonics* **4**, 363–368 (2017).

33. Salehi, A., Chen, Y., Fu, X., Peng, C. & So, F. Manipulating Refractive Index in Organic Light-Emitting Diodes. *ACS Appl. Mater. Interfaces* **10**, 9595–9601 (2018).

34. Chen, Y. J. *et al.* A Vision toward Ultimate Optical Out-Coupling for Organic Light-Emitting Diode Displays: 3D Pixel Configuration. *Adv. Sci.* **5**, (2018).

35. Möller, S. & Forrest, S. R. Improved light out-coupling in organic light emitting diodes employing ordered microlens arrays. *J. Appl. Phys.* **91**, 3324–3327 (2002).

36. Reineke, S. *et al.* White organic light-emitting diodes with fluorescent tube efficiency. *Nature* **459**, 234–238 (2009).

37. Sung, Y. H. *et al.* Air void optical scattering structure for high-brightness organic light emitting diodes. *Ceram. Int.* **43**, S455–S459 (2017).

38. Song, J. *et al.* Lensfree OLEDs with over 50% external quantum

efficiency via external scattering and horizontally oriented emitters. *Nat. Commun.* **9**, (2018).

39. Jeon, S. *et al.* High-Quality White OLEDs with Comparable Efficiencies to LEDs. *Adv. Opt. Mater.* **6**, 1–8 (2018).

40. Zhou, J. G. *et al.* Nano-modified indium tin oxide incorporated with ideal microlens array for light extraction of OLED. *J. Mater. Chem. C* **7**, 3958–3964 (2019).

41. Li, Z. *et al.* Highly efficient organic light-emitting diodes employing the periodic micro-structured ITO substrate fabricated by holographic lithography. *Org. Electron.* **75**, 105438 (2019).

42. Kim, A., Huseynova, G., Lee, J. & Lee, J. H. Enhancement of out-coupling efficiency of flexible organic light-emitting diodes fabricated on an MLA-patterned parylene substrate. *Org. Electron.* **71**, 246–250 (2019).

43. Yen, J. H., Wang, Y. J., Hsieh, C. A., Chen, Y. C. & Chen, L. Y. Enhanced light extraction from organic light-emitting devices through non-covalent or covalent polyimide-silica light scattering hybrid films. *J. Mater. Chem. C* **8**, 4102–4111 (2020).

44. Koo, W. H. *et al.* Light extraction from organic light-emitting diodes enhanced by spontaneously formed buckles. *Nat. Photonics* **4**, 222–226 (2010).

45. Chang, H. W. *et al.* Nano-particle based scattering layers for optical efficiency enhancement of organic light-emitting diodes and organic solar cells. *J. Appl. Phys.* **113**, 204502 (2013).

46. Ou, Q. D. *et al.* Extremely efficient white organic light-emitting diodes for general lighting. *Adv. Funct. Mater.* **24**, 7249–7256 (2014).

47. Youn, W., Lee, J., Xu, M., Singh, R. & So, F. Corrugated sapphire substrates for organic light-emitting diode light extraction. *ACS Appl. Mater. Interfaces* **7**, 8974–8978 (2015).

48. Koh, T. W., Spechler, J. A., Lee, K. M., Arnold, C. B. & Rand, B. P. Enhanced Outcoupling in Organic Light-Emitting Diodes via a High-Index Contrast Scattering Layer. *ACS Photonics* **2**, 1366–1372 (2015).

49. Kim, J. J. *et al.* Biologically Inspired Organic Light-Emitting Diodes. *Nano Lett.* **16**, 2994–3000 (2016).

50. Riedel, D., Wehlus, T., Reusch, T. C. G. & Brabec, C. J. Polymer-based scattering layers for internal light extraction from organic light emitting diodes. *Org. Electron.* **32**, 27–33 (2016).

51. Wu, W. T., Hsu, C. M., Lin, W. M., Tsai, D. H. & Peng, U. J. Optical

and electrical effects of nickel oxide interlayer for anode-recessed organic light-emitting diodes. *Org. Electron.* **30**, 219–224 (2016).

52. Levermore, P. A. *et al.* 52.4: Highly efficient phosphorescent OLED lighting panels for solid state lighting. *48th Annu. SID Symp. Semin. Exhib. 2010, Disp. Week 2010* **2**, 786–789 (2010).

53. Coburn, C., Jeong, C. & Forrest, S. R. Reliable, All-Phosphorescent Stacked White Organic Light Emitting Devices with a High Color Rendering Index. *ACS Photonics* **5**, 630–635 (2018).

54. Mulder, C. L., Celebi, K., Milaninia, K. M. & Baldo, M. A. Saturated and efficient blue phosphorescent organic light emitting devices with Lambertian angular emission. *Appl. Phys. Lett.* **90**, 211109 (2007).

55. Zhou, L. *et al.* Light manipulation for organic optoelectronics using bio-inspired moth's eye nanostructures. *Sci. Rep.* **4**, (2014).

56. Xiang, H. Y. *et al.* Outcoupling-Enhanced Flexible Organic Light-Emitting Diodes on Ameliorated Plastic Substrate with Built-in Indium-Tin-Oxide-Free Transparent Electrode. *ACS Nano* **9**, 7553–7562 (2015).

57. Park, W.-Y., Cheong, H.-W., Lee, C. & Whang, K.-W. Design of highly efficient RGB top-emitting organic light-emitting diodes using finite element method simulations. *Opt. Express* **24**, 24018 (2016).

58. Han, K. H. *et al.* Optical Analysis of Power Distribution in Top-Emitting Organic Light Emitting Diodes Integrated with Nanolens Array Using Finite Difference Time Domain. *ACS Appl. Mater. Interfaces* **10**, 18942–18947 (2018).

59. Nien, C. K. & Yu, H. H. The applications of biomimetic cicada-wing structure on the organic light-emitting diodes. *Mater. Chem. Phys.* **227**, 191–199 (2019).

60. Jeon, S. *et al.* Vacuum nanohole array embedded phosphorescent organic light emitting diodes. *Sci. Rep.* **5**, 1–7 (2015).

61. Hippola, C. *et al.* Enhanced Light Extraction from OLEDs Fabricated on Patterned Plastic Substrates. *Adv. Opt. Mater.* **6**, 1–11 (2018).

62. Kim, K. H. & Park, S. Y. Enhancing light-extraction efficiency of OLEDs with high- and low-refractive-index organic-inorganic hybrid materials. *Org. Electron.* **36**, 103–112 (2016).

63. Chen, S., Zhao, Z., Tang, B. Z. & Kwok, H. S. Growth methods, enhanced photoluminescence, high hydrophobicity and light scattering of 4,4′-bis(1,2,2-triphenylvinyl)biphenyl nanowires. *Org. Electron.* **13**, 1996–2002 (2012).

64. Kim, J. B., Lee, J. H., Moon, C. K., Kim, S. Y. & Kim, J. J. Highly enhanced light extraction from surface plasmonic loss minimized organic light-emitting diodes. *Adv. Mater.* **25**, 3571–3577 (2013).

65. Park, Y. S. *et al.* Crystallization-assisted nano-lens array fabrication for highly efficient and color stable organic light emitting diodes. *Nanoscale* **9**, 230–236 (2017).

66. Shin, H. *et al.* Sky-Blue Phosphorescent OLEDs with 34.1% External Quantum Efficiency Using a Low Refractive Index Electron Transporting Layer. *Adv. Mater.* **28**, 4920–4925 (2016).

67. Kim, K. H., Moon, C. K., Sun, J. W., Sim, B. & Kim, J. J. Triplet Harvesting by a Conventional Fluorescent Emitter Using Reverse Intersystem Crossing of Host Triplet Exciplex. *Adv. Opt. Mater.* **3**, 895–899 (2015).

68. Moon, C. K., Huh, J. S., Kim, J. M. & Kim, J. J. Electronic Structure and Emission Process of Excited Charge Transfer States in Solids. *Chem. Mater.* **30**, 5648–5654 (2018).

69. Sakamoto, T. & Fujimoto, K. Photo-Cross-Linking Reaction in Nucleic Acids: Chemistry and Applications. *Modif. Nucleic Acids. Nucleic Acids Mol. Biol.* **31**, 145–157 (2016).

70. Lee, J. H. *et al.* An exciplex forming host for highly efficient blue organic light emitting diodes with low driving voltage. *Adv. Funct. Mater.* **25**, 361–366 (2015).

71. Kim, K. *et al.* Dual pattern for enhancing light extraction efficiency of white organic light-emitting diodes. *Org. Electron.* **57**, 201–205 (2018).

72. Moon, C.-K., Kim, S.-Y., Lee, J.-H. & Kim, J.-J. Luminescence from oriented emitting dipoles in a birefringent medium. *Opt. Express* **23**, A279 (2015).

73. Will, P. *et al.* Efficiency of Light Outcoupling Structures in Organic Light-Emitting Diodes: 2D TiO 2 Array as a Model System. *Adv. Funct. Mater.* **29**, 1901748 (2019).

74. Jin, Y. *et al.* Solving efficiency-stability tradeoff in top-emitting organic light-emitting devices by employing periodically corrugated metallic cathode. *Adv. Mater.* **24**, 1187–1191 (2012).

75. Kim, J., Qu, Y., Coburn, C. & Forrest, S. R. Efficient Outcoupling of Organic Light-Emitting Devices Using a Light-Scattering Dielectric Layer. *ACS Photonics* **5**, 3315–3321 (2018).

76. Liu, Y. F. *et al.* Viewing-angle independence of white emission from

microcavity top-emitting organic light-emitting devices with periodically and gradually changed cavity length. *Org. Electron.* **14**, 1597–1601 (2013).

77. Fuchs, C. *et al.* Quantitative allocation of Bragg scattering effects in highly efficient OLEDs fabricated on periodically corrugated substrates. *Opt. Express* **21**, 16319 (2013).

78. Schwab, T. *et al.* Coherent mode coupling in highly efficient top-emitting OLEDs on periodically corrugated substrates. *Opt. Express* **22**, 7524 (2014).

79. Park, W. Y., Kwon, Y., Cheong, H. W., Lee, C. & Whang, K. W. Increased light extraction efficiency from top-emitting organic light-emitting diodes employing a mask-free plasma-etched stochastic polymer surface. *J. Appl. Phys.* **119**, 95502 (2016).

80. Xu, K., Lu, C., Huang, Y., Hu, J. & Wang, X. Enhanced outcoupling efficiency and removal of the microcavity effect in top-emitting OLED by using a simple vapor treated corrugated film. *RSC Adv.* **7**, 54876–54880 (2017).

81. Jin, Y., Zou, D., Wang, K., Wu, Z. & Xiang, C. Optimization of period and thickness of the corrugated Ag cathode for efficient cross coupling between SPP and microcavity modes in top-emitting OLEDs. *Opt. Mater. Express* **7**, 2096 (2017).

82. Will, P. A. *et al.* Scattering quantified: Evaluation of corrugation induced outcoupling concepts in organic light-emitting diodes. *Org. Electron.* **58**, 250–256 (2018).

83. Kim, N. S., Lee, W. Y., Jung, S. H. & Suh, M. C. Light modulation of top emission organic light emitting diodes showing strong microcavity effect by applying multilayered scattering film. *Opt. Express* **26**, 1185 (2018).

84. Yang, C. J. *et al.* Microcavity top-emitting organic light-emitting devices integrated with microlens arrays: Simultaneous enhancement of quantum efficiency, cd/A efficiency, color performances, and image resolution. *Appl. Phys. Lett.* **91**, 253508 (2007).

85. Wrzesniewski, E. *et al.* Enhancing light extraction in top-emitting organic light-emitting devices using molded transparent polymer microlens arrays. *Small* **8**, 2647–2651 (2012).

86. Liu, C. C. *et al.* Microcavity top-emitting organic light-emitting devices integrated with diffusers for simultaneous enhancement of efficiencies and viewing characteristics. *Appl. Phys. Lett.* **94**, 103302 (2009).

87. Thomschke, M., Reineke, S., Lüssem, B. & Leo, K. Highly efficient white top-emitting organic light-emitting diodes comprising laminated microlens films. *Nano Lett.* **12**, 424–428 (2012).

88. Pyo, B. *et al.* A nanoporous polymer film as a diffuser as well as a light extraction component for top emitting organic light emitting diodes with a strong microcavity structure. *Nanoscale* **8**, 8575–8582 (2016).

89. Yin, M. *et al.* Efficient and angle-stable white top-emitting organic light emitting devices with patterned quantum dots down-conversion films. *Org. Electron.* **56**, 46–50 (2018).

90. Liu, Y. F. *et al.* Polymer encapsulation of flexible top-emitting organic light-emitting devices with improved light extraction by integrating a microstructure. *Org. Electron.* **15**, 2661–2666 (2014).

91. Schaefer, T., Schwab, T., Lenk, S. & Gather, M. C. White top-emitting organic light-emitting diodes with solution-processed nano-particle scattering layers. *Appl. Phys. Lett.* **107**, 233301 (2015).

92. Jang, S. *et al.* Spontaneously formed organic wrinkle structure for top-emitting organic light emitting diodes. *J. Ind. Eng. Chem.* **80**, 490–496 (2019).

93. Liu, H. *et al.* Synthesis of organic one-dimensional nanomaterials by solid-phase reaction. *J. Am. Chem. Soc.* **125**, 10794–10795 (2003).

94. Yang, F., Shtein, M. & Forrest, S. R. Controlled growth of a molecular bulk heterojunction photovoltaic cell. *Nat. Mater.* **4**, 37–41 (2005).

95. Hsiao, Y. S., Whang, W. T., Suen, S. C., Shiu, J. Y. & Chen, C. P. Morphological control of CuPc and its application in organic solar cells. *Nanotechnology* **19**, 415603 (2008).

96. Zhao, Y. S. *et al.* Photoluminescence and electroluminescence from tris (8-hydroxyquinoline) aluminum nanowires prepared by adsorbent-assisted physical vapor deposition. *Adv. Funct. Mater.* **16**, 1985–1991 (2006).

97. Chen, W., Peng, Q. & Li, Y. Alq3 nanorods: Promising building blocks for optical devices. *Adv. Mater.* **20**, 2747–2750 (2008).

98. Cho, C. P. & Perng, T. P. On the dendritic growth and field emission of amorphous AlQ3 nanowires. *Org. Electron.* **11**, 115–122 (2010).

99. Liu, H. *et al.* Field emission properties of large-area nanowires of organic charge-transfer complexes. *J. Am. Chem. Soc.* **127**, 1120–1121 (2005).

100. Tian, F., Liu, W. & Wang, C. R. Controllable preparation of copper

tetracyanoquinodimethane nanowire and the field emission study. *J. Phys. Chem. C* **112**, 8763–8766 (2008).

101. Cui, S. *et al.* Fabrication and field-emission properties of large-area nanostructures of the organic charge-transfer complex Cu-TCNAQ. *Adv. Mater.* **20**, 309–313 (2008).

102. Chen, S., Qin, W., Zhao, Z., Tang, B. Z. & Kwok, H. S. One-step fabrication of organic nanoparticles as scattering media for extracting substrate waveguide light from organic light-emitting diodes. *J. Mater. Chem.* **22**, 13386–13390 (2012).

103. Choi, Y. H., Jeon, Y. P., Choo, D. C. & Kim, T. W. Enhancement of out-coupling efficiency due to an organic scattering layer in organic light-emitting devices. *Org. Electron.* **22**, 197–201 (2015).

104. Wang, W., Peng, H., Wang, S. & Chen, S. Top-emitting organic light-emitting diodes integrated with thermally evaporated scattering film for reducing angular dependence of emission spectra. *Org. Electron.* **24**, 195–199 (2015).

105. Wang, Z., Chen, Z., Xiao, L. & Gong, Q. Enhancement of top emission for organic light-emitting diode via scattering surface plasmons by nano-aggregated outcoupling layer. *Org. Electron.* **10**, 341–345 (2009).

106. Zhao, Y. S., Wu, J. & Huang, J. Vertical organic nanowire arrays: Controlled synthesis and chemical sensors. *J. Am. Chem. Soc.* **131**, 3158–3159 (2009).

107. Huang, K. J., Hsiao, Y. S. & Whang, W. T. Low-temperature formation of self-assembled 1,5-diaminoanthraquinone nanofibers: Substrate effects and field emission characteristics. *Org. Electron.* **12**, 686–693 (2011).

108. Zheng, J. Y. *et al.* Wire-on-wire growth of fluorescent organic heterojunctions. *J. Am. Chem. Soc.* **134**, 2880–2883 (2012).

109. Riel, H., Karg, S., Beierlein, T., Rieß, W. & Neyts, K. Tuning the emission characteristics of top-emitting organic light-emitting devices by means of a dielectric capping layer: An experimental and theoretical study. *J. Appl. Phys.* **94**, 5290–5296 (2003).

110. Kuei, C. Y. *et al.* Bis-Tridentate Ir(III) Complexes with Nearly Unitary RGB Phosphorescence and Organic Light-Emitting Diodes with External Quantum Efficiency Exceeding 31%. *Adv. Mater.* **28**, 2795–2800 (2016).

111. Kim, K. H. *et al.* Controlling Emitting Dipole Orientation with Methyl Substituents on Main Ligand of Iridium Complexes for Highly

Efficient Phosphorescent Organic Light-Emitting Diodes. *Adv. Opt. Mater.* **3**, 1191–1196 (2015).

112. Kim, K. H., Moon, C. K., Lee, J. H., Kim, S. Y. & Kim, J. J. Highly efficient organic light-emitting diodes with phosphorescent emitters having high quantum yield and horizontal orientation of transition dipole moments. *Adv. Mater.* **26**, 3844–3847 (2014).

113. Kim, K. H. *et al.* Phosphorescent dye-based supramolecules for high-efficiency organic light-emitting diodes. *Nat. Commun.* **5**, (2014).

114. Kim, K. H. *et al.* Crystal Organic Light-Emitting Diodes with Perfectly Oriented Non-Doped Pt-Based Emitting Layer. *Adv. Mater.* **28**, 2526–2532 (2016).

115. Lee, D. R. *et al.* Above 30% external quantum efficiency in green delayed fluorescent organic light-emitting diodes. *ACS Appl. Mater. Interfaces* **7**, 9625–9629 (2015).

116. Kaji, H. *et al.* Purely organic electroluminescent material realizing 100% conversion from electricity to light. *Nat. Commun.* **6**, 1–8 (2015).

117. Udagawa, K., Sasabe, H., Igarashi, F. & Kido, J. Simultaneous Realization of High EQE of 30%, Low Drive Voltage, and Low Efficiency Roll-Off at High Brightness in Blue Phosphorescent OLEDs. *Adv. Opt. Mater.* **4**, 86–90 (2016).

118. Sun, Y. & Forrest, S. R. Organic light emitting devices with enhanced outcoupling via microlenses fabricated by imprint lithography. *J. Appl. Phys.* **100**, 1–7 (2006).

119. Cheng, Y. H., Wu, J. L., Cheng, C. H., Syao, K. C. & Lee, M. C. M. Enhanced light outcoupling in a thin film by texturing meshed surfaces. *Appl. Phys. Lett.* **90**, 2005–2008 (2007).

120. Tsutsui, T., Yahiro, M., Yokogawa, H., Kawano, K. & Yokoyama, M. Doubling coupling-out efficiency in organic light-emitting devices using a thin silica aerogel layer. *Adv. Mater.* **13**, 1149–1152 (2001).

121. Sun, Y. & Forrest, S. R. Enhanced light out-coupling of organic light-emitting devices using embedded low-index grids. *Nat. Photonics* **2**, 483–487 (2008).

122. Lee, Y. J. *et al.* A high-extraction-efficiency nanopatterned organic light-emitting diode. *Appl. Phys. Lett.* **82**, 3779–3781 (2003).

123. Do, Y. R., Kim, Y. C., Song, Y. W. & Lee, Y. H. Enhanced light extraction efficiency from organic light emitting diodes by insertion of a two-dimensional photonic crystal structure. *J. Appl. Phys.* **96**, 7629–

7636 (2004).

124. Kim, E. *et al.* A Facile Route to Efficient, Low-Cost Flexible Organic Light-Emitting Diodes: Utilizing the High Refractive Index and Built-In Scattering Properties of Industrial-Grade PEN Substrates. *Adv. Mater.* **27**, 1624–1631 (2015).

125. Altun, A. O. *et al.* Corrugated organic light emitting diodes for enhanced light extraction. *Org. Electron.* **11**, 711–716 (2010).

126. Huh, J. W. *et al.* A randomly nano-structured scattering layer for transparent organic light emitting diodes. *Nanoscale* **6**, 10727–10733 (2014).

127. Li, L. *et al.* A solution processed flexible nanocomposite electrode with efficient light extraction for organic light emitting diodes. *Sci. Rep.* **4**, 1–8 (2014).

128. Kim, Y. & Do, Y. R. Nanohole-templated organic light-emitting diodes fabricated using laser-interfering lithography : moth-eye lighting. *Opt. Express* **13**, 1598–1603 (2005).

129. Khadir, S. *et al.* Localized surface plasmon enhanced emission of organic light emitting diode coupled to DBR-cathode microcavity by using silver nanoclusters. *Opt. Express* **23**, 23647 (2015).

130. Shin, J. W. *et al.* Random nano-structures as light extraction functionals for organic light-emitting diode applications. *Org. Electron.* **15**, 196–202 (2014).

131. Dang, G. *et al.* Comparison of Dry and Wet Etch Processes for Patterning SiO[sub 2]/TiO[sub 2] Distributed Bragg Reflectors for Vertical-Cavity Surface-Emitting Lasers. *J. Electrochem. Soc.* **148**, G25 (2001).

132. Mehta, S. M. & Patel, S. R. The Behavior of Solutions of Titanium Dioxide in Sulfuric Acid in the Presence of Metallic Sulfates. *J. Am. Chem. Soc.* **73**, 224–226 (1951).

133. Okazaki, S. *et al.* Wet etching of amorphous TiO2 thin films using H 3PO4-H2O2 aqueous solution. *Jpn. J. Appl. Phys.* **52**, (2013).

134. Lee, J. H., Wu, C. I., Liu, S. W., Huang, C. A. & Chang, Y. Mixed host organic light-emitting devices with low driving voltage and long lifetime. *Appl. Phys. Lett.* **86**, 1–3 (2005).

135. Cho, Y. J., Yook, K. S. & Lee, J. Y. A universal host material for high external quantum efficiency close to 25% and long lifetime in green fluorescent and phosphorescent OLEDs. *Adv. Mater.* **26**, 4050–4055 (2014).

136. Chen, C. H. *et al.* Highly efficient orange and deep-red organic light emitting diodes with long operational lifetimes using carbazole-quinoline based bipolar host materials. *J. Mater. Chem. C* **2**, 6183–6191 (2014).

137. Kim, S. M., Yun, J. H., Han, S. H. & Lee, J. Y. A design strategy of bipolar host materials for more than 30 times extended lifetime in phosphorescent organic light-emitting diodes using benzocarbazole and quinazoline. *J. Mater. Chem. C* **5**, 9072–9079 (2017).

138. Kim, J. M., Lee, C. H. & Kim, J. J. Mobility balance in the light-emitting layer governs the polaron accumulation and operational stability of organic light-emitting diodes. *Appl. Phys. Lett.* **111**, 1–6 (2017).

139. Ihn, S. G. *et al.* An Alternative Host Material for Long-Lifespan Blue Organic Light-Emitting Diodes Using Thermally Activated Delayed Fluorescence. *Adv. Sci.* **4**, 1600502 (2017).

140. Kim, J. M. & Kim, J. J. Charge transport layers manage mobility and carrier density balance in light-emitting layers influencing the operational stability of organic light emitting diodes. *Org. Electron.* **67**, 43–49 (2019).

141. Hong, S., Kim, J. W. & Lee, S. Lifetime enhanced phosphorescent organic light emitting diode using an electron scavenger layer. *Appl. Phys. Lett.* **107**, 1–5 (2015).

142. Tsang, D. P. K. & Adachi, C. Operational stability enhancement in organic light-emitting diodes with ultrathin Liq interlayers. *Sci. Rep.* **6**, 1–10 (2016).

143. Zhang, Y., Lee, J. & Forrest, S. R. Tenfold increase in the lifetime of blue phosphorescent organic light-emitting diodes. *Nat. Commun.* **5**, 1–7 (2014).

144. Nakanotani, H., Masui, K., Nishide, J., Shibata, T. & Adachi, C. Promising operational stability of high-efficiency organic light-emitting diodes based on thermally activated delayed fluorescence. *Sci. Rep.* **3**, 1–6 (2013).

145. Lee, J. *et al.* Hot excited state management for long-lived blue phosphorescent organic light-emitting diodes. *Nat. Commun.* **8**, (2017).

146. Kim, S. *et al.* Degradation of blue-phosphorescent organic light-emitting devices involves exciton-induced generation of polaron pair within emitting layers. *Nat. Commun.* **9**, 1–11 (2018).

147. Regnat, M. *et al.* Routes for Efficiency Enhancement in Fluorescent

TADF Exciplex Host OLEDs Gained from an Electro-Optical Device Model. *Adv. Electron. Mater.* **6**, 1–8 (2020).

148. Aziz, H. & Popovic, Z. D. Degradation phenomena in small-molecule organic light-emitting devices. *Chem. Mater.* **16**, 4522–4532 (2004).

149. Schmidbauer, S., Hohenleutner, A. & König, B. Chemical degradation in organic light-emitting devices: Mechanisms and implications for the design of new materials. *Adv. Mater.* **25**, 2114–2129 (2013).

150. Scholz, S., Kondakov, D., Lüssem, B. & Leo, K. Degradation mechanisms and reactions in organic light-emitting devices. *Chem. Rev.* **115**, 8449–8503 (2015).

151. Zhao, C. & Duan, L. Review on photo- And electrical aging mechanisms for neutral excitons and ions in organic light-emitting diodes. *J. Mater. Chem. C* **8**, 803–820 (2020).

152. Zhang, D., Wei, P., Zhang, D. & Duan, L. Sterically Shielded Electron Transporting Material with Nearly 100% Internal Quantum Efficiency and Long Lifetime for Thermally Activated Delayed Fluorescent and Phosphorescent OLEDs. *ACS Appl. Mater. Interfaces* **9**, 19040–19047 (2017).

153. Berleb, S., Brütting, W. & Paasch, G. Interfacial charges and electric field distribution in organic hetero-layer light-emitting devices. *Org. Electron.* **1**, 41–47 (2000).

154. Noguchi, Y., Brütting, W. & Ishii, H. Spontaneous orientation polarization in organic light-emitting diodes. *Jpn. J. Appl. Phys.* **58**, (2019).

155. Noguchi, Y. *et al.* Influence of the direction of spontaneous orientation polarization on the charge injection properties of organic light-emitting diodes. *Appl. Phys. Lett.* **102**, (2013).

156. Kinjo, H. *et al.* Significant relaxation of residual negative carrier in polar Alq3 film directly detected by high-sensitivity photoemission. *Appl. Phys. Express* **9**, 3–7 (2016).

157. Altazin, S. *et al.* Simulation of OLEDs with a polar electron transport layer. *Org. Electron.* **39**, 244–249 (2016).

158. Hofmann, A. J. L. *et al.* Dipolar Doping of Organic Semiconductors to Enhance Carrier Injection. *Phys. Rev. Appl.* **12**, 1 (2019).

159. Jäger, L., Schmidt, T. D. & Brütting, W. Manipulation and control of the interfacial polarization in organic light-emitting diodes by dipolar doping. *AIP Adv.* **6**, 95220 (2016).

160. Osada, K. *et al.* Observation of spontaneous orientation polarization in

evaporated films of organic light-emitting diode materials. *Org. Electron.* **58**, 313–317 (2018).

161. Lee, J. H., Shin, H., Kim, J. M., Kim, K. H. & Kim, J. J. Exciplex-forming co-host-based red phosphorescent organic light-emitting diodes with long operational stability and high efficiency. *ACS Appl. Mater. Interfaces* **9**, 3277–3281 (2017).

162. Noguchi, Y. *et al.* Charge accumulation at organic semiconductor interfaces due to a permanent dipole moment and its orientational order in bilayer devices. *J. Appl. Phys.* **111**, 114508 (2012).

163. Van Mensfoort, S. L. M. *et al.* Electron transport in the organic small-molecule material BAlq - The role of correlated disorder and traps. *Org. Electron.* **11**, 1408–1413 (2010).

164. Carvelli, M., Van Reenen, A., Janssen, R. A. J., Loebl, H. P. & Coehoorn, R. Exciton formation and light emission near the organic-organic interface in small-molecule based double-layer OLEDs. *Org. Electron.* **13**, 2605–2614 (2012).

165. Hung, W. Y. *et al.* The first tandem, all-exciplex-based woled. *Sci. Rep.* **4**, 4–9 (2014).

166. Brütting, W., Berleb, S. & Mückl, A. G. Device physics of organic light-emitting diodes based on molecular materials. *Org. Electron.* **2**, 1–36 (2001).

초 록

1965 년, 안트라센 단결정에서 유기물의 첫 전기 발광이 발견된 이후, 유기 발광소자는 많은 발전을 거듭해 최근 소형 디스플레이의 주류를 이뤘다. 또한 유기 발광소자는 적은 기판 의존성을 갖기 때문에 플렉시블 디스플레이나 투명 디스플레이와 같은 차세대 디스플레이로 활용될 수 있는 잠재력을 갖고 있다. 유기 발광소자에서 남은 과제는 높은 효율과 구동 안정성이다.

일반적으로 유기물은 넓은 발광스펙트럼을 보이기 때문에, 유기 발광소자는 연색성이 높은 조명으로 사용될 수 있다. 또한, 광학 공진 구조 최적화를 통해 높은 색순도의 디스플레이로도 활용될 수 있다. 하지만 유기 발광소자가 방출한 광자의 절반 이상은 높은 굴절률의 유기물 및 기판으로 인한 내부 전반사로 소멸된다. 따라서, 유기 발광소자의 효율을 올리고 전력 소모를 감소시키기 위해 광추출 기술은 필요하다. 이에 더불어, 위에서 언급한 바와 같이 소자의 구동시간에 대한 고려도 필요하다. 유기 발광소자의 짧은 구동 수명에 대한 연구는 많이 있고, 몇몇 메커니즘이 발표되었지만, 아직 소자 열화의 전반을 설명할 수 있는 이론은 전무하다. 그럼에도 불구하고, 높은 구동 안정성을 위해선

유기 발광소자를 구성하는 층의 안정성을 고려해야 하는 것은 자명하다.

본 논문은 2 가지 연구주제: (1) 단순하면서도 효율적인 조명용 그리고 디스플레이용 광추출 구조, 그리고 (2) 자발적 배향 분극 분자를 활용한 소자의 수명 향상에 대한 내용을 다루고 있다.

제 1 장은 유기 발광소자에 대한 간략한 서론을 담고 있다.

제 2 장은 파란색 하부 발광형 유기 발광소자의 외부 광추출 효율 향상을 위한 손쉬우면서도 효율적인 랜덤 유기 마이크로 구조(DACM)에 대한 내용을 담고 있다. TCTA 와 B4PyMPM 혼합 용액을 필름에 드롭 캐스팅 후 UV 경화 시키면 무작위 모양의 마이크로 구조물이 형성되었고, 회절 무늬가 없어 광추출로 적합했다. DACM 필름을 부착한 소자는 44.3%의 외부 광자 효율을 가졌고, 광추출 구조가 없는 소자 평판 소자 대비 35%의 향상을 보였다. 또한, 마이크로 렌즈 어레이 필름에 향상량인 22% 보다 높은 수치를 기록했다. 이 구조는 기판에 상관없이 대면적 공정이 가능하고, 저렴한 제작 공정, 클로로포름과 같은 알킬 할라이드 용매에 강했으며, 구조 컨트롤도 가능하기 때문에 조명용으로 매우 효율적이고, 디스플레이용으로 활용될 잠재력이 있다.

제 3 장은 진공 열증착을 통해 손상 없이 형성한 상부 발광형 유기 발광소자용 광추출 구조에 대한 내용을 담고 있다. 상부 발광형 소자는 높은 픽셀 종횡비, 흐려짐 없는 이미징, 높은 색 순도로 인해 소형 디스플레이에 활용되고 있다. 하지만, 이러한 이점을 얻는 강공진 구조는 금속 전극에 의한 높은 광학 손실을 야기한다. 게다가 상부 발광형 소자에는 빛의 경로에 기판이 없는 까닭에 손상 없는 공정이 어렵다. 우리는 1,5-diaminoanthraquinone (DAAQ) 유기물의 진공 열증착을 통해 상부 발광형 소자의 은 (Ag) 박막 위에 손상 없이 광추출 구조를 형성했다. DAAQ 는 은 박막 위에서 증착 즉시 결정화되었으며, 기판에 수직 방향으로 나노와이어를 형성했다. 나노와이어 어레이의 높이, 둘레, 그리고 주기는 증착 속도 및 두께로 조절 가능했다. 이를 상부 발광형 소자에 접목시켰고, 좁은 반치폭의 소자에서는 8.6%, 넓은 반치폭의 소자에서는 10.6%의 향상량을 얻었다. 이 방법은 쉬우며, 소자에 손상을 주지 않아 열화 시키지 않으며, 패터닝 공정이 필요 없고, 진공공정이 가능한 까닭에 매우 유용하다.

제 4 장은 내부 광추출 구조의 패터닝 특성의 중요성에 대해 서술한다. 내부 광추출 구조를 디스플레이에 활용하기 위해선 박막 트랜지스터 (TFT) 와 유기 발광소자 전극 사이에 신호를 주고받을 수 있는 통로, 즉 비아홀 (viahole) 이 필요하다. 내부 광추출

구조는 위치가 박막 트랜지스터와 유기 발광소자 사이에 위치한 까닭에, 구조 설계 시 viahole 패터닝을 고려해야 하지만, 지금까지 이런 고려는 적었다. 또한, 일반적인 내부 광추출구조는 고 굴절 물질 내에, 낮은 굴절률의 광 결정이 위치하는데, 이종의 물질은 식각 용액에 대해 서로 다른 에칭 선택비 (etching selectivity)를 갖기 때문에, 내부 광추출구조의 손상 없이 패터닝이 가능한 식각 용액을 찾는 것 또한 필요하다. 우리는 SiO_x 스캐터와 TiO_2 평탄층을 갖는 내부 광추출 구조의 비아홀 패터닝을 성공적으로 구현한 소자를 보고한다. SiO_x 와 TiO_2 에 대해 유사한 에칭 선택비를 갖는 buffered oxide etchant (BOE) 와 인산 (H_3PO_4) 의 혼합 식각 용액을 활용해 언더컷 (undercut) 문제가 해결된 비아홀 패터닝 공정을 확립했으며, 제작된 유기 발광소자의 낮은 누설 전류 및 손상 없는 광추출 효율을 통해 비아홀 패터닝이 성공적으로 되었음을 실험적으로 보였다.

제5장은 전자 전달층 (Electron transporting layer, ETL) 의 안정성을 향상시키기 위한 방법을 담고 있다. 영구 쌍극자 모멘트 (permanent dipole moment)의 정렬이 비정질의 Alq_3 유기물에서도 발현됨을 발견한 이후, 여러 전자전달물질에서 이러한 특성 (배향 분극, orientation polarization)이 나타남이 밝혀졌다. 지금까진 배향 분극이 소자의 전기적 특성에 어떻게 영향을 끼치는지에 대한

연구가 주류를 이뤘다. 하지만 우리는 배향 분극이 유기 발광소자의 수명에 어떤 영향을 주는지 밝혔다. 소자의 에너지 전달 과정에 참여하지 않는 BAlq 분자를 활용해 전자 전달층과 발광층 (EML) 사이에 음의 표면 전하 밀도를 높혔을 때, 소자의 구동 수명이 증가함을 보였다. 또한 물질의 열화 정도를 파악할 수 있는 전압 변화가 낮아짐을 통해 BAlq 에 의한 표면전하 변화가 전자전달층의 안정성을 올림을 알 수 있었다. 또한 분극된 층이 발광층과의 계면에 위치할 경우에서만 수명이 증가하는 결과를 통해 정공 차단층 (hole blocking layer, HBL) 이 음의 표면 전하를 발광층과의 계면에 가질 경우, 향상된 수명을 얻을 수 있다는 결론을 얻었으며, 이를 통해 분자의 배향 분극 특성도 소자의 수명향상을 위해 고려해야 함을 보였다.

주요어: 유기발광소자, 광추출 효율, 광추출 구조, 구동 수명, 자발적 배향 분극

학번: 2015-20870

CURRICULUM VITAE

Yoonjay Han

Department of Materials Science & Engineering

Seoul National University, Seoul, 08826, Korea

+82-2-875-2412 (Office)

E-mail: yoonjay@snu.ac.kr

Education

2015.03 ~ 2020.08 **Ph.D.** in Materials Science & Engineering
Supervisor: Professor Jang-Joo Kim
Seoul National University, Seoul, Korea

2013.03 ~ 2015.02 **B.S.** in Materials Science and Engineering
Yonsei University, Seoul, Korea

2009.03 ~ 2013.02 Materials Science and Engineering
Hanyang University, Seoul, Korea

Research Interests

Organic light-emittng diodes, Light extraction efficiency, Light extraction structure, Operation lifetime, Layer chemical stability of transporting layer, spontaneous orientation polarization

Professional Skills

- Design and fabrication of organic electronic devices: Thermal vacuum evaporator, Glove-box, Spin-coater
- The optoelectronic analysis on organic semiconductors: UV-vis-NIR absorption spectroscopy, OLEDs characteristic measurements, PL efficiency measurement, Angle dependent PL analysis, Angle EL analysis
- The electrical characterization of OLEDs: impedance analysis
- The structural characterization of organic semiconductors: α-STEP, AFM
- Wet etching
- Photolithography
- Density functional theory (DFT) calculations
- Finite difference time domain calculations
- Ray tracing calculations

Scholarship and Fellowship

- Brain Korea 21 Scholarship (2015.02 ~)

List of Publications

1. Young-Sam Park*, Kyung-Hoon Han, Jehan Kim, Doo-Hee Cho, Jonghee Lee, **Yoonjay Han**, Jong Tae Lim, Nam Sung Cho, Byounggon Yu, Jeong-Ik Lee, and Jang-Joo Kim*, "Crystallization-assisted nano-lens array fabrication for highly efficient and color stable organic light emitting diodes ", *Nanoscale* **9**, 230 (2017)

2. Young Hoon Sung, Kyung-Hoon Han, Yang Doo Kim, **Yoonjay Han**, Jang-Joo Kim*, and Heon Lee*, "Air void optical scattering structure for high-brightness organic light emitting diodes ", *Ceram. Int.* **43**, S455-S459 (2017)

3. Kwan Kim, Kyoung-Hoon Han, Yang-Doo Kim, Daihong Huh, **Yoonjay Han**, Heon Lee*, and Jang-Joo Kim*, "Dual pattern for enhancing light extraction efficiency of white organic light-emitting diodes", *Org. Electron.* **57**, 201-205 (2018)

4. Kyung-Hoon Han, Young-Sam Park*, Doo-Hee Cho, **Yoonjay Han**, Jonghee Lee, Byoung-Gon Yu, Nam Sung Cho, Jeong-Ik Lee, and Jang-Joo Kim*, "Optical Analysis of Power Distribution in Top-Emitting Organic Light Emitting Diodes Integrated with Nanolens Array Using Finite Difference Time Domain ", *ACS Appl. Mater. Interfaces* **10**, 18942-18947 (2018)

5. Kyung-Hoon Han, Kwan Kim, **Yoonjay Han**, Yang-Doo Kim,

Hyoungcheol Lim, Daihong Huh, Hyun Shin, Heon Lee*, and Jang-Joo Kim*, "Highly Efficient Tandem White OLED Using a Hollow Structure", *Adv. Mater. Interfaces* **7**, 1901509 (2020)

6. **Yoonjay Han**, Kyung-Hoon Han, and Jang-Joo Kim*, "Random Nanowire Arrays Spontaneously Formed via Vacuum Deposition for Enhancing Light Extraction from Inverted Top-Emitting Organic Light-Emitting Diodes", *Fibers and Polymers* (2020, accepted)

7. **Yoonjay Han**, Chang-Ki Moon*, Kwan Kim, Heon Lee, and Jang-Joo Kim*, "Random Organic Nano-textured Microstructures by Photo-Induced Crosslinking for Light Extraction of Blue OLEDs", *Org. Electron.* (2020, accepted)

8. **Yoonjay Han**, Chang-Ki Moon*, and Jang-Joo Kim*, "Improving Operation Lifetime of OLEDs using Spontaneous Orientation Polarization", (2020, in preparation)

9. Beom-Soo Kim, **Yoonjay Han**, and Jang-Joo Kim*, "Growth mechanism of CH_3NH_3I in a vacuum processed perovskite", (2020, submitted)

List of Presentations

International Conference

1. **Yoonjay Han**, Doo-Hee Cho, Jeong-Ik Lee and Jang-Joo Kim, "Via hole of out-coupling layer for OLED displays", The 7th International Workshop on Flexible & Printable Electronics (2015 IWFPE), November 4-6 (November 5), 2015, Korea (Poster)
2. **Yoonjay Han**, Doo-Hee Cho, Kyung-Hoon Han, Jin-Wook Shin, Seung Koo Park, Jeong-Ik Lee, and Jang-Joo Kim, “Via Hole Patterning of Internal Scattering Layer for Electrical Connection between OLEDs and TFTs without Damaging Its Optical Enhancements”, The 12th International Conference on Electroluminescence and Optoelectronic Devices (ICEL 2018), October 14-17 (October 16), 2018, Korea (Poster)
3. **Yoonjay Han**, Chang-Ki Moon, and Jang-Joo Kim, "Light Extraction Layer using Photo Induced Charge Transfer", The 11th Asian Conference on Organic Electronics (A-COE 2019), Novembe 6-9 (November 8), 2019, Taiwan (Poster)